Finnmarkian EMP monazite ages and PT calculations of high grade rocks in the Central Belt of the Seve Nappe Complex, northern Jämtland and southern Västerbotten, Sweden.

MSc Thesis
Matthijs A. Hogerwerf*
*e-mail: M.A.Hogerwerf@gmail.com

July 2010
Faculty of Geosciences
Utrecht University

Supervisor:
Dr. H.L.M. Van Roermund

Abstract

The Scandinavian Caledonides consists of a series of Nappe Complexes that were transported in early Paleozoic times, from west to east over the Baltic Shield. This Allochthonous Nappe Complex is subdivided from bottom to top into Lower, Middle, Upper and Uppermost Allochthons. The investigated metamorphic complex, called the Seve Nappe Complex (SNC) in Sweden, defines the lower part of the Upper Allochthon in the counties of N. Jämtland and S. Västerbotten. Here the SNC is subdivided into three NS running belts, from top to bottom, called the Western, Central and Eastern Belts. The metamorphic grade (=temp; °C) of the SNC increases from the structural top (Western Belt; lower amphibolites facies) downwards (Central Belt; upper amphibolite- to granulite facies) and than decreases again (Eastern Belt; lower amphibolite- upper greenschist facies). However, although from north to south the metamorphic temperature, defined by mineral assemblages in the Central Belt of the SNC, remains (approximately) the same, this is not the case with associated metamorphic pressures. Associated metamorphic pressures (i.e. depths) in the Central Belt vary orders of magnitude when northern, central and southern sequents are mutually compared. In contrast, characteristic metamorphic mineral assemblages in the over- and underlying Western and Eastern Belts do not reveal this particularity. This change in metamorphic facies, from north to south is exclusively restricted to the Central Belt of the SNC and has never been explained before. The aim of the research project is to date the characteristic mineral assemblages in northern (Marsfjället gneiss) and central (Avardo gneiss) domains of the Central Belt using the chemical age dating EMP technique applied to monazites from samples collected in the summer of 2009 and to determine the formal metamorphic PT conditions of these rocks using the theoretical program Theriak-Domino applied to bulk rock compositions obtained by XRF. The EMP monazite ages of monazite grains included in peak metamorphic mineral assemblages, combined with detailed geothermobarometric work, is used to evaluate existing geodynamic models that can explain the variation in metamorphic facies. The age (T(0)) that has been found for the northern part of the Central Belt of the SNC is 497.3 +/- 3 Ma. The HP rocks in the central part are slightly younger, T(0) = 490.6 +/- 3 Ma. These ages are interpreted as Finnmarkian. The accompanied PT conditions for the rocks of the northern part, obtained by the program Theriak-Domino, are between ~12-17 kbar and ~550-800 ^{o}C. This is interpreted as a single stage of continental subduction followed by eduction in the SNC of N. Jämtland and S. Västerbotten. Renewed thrusting occurred during Scandian.

Table of contents

1. Introduction ……..4

2. Geology of the Scandinavian Caledonides 9
   2.1. Plate tectonic framework 9
   2.2. Anatomy / geometry 11
   2.3. Metamorphic grade 13

3. Methods 14
   3.1. Sampling 14
   3.2. Optical microscopy & EMP Analysis 15
   3.3. X-Ray Fluoresence 15
   3.4. TheriakDomino and metamorphic PT determinating 15
   3.5. ACF-A'KF diagrams 15

4. Geodynamic models 17
   4.1. Gee (1975) 17
   4.2. Brueckner and Van Roermund (2004) 19
   4.3. Hacker and Gans (2005)…….24
   4.4. Roberts (2002) 26

5. Monazites 30
   5.1. What are monazites and under what conditions do they form 30
   5.2. Crystal structure and chemistry 31
   5.3. Types of zoning 32

6. Results 35
   6.1. Field Observations 35
   6.2. Microstructure and mineral assemblage 38
   6.3. Monazite ages 41
      6.3.1 Standard …….41
      6.3.2 Marsfjället Gneiss / Northern part ……..42
      6.3.3 Avardo gneiss ……44
   6.4. Detailed features of dated monazites 46
   6.5. Bulk rock chemistry 49
   6.6. ACF – A'KF diagrams 50
   6.7. PT conditions 51
      6.7.1 Program Theriak-Domino ……51
      6.7.2 PT plots ……51
      6.7.3 PT discussion ……54
   6.8. EMP Mineral analysis 57
      6.8.1 Location mineral analysis 57
      6.8.2 Result mineral analysis 61
      6.8.3 Endmember diagram according to Theriak-Domino……...67
   6.9. Svartsjöbäcken schist 70

7. Discussion 72
   7.1. Age determination 72
      7.1.1 Reliability results…….....72

7.1.2 What is already known / comparison outcoming ages ..……73
7.2. PT conditions 74
7.2.1 (U)HP conditions ……75
7.2.2 Water ……...77
7.2.3 Microstructure and mineral assemblages……..……79
7.2.4 EMP Mineral analysis ……..……..80
7.2.5 Obtained PT conditions compared to what is already known ……..……80
7.3. Conceptional model 80
7.3.1 Peridotite bodies ……...80
7.3.2 Why are previous geodynamic models incorrect/incomplete ……..……..81
7.3.3 Own adaptation ……84
7.4. Svartsjöbäcken schist 85
7.5. Future 85
7.5.1 Other relevant investigations/projects ……85
7.5.2 What needs to be done ……86

8. Conclusions .....……87

9. Acknowledgements 89

10. References 90

1. Introduction

The (Scandinavian) Caledonides

The formation of the Caledonides all started during the closure of the Aegir and Iapetus Oceans followed by the continental collision between Baltica and Laurentia, which caused the formation of the Caledonides, including the formation of allochthons nappe complexes in the Scandinavian Caledonides. The nappes were trusted to the east over the Baltoscandian basement and autochthonous sedimentary cover. Up to the 1980's models of the Caledonides revealed passive continental margins, in early Palaeozoic times (the time table in appendix 11.1 is handled as reference in this master thesis), along the eastern margins of Iapetus Ocean. Imbrication of the Western Baltic margin occurred during the Scandian (Gee, 1975) resulting in a continuously westward dipping basement overthrust by allochthonous nappes tappening off towards the west. This way the nappe structure was explained by overthrusting. However, ideas that are more recent reject this model and come up with a new model that allows the rigid basement to subduct and educt again in a relatively short period. This way, observations like peridotites (Brueckner and Van Roermund, 2008) as well as eclogites (Van Roermund, 1985) can be explained better.

The Nappes of the Caledonides have a structure that can be divided from bottom to the top into five main complexes: the Autochthon, Lower Allochthon, Middle Allochthon, Upper Allochthon and the Uppermost Allochthon (Gee, 1985; Fig. 1). The Lower and Middle Allochthons are mainly shelf and continental rise successions of the Baltic Shelf. The Uppermost Allochthon constitutes a Scandinavian part that is likely formal Laurentia (Roberts, 2002). The Upper Allochthon is mainly oceanic (ophiolitic), with diverse magmatic arcs and marginal basin associations possibly from the Iapetus Ocean. The Upper Allochthon is subdivided into two major nappe complexes: the Köli Nappe Complex (KNC) on top and the Seve Nappe Complex (SNC) at the bottom. The SNC can be subdivided into the Eastern, Central and Western Belt (Zwart, 1974; Van Roermund 1985, 1989). The highest grade (=temp; °C) metamorphic rocks of the SNC are located in the Central Belt and define three different types of metamorphic facies. In the northern part, high-pressure granulite facies rocks occur which consists of kyanite and k-feldspar in pelitic schists and gneisses and grt-cpx-plag in metabasic rocks (Trouw, 1969). In the central part eclogite facies rocks are exposed (Van Roermund, 1985) and in basic rocks within the southern domain, low pressure granulite facies rocks (sillimanite - k-feldspar/2 pyroxene plagioclase) are found within pelites and metabasics (Van der Stijl, 1976). So the metamorphic grade (=temp; °C) of the SNC increases from the structural top (Western Belt; lower amphibolites facies) downwards (Central Belt; upper amphibolite- to granulite facies) and then decreases again (Eastern Belt; lower amphibolite- upper greenschist facies). An exception is the area around Tjeliken (Van Roermund and Bakker, 1984; v. Roermund, 1985; 1989). Here an extra HP lens

is integrated within the Eastern Belt, but this has been ignored in the present study. However, although from north to south the metamorphic temperature, defined by mineral assemblages in the Central Belt of the SNC, remains (approximately) the same, this is not the case with associated metamorphic pressures (Fig. 5). Associated metamorphic pressures (i.e. depths) in the Central Belt vary orders of magnitude when northern, central and southern parts are compared. In contrast, characteristic metamorphic mineral assemblages in the over- and underlying Western and Eastern Belts do not reveal this particularity (except for Tjeliken). This change in metamorphic facies, from north to south and exclusively restricted to the Central Belt of the SNC, has never been explained. The eclogite facies mineral assemblage in the Central Belt is dated as being 454 Ma, Scandian stage (Brueckner and Van Roermund, 2008). The reason for the strong variation in metamorphic pressure, while metamorphic temperature remains approximately constant, within rocks defining the Central Belt of the SNC is unknown. On a larger, regional scale (Fig. 1), the metamorphic facies variations described above seems to be dated. The Norbotton region in the north is dated at 500 Ma (Mørk et al, 1988), the central part at 454 Ma (Brueckner and Van Roermund, 2008) and the southern part as 425 Ma (a.o. Claesson, 1987). What is not known however is how this 3-fold age spread is distributed within the research area and what its effect is on the nappe stacking process? This information is crucial to construct a proper geodynamic model. Figure 2 illustrates a tectonostratigraphic map of the fieldwork area with sample locations within the Marsfjället gneiss, Avardo gneiss, Sjouten unit and Svartsjöbäcken schist. Another more detailed illustration of the fieldwork area can be found in Appendix 11.2.

Aim & Approach

The main aim of this master thesis is to use the electron microprobe to date monazites in these high-grade mineral assemblages of the central belt of the SNC. Secondly, to determine the PT conditions during the formation of the high grade mineral assemblages. I.e. metamorphic conditions, microstructures of the selected samples, (special) monazites, and Electron Micro Probe (EMP) mineral analysis will all be evaluated. Monazite ages, combined with detailed geothermobarometric work applied to the characteristic mineral assemblages will be used to reconstruct a PT time path of Central belt metamorphic rocks. Subsequently these data will be evaluated to see if they can be used to discuss existing geodynamic models for the formation of the SNC. These geodynamic models should explain the variation in metamorphic grade exclusively restricted to the central belt of the SNC in N Jämtland and S. Västerbotten, Central Sweden. As such this new data will strengthen or give new insights about the fundamental question whether Caledonian Nappe transport in this part of the Scandinavian Caledonides occurred during one or more orogenic events widely separated in time or not.

Dating of the metamorphic rocks has been done with the use of the mineral monazite; a rare earth element phosphate. After sampling monazite bearing rocks from several EW cross-sections across the SNC in N. Jämtland and S. Västerbotten, Central Sweden, the samples were studied using optical- and

electron-optical techniques c.q. the mineral composition and monazite-ages were determined using the EMP of the Earth Science Department of the Utrecht University. For monazite age dating, the technique of Suzuki and Adachi (1991) is used. Bulk rock chemistry of the samples are determined by XRF which provided the input data for ACF-A'KF diagrams, that give the possibility for quantitative evaluation of metamorphic conditions, as well as determination of the PT conditions with the use of the computer program Theriak-Domino. The computer program Theriak-Domino provided pseudo sections (PT diagram) with possible PT stability fields illustrated by the microstructure and mineral analysis.

Figure 1 (next page): Tectonostratigraphic map of the Scandinavian Caledonides illustrating the main Allochthons and complexes. The fieldwork area is located within the central black square and enlarged in the bottom right side image. (Modified after Gee et al., 1985)

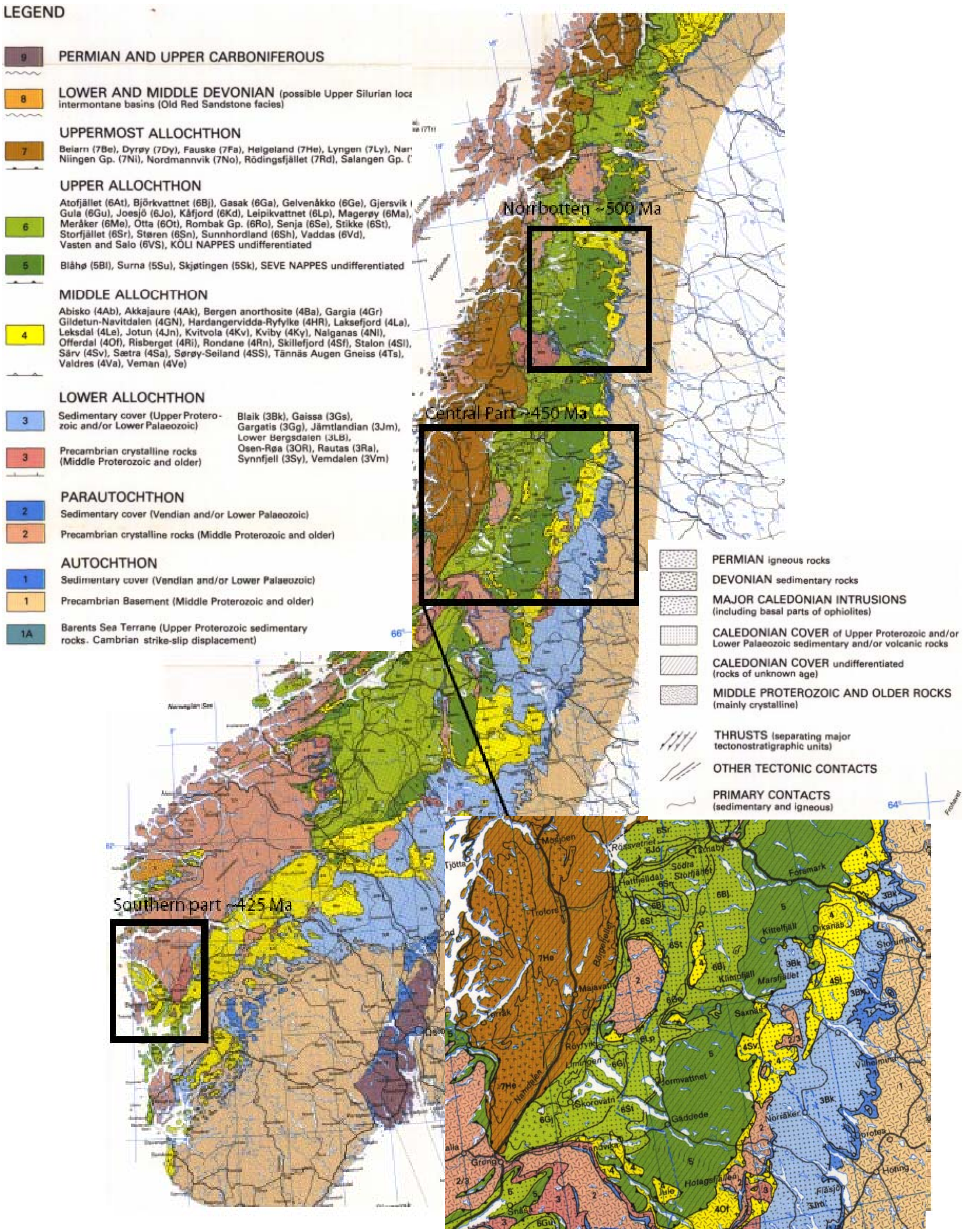
LEGEND
PERMIAN AND UPPER CARBONIFEROUS
LOWER AND MIDDLE DEVONIAN (possible Upper Silurian loca
intermontane basins (Old Red Sandstone facies)
UPPERMOST ALLOCHTHON
Beiarn (7Be), Dyrøy (7Dy), Fauske (7Fa), Helgeland (7He), Lyngen (7Ly), Nar
Niingen Gp. (7Ni), Nordmannvik (7No), Rödingsfjället (7Rd), Salangen Gp. (
UPPER ALLOCHTHON
Atofjället (6At), Björkvattnet (6Bj), Gasak (6Ga), Gelvenåkko (6Ge), Gjersvik
Gula (6Gu), Joesjö (6Jo), Kåfjord (6Kd), Leipikvattnet (6Lp), Magerøy (6Ma),
Meråker (6Me), Otta (6Ot), Rombak Gp. (6Ro), Senja (6Se), Stikke (6St),
Storfjället (6Sr), Støren (6Sn), Sunnhordland (6Sh), Vaddas (6Vd),
Vasten and Salo (6VS), KÖLI NAPPES undifferentiated
Blåhø (5Bl), Surna (5Su), Skjøtingen (5Sk), SEVE NAPPES undifferentiated
MIDDLE ALLOCHTHON
Abisko (4Ab), Akkajaure (4Ak), Bergen anorthosite (4Ba), Gargia (4Gr)
Gildetun-Navitdalen (4GN), Hardangervidda-Ryfylke (4HR), Laksefjord (4La),
Leksdal (4Le), Jotun (4Jn), Kvitvola (4Kv), Kviby (4Ky), Nalganas (4Nl),
Offerdal (4Of), Risberget (4Ri), Rondane (4Rn), Skillefjord (4Sf), Stalon (4Sl),
Särv (4Sv), Sætra (4Sa), Sørøy-Seiland (4SS), Tännäs Augen Gneiss (4Ts),
Valdres (4Va), Veman (4Ve)
LOWER ALLOCHTHON
Sedimentary cover (Upper Proterozoic and/or Lower Palaeozoic)
Precambrian crystalline rocks (Middle Proterozoic and older)
Blaik (3Bk), Gaissa (3Gs), Gargatis (3Gg), Jämtlandian (3Jm), Lower Bergsdalen (3LB), Osen-Røa (3OR), Rautas (3Ra), Synnfjell (3Sy), Vemdalen (3Vm)
PARAUTOCHTHON
Sedimentary cover (Vendian and/or Lower Palaeozoic)
Precambrian crystalline rocks (Middle Proterozoic and older)
AUTOCHTHON
Sedimentary cover (Vendian and/or Lower Palaeozoic)
Precambrian Basement (Middle Proterozoic and older)
Barents Sea Terrane (Upper Proterozoic sedimentary rocks. Cambrian strike-slip displacement)
Norrbotten ~500 Ma
Central Part ~450 Ma
Southern part ~425 Ma
PERMIAN igneous rocks
DEVONIAN sedimentary rocks
MAJOR CALEDONIAN INTRUSIONS (including basal parts of ophiolites)
CALEDONIAN COVER of Upper Proterozoic and/or Lower Palaeozoic sedimentary and/or volcanic rocks
CALEDONIAN COVER undifferentiated (rocks of unknown age)
MIDDLE PROTEROZOIC AND OLDER ROCKS (mainly crystalline)
THRUSTS (separating major tectonostratigraphic units)
OTHER TECTONIC CONTACTS
PRIMARY CONTACTS (sedimentary and igneous)

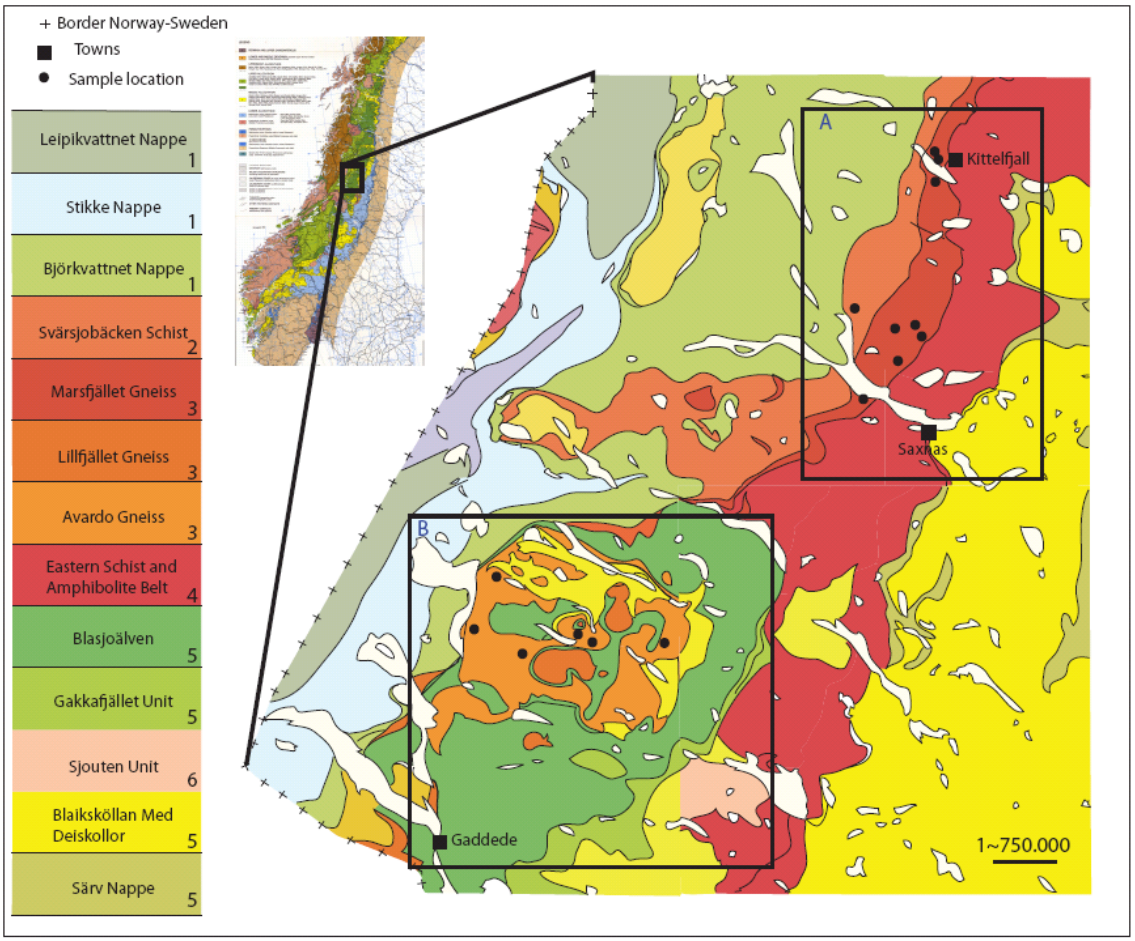

Figure 2: Tectonostratigraphic map of the fieldwork area illustrating the sample locations Marsfjället gneiss (Central Belt; Square A), Svartsjöbäcken schist (Western Belt; Square A), Avardo Gneiss (local name for Central Belt gneiss in the area around Härbergsdalen; Square B) and Sjouten Unit / Tjeliken (square B). Modified after SGU, 1991. The inserted map in the upper left corner of the figure is modified after Gee et al., 1985. The rectangular insets refer to the Marsfjället (north) and Tängen-Inviken area (south). Scale ~ 1:750.000 (note that the size of the Marsfjället and Tängen-Inviken area together is approximately the same size as the counties Utrecht and S. Holland combined). Number indications in name units: 1 = KNC, 2 = Western Belt, 3 = Central Belt, 4 = Eastern Belt, 5 = Särv Nappes, 6 = Sjouten Unit.

2. Geology of the Scandinavian Caledonides

2.1. Plate tectonic framework

Before the Scandinavian Caledonides were formed there was one supercontinent Rhodinia. The Grenvillian-Sveconorwegian Orogeny took place (approximately 1000-800 Ma) and incorporated the early Laurentian Shield and the East European Platform (formation of supercontinent Rhodinia). In post-Grenvillian time, sedimentation of the late Riphean prevailed during the basinal deposits (SGU Uppsala, 1998). Between 760-750 Ma a subarctic climate caused the presence of tillites and tilloids in the Lower Allochthon (Hotagen and Särv Nappes). At 650 Ma Rhodinia breaks up in Laurentia and Baltica, which caused the opening of the Laurentian-Baltic megaplatform. This coincided with basaltic dike intrusions along the rift zone (Gee, 1975) followed by the formation of an ocean floor (Iapetus Ocean). Within this ocean, also some microcontinents and island arcs were present (SGU Uppsala, 1998). After the opening, the tectonic regime changed from rifting to convergence, causing the clousure of the Iapetus ocean. The next step took place between the Late Cambrium and the Early Devonian when four major compressive/transpressive events occurred, all related to the closure of the Iapetus followed by the first continental collision. Microcontinents and island arcs were picked up during this closure before the actual collision of Baltica and Laurentia. These events are called the Finnmarkian (Late Cambrium, 542-500 Ma), the Trondheim (Early Arenig, 479-468 Ma)), the Taconian (Mid-Late Ordovician, 472-444 Ma) along the western margin of the Iapetus, the Jämtlandian (454 Ma; Brueckner and Van Roermund, 2004; see also Brueckner and Van Roermund, 2008) along the eastern margin of Iapetus Ocean affecting the western margin of Baltica and finally the Scandian event (Early Devonian, 430-398 Ma; Roberts 2002).

Palaeomagnetic reconstructions illustrated in figure 3, record the gradually change in positions of Baltica in space and time. From this figure it can be seen that there has been a major shift from below 60^{o} on the southern hemisphere to today's position at approximately 60^{o} on the northern hemisphere. Secondly, an 180^{o} anticlockwise rotation of Baltica occurred during the time period of 500-440 Ma (Torsvik and Cocks, 2005). A mechanism for this rotation is thus far lacking. Figure 4 is illustrating a plate reconstruction from Early Ordovician (480 Ma) to Late Silurian (420 Ma) times. Highlighted are the positions of Baltica, Siberia and Laurentia (Torsvik, 1998; Torsvik et al., 1998; Cocks and Torsvik, 2002).

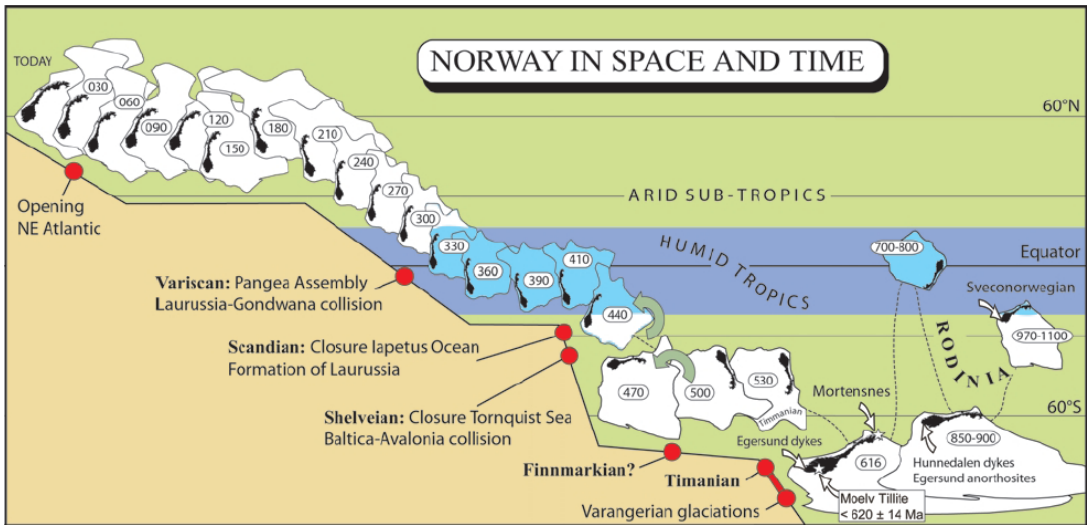

Figure 3: Baltica in space and time. Illustrating the shift from the southern hemisphere to the Northern hemisphere in the last 900 Myr (after: Torsvik and Cocks, 2005).

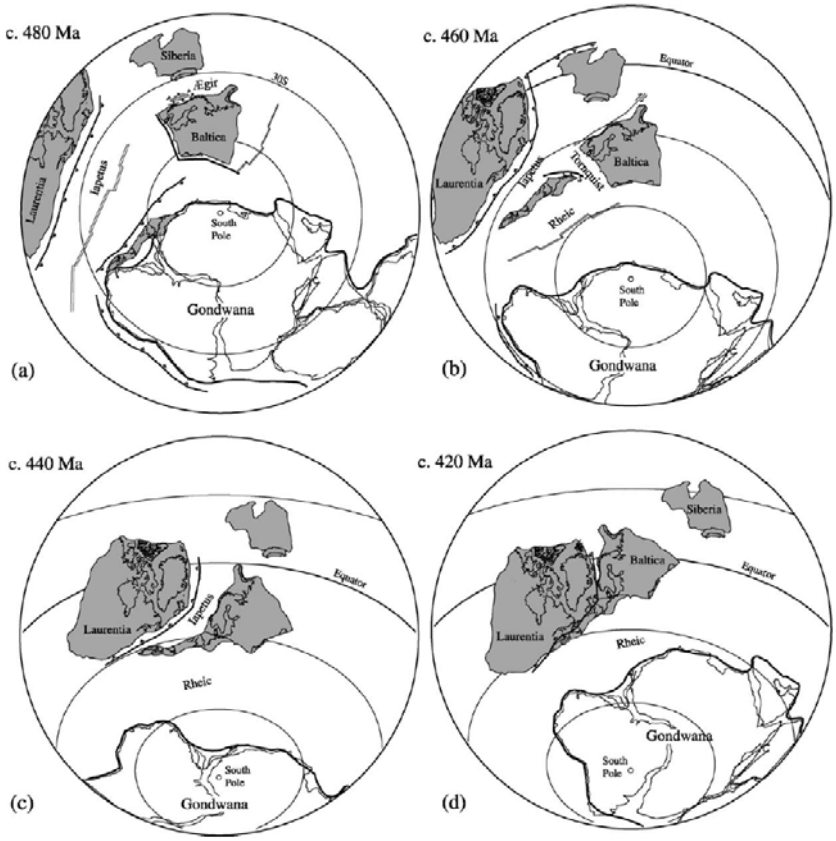

Figure 4: Palaeomagnetic reconstructions from Early Ordovician to Late Silurian time. Illustrating gradually changing positions of Baltica, Siberia and Laurentia. Reconstructions are based on Torsvik (1998), Torsvik et al., (1996) and Cocks and Torsvik (2002) with small modifications by Roberts 2003. (a) Situation at approximately 480 Ma coeval with the Trondheim event (the Baltoscandian margin of Baltica faced Siberia at this time but Baltica was rotating anticlockwise (Roberts, 2003). (b) Mid to Late Ordovician boundary at the Taconian event along the margin of Laurentia. (c) Early Silurian situation with a rapid closing Iapetus ocean. (d) Late Silurian at the Scandian continent – continent collision event. (After: Roberts, 2002).

2.2. Anatomy / geometry of the Scandinavian Caledonides

The geology of the Scandinavian Caledonides is complex (Fig. 1). The current structure is dominated by several nappe complexes, generally thinning westwards (Gee, 1985) that were transported in Early Paleaozoic times, from west to east over the Baltic Shield. These Allochthonous nappe complexes are situated on top of the Autochthon basement and form five tectonic major units. These main complexes are from bottom to top the Autochthon basement, Lower Allochthon, Middle Allochthon, Upper Allochthon and the Uppermost Allochthon (Gee, 1985; Roberts, 2003; Fig. 1). The Autochthon consists of Precambrian Baltica basement overlain by Vendian through Upper Silurian sedimentary rocks (Hacker and Gans, 2005). The Lower Allochthon is composed of Late Precambrian to lower Palaeozoic metasedimentary rocks and underlying crystalline basement (SGU, Uppsala 1998). All Allochthons are internally deformed by thrust faults, limited faults and normal faults. The intensity of the deformation is highest near thick bodies, where shortening by stacking tectonics occurred. The Lower Allochthon may vary in rock type between rigid quartzites, soft metasediments and basement porphyries. The sole-thrust dominating in the east of the Caledonides dips westward with an angle varying between 0.5 to 1 degree (SGU Uppsala, 1998; Greiling et al., 1998). Crystalline and sedimentary rocks derived from Baltica form the Middle Allochthon. The Upper Allochthon consists of rocks that originate from the transition zone between the western continental margin of Baltica and Eastern Iapetus. The Uppermost Allochthon consists of fragment of Laurentia (Hacker and Gans, 2009; Brueckner and Van Roermund, 2008).

The Upper Allochthon in Sweden can be subdivided into the Köli Nappe Complex (greenschist facies; oceanic domain) and SNC (continental domain). In the counties N. Jämtland and S. Västerbotten in central Sweden, the SNC is defined by the lower part of the Upper Allochthon and can be subdivided into three NS running belts (Fig. 2). From top to bottom called the Western, Central and Eastern Belts (Zwart, 1974). The boundary between the Central and Eastern Belt is tectonic. The Köli Nappe Complex (KNC) overlies the Western Belt; the Eastern Belt is underlain by nappes that belong to the lower Allochthon (a.o. Särv nappe). Both major contacts, sandwiching the entire SNC, are interpreted to be tectonic in nature. In the central part of the area, the Western Belt is missing due to truncation by the overlying KNC. According to SGU Uppsala (1998), the original rocks of the Seve Nappes were sediments and submarine volcanics, which originated on the ocean floor of the Iapetus Ocean where no crystalline basement is involved. According to Brueckner and Van Roermund (2008) this is not true and Seve Nappes do include more material derived from Western Baltica (including basement units). Nowadays the rocks appear as light coloured gneisses, crystalline limestones and ultra-basites. The Köli rock sequence contains volcanic rocks and shows features of island arc sedimentation. Svartsjöbäcken schist can be found on top of the Central Belt and is called the Western Belt. These schists are separated from the Central Belt by a transition zone. On top of this Western Belt lies the KNC. This is a tectonic belt (SGU Uppsala, 1998). The KNC is divided into three groups; Upper,

Middle and Lower Köli. They are all foliated mafic to felsic igneous rocks (Gee, 1985). Seve Nappes rocks are interpreted to be Late Precambrian to Cambrian of age and originated from the Baltoscandian continental margin to ocean-continental transition. These rocks consist of mica schist, amphibolite and quartzofeldspathic gneisses (Hacker and Gans, 2009). This is presented in Table 1 below (Zwart, 1974)

Tectonic unit		Rock Type	Metamorphic zone
Köli		Keratophyre, greenschist, calcareous phyllite, limestone, conglomerate, quartz-keratophyre, greenschist, black phyllite	Chlorite and Biotite
Seve	Western Belt	Garnet-mica schist Quartzitic garnet-mica schist with amphibolites	Garnet and Staurolite-kyantite
	Central Belt	Migmatic ky/sill-k-feldspar gneiss (with eclogites) +/- other rocks Quartzo-feldspatic gneiss amphibolite (hbl, cpx, gar) ky-k-feldspar gneiss (+sill)	Kyanite-potassium feldspar Sill-KFS Plagioclase is above the amphibolite temperatures
	Eastern Belt	Meta-arkose and quartzite Garnet-mica schist, marble amphibolite garnet-mica schist	Staurolite-kyanite and Garnet HP lenses

Table 1 (modified after Zwart, 1974): Illustration of the Upper Allochthon with the subdivided tectonic units with there present rock types and metamorphic zone. Note: there is a major tectonic contact between the Köli and Seve Nappe.

The structure and metamorphism of the Seve-Köli Nappe Complex (SKNC), and its implications concerning the formation of metamorphic nappes are described on the base of lithologic, metamorphic and structural criteria. Units between the SNC are separated by mylonite zones, while between the Seve Nappe and the nappes attached (Köli and Särv Nappes) this contact is considered tectonic. This thrust contact of the SNC can be followed along a strike for with length of up to 900 km. The width of the Seve Nappes is approximately 80 to 100 km (Zwart, 1974).

2.3. Metamorphic grade

Figure 5 below is a simplified metamorphic map of the fieldwork area illustrating differences in metamorphic PT conditions throughout the area. This figure clearly summarises the major topic of this master thesis as stated earlier.

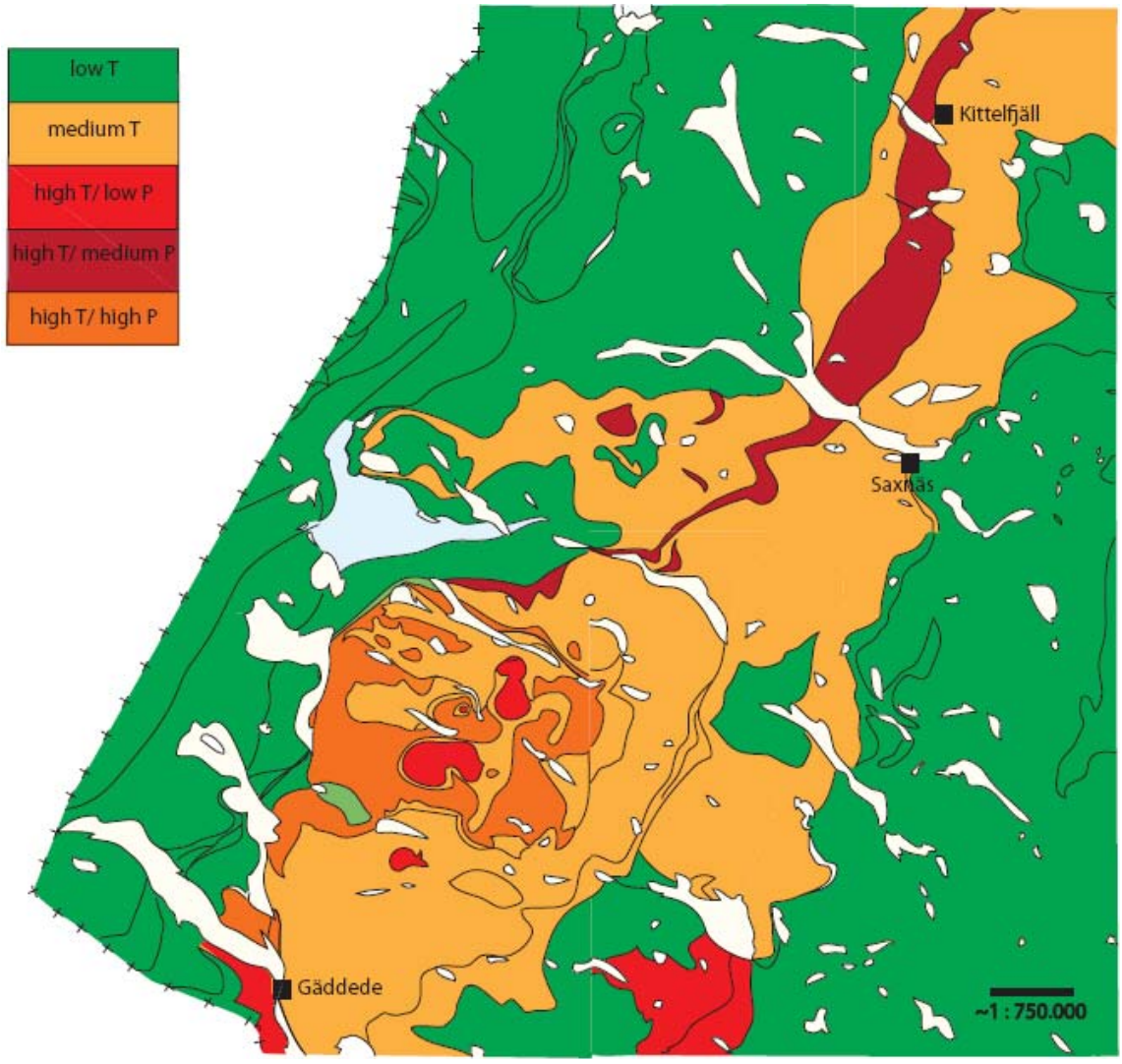

Figure 5: Simplified metamorphic map of the fieldwork area indicating low T, medium T, high T/low P, High T / medium P and high T/high P terranes (Sveriges Geologiska Undersokning, 1991). Scale ~ 1:750.000

What is not visible in this figure are the major tectonic contacts between the SNC and the KNC and nappes from the Lower Allochthon. These are situated between the low temperature and medium to high temperature rocks. Samples are essentially taken from the high T / medium P metamorphic rocks, located in the central part, as well as from high T / high P rocks, located in the southern domain. These locations are illustrated in figure 2.

3. Methods

3.1. Samples

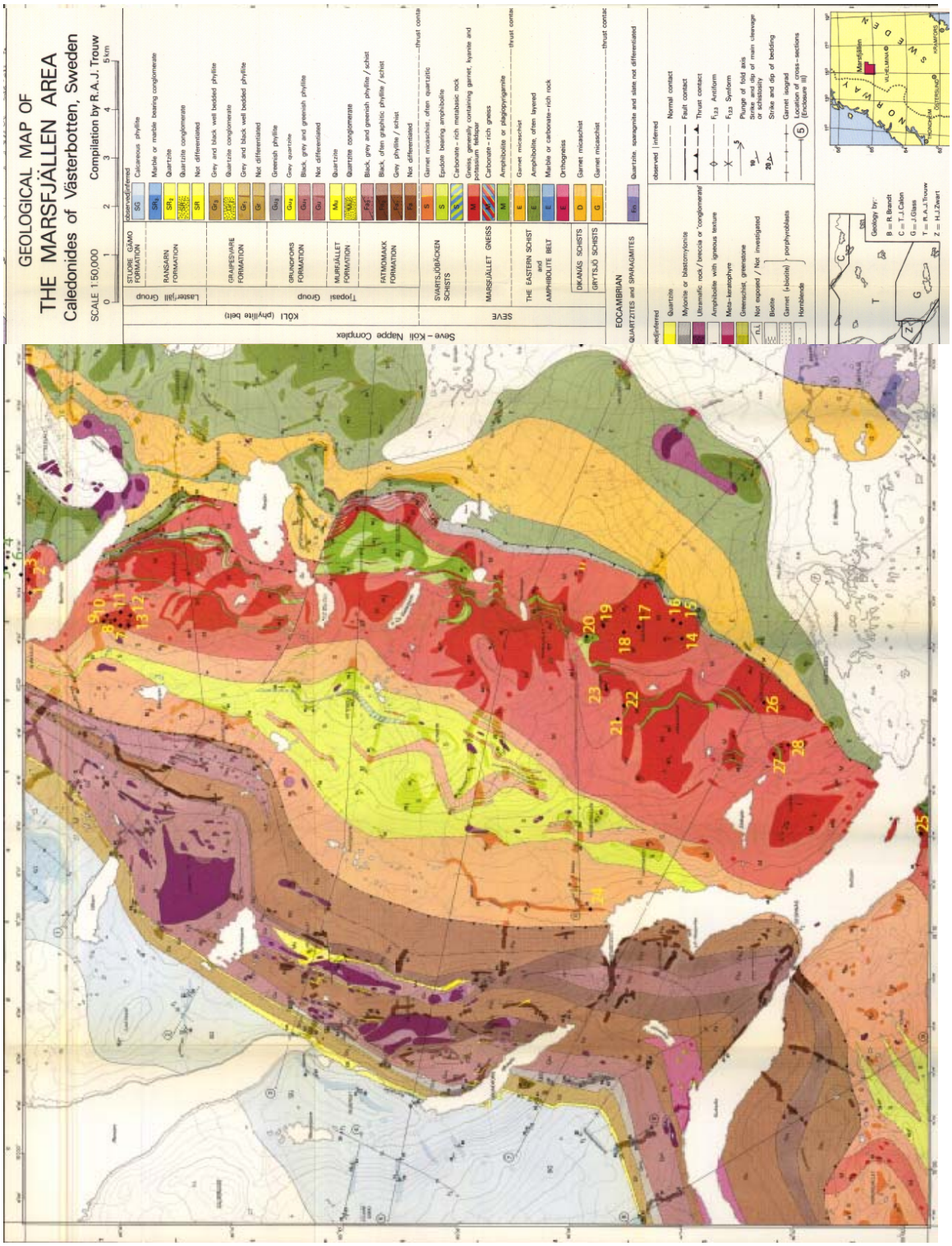

Figure 6: Geological map of the Marsfjällen area, Caledonides of Västerbotten, Sweden (Trouw, 1979). Sample locations and accompanied numbers are illustrated in yellow (and green).

28 Samples have been collected in the Marsfjällen area (Fig. 2; Fig. 6; Appendix 11.2.2) and 20 samples in the Tängen-Inviken area (Fig. 2; Appendix 11.2.3). Samples 1 to 28 are all from the northern part. Sample 24 comes from the Svartsjöbäcken schist (Fig. 6). The 20 samples of the high pressure rocks (Avardo Gneiss and Sjouten Unit) from the Tängen-Inviken are numbered from 33-38, 45-46, 51-52, 58-64 and 68-69II for the Avardo Gneiss and 47-50 for the Sjouten Unit (Appendix 11.2.3). Representative samples were taken back home to the lab. Thin sections have been made of nearly all the collected samples and two rock samples of the Marsfjällen area have been crushed in order to get the bulk rock chemical composition. The thin sections are used for optical microscopy to investigate the mineral content and possible structures. The thin sections are also used for Electron Microprobe (EMP) analysis to investigate detailed mineral chemistry for analysis of the metamorphic grade and the age of the rocks.

3.2. Optical microscopy & EMP Analysis

The collected samples have been prepared in the lab to produce thin sections that were subsequently studied using optical- and electron-optical techniques. Optical microscopy is used for making plain and cross-polarized light images of the thin sections. Electron-optical techniques are used for Backscattered electron (BSE) imaging. Monazite-age determination has been carried out using the EMP in the Earth Science Department of the Utrecht University. For monazite age dating the technique of Suzuki and Adachi (1991) was used. Another tool of the EMP is the determination of chemical compositions. This can be done on a micron scale. This technique is described by Reed (1983) and Fialin et al., (1999).

3.3. X-Ray Fluorescence

Representative parts of two rock samples of the Marsfjällen area have been crushed and prepared for X-Ray Fluorescence. The analytical technique X-Ray Fluorescence (XRF) will provide bulk rock compositions of these representative rock samples. This technique is described by Norrish et al., 1967 and Leake et al., 1969.

3.4. TheriakDomino for metamorphic PT determination

Determination of the metamorphic PT conditions has been done with the use of the computer program TheriakDomino. The computer program TheriakDomino provide pseudo sections of PT diagram with possible PT stability fields. The technique used here is described in the manual of THERIAK-DOMINO Vers. 20.03.07 User's Guide *Christian de Capitani Konstantin Petrakakis.* Bulk rock chemical analyses are needed as input data.

3.5. ACF-A'KF diagrams

Bulk rock chemical compositions are the input data for the making of ACF-A'KF diagrams that give the possibility for quantitative evaluation of metamorphic conditions. This technique is described in

‘Metamorphic rocks and their geodynamic significance (a petrological handbook)’ by Jacques Kornbrobst (2002).

4. Geodynamic models

There are several geodynamic models about the formation of the Scandinavian Caledonides. The first one who described the nappe structure in the Caledonides of S. Västerbotten and N. Jämtland and its relation to the metamorphic grade was H. Zwart (1975). Gee (1975) proposed a geodynamic model where he assumed that there was one large rigid basement plate where all nappes were pushed over, i.e. the major tectonic contact between the basement and nappes was integrated as a décollement surface (at that time plate tectonics didn't exist). After Gee (1975), several scientists have tried to come up with alternative models. Just to mention a few: Roberts (2003) and Hacker and Gans (2007) have incorporated the concept of plate tectonics and made a geodynamic model that describes the nappe structure. Another model that describes the formation of the Scandinavian Caledonides is the model of Brueckner and Van Roermund (2004). They describe subduction of a rigid oceanic and continental plate, which endured slab break-off after continental subduction. After this break-off, the continental plate 'educts' back again and returns to the surface. These different geodynamic models will be described in the following chapters.

4.1. Gee (1975)

The geodynamic model of Gee (1975) is visualised in figures 7 and 8. Within these figures, a schematic geodynamic model is shown between Middle Silurian (~430-420 Ma) to Middle Devonian (~400-385). The main idea here is the major tectonic contact between the basement and nappes, which is integrated as a décollement surface. After initial extension (formation of rift basins) which was related to the opening/formation of the Iapetus Ocean, convergence started. The latter resulted in the illustrated structures in figures 7 and 8. Here the SKNC is depressed, metamorphosed, intruded and thrusted on the Särv Nappe. After this underthrusting, partial mobilization of the basement resulted in uplift in the west.

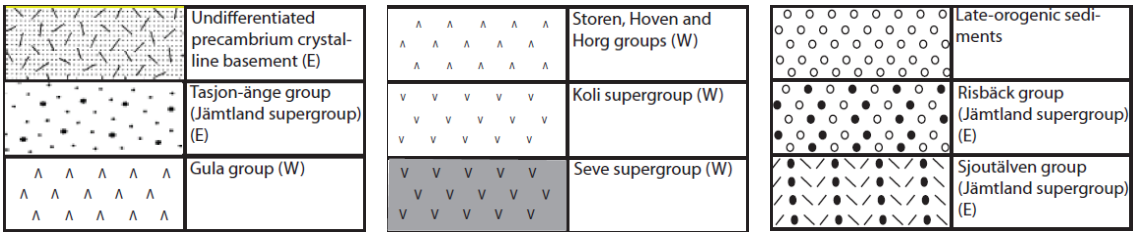

Legend figures 7 and 8.

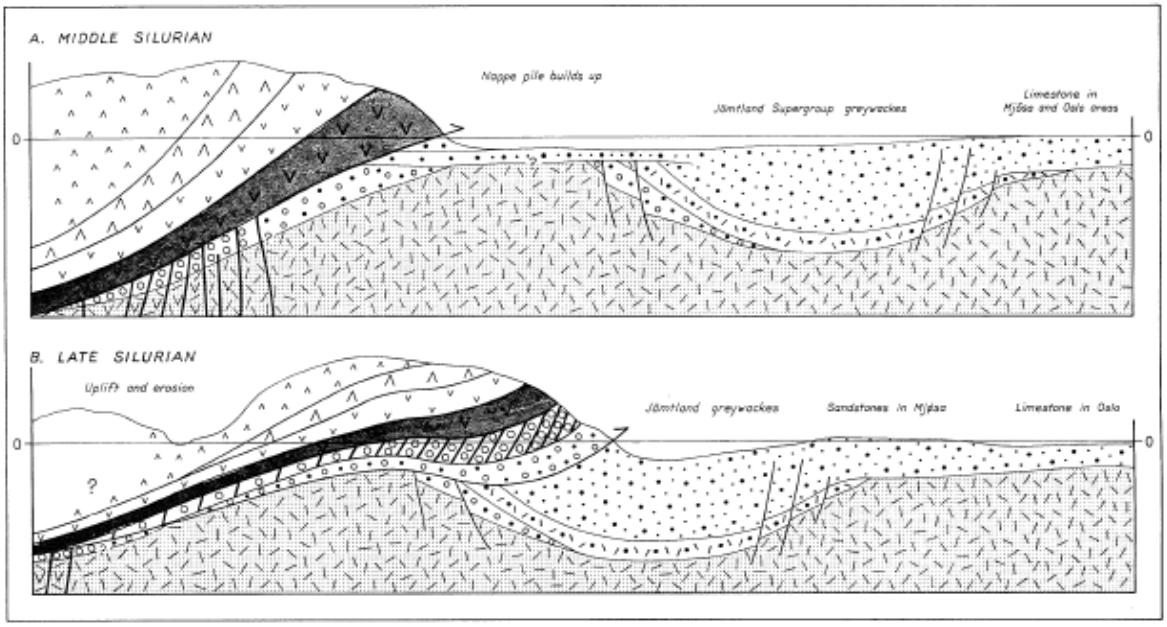

Figure 7: Schematic geodynamic model at Early-Middle and Middle-Late Silurian time (Gee, 1975). (a) Early Middle Silurian time: Baltoscandian margin continues to underthrust the Greenlandian Margin. SKNC is depressed, metamorphosed, intruded and thrust on to the Särv Group. Deposition is still going on in Jämtland. (b) Middle-Late Silurian time: Continued underthrusting.

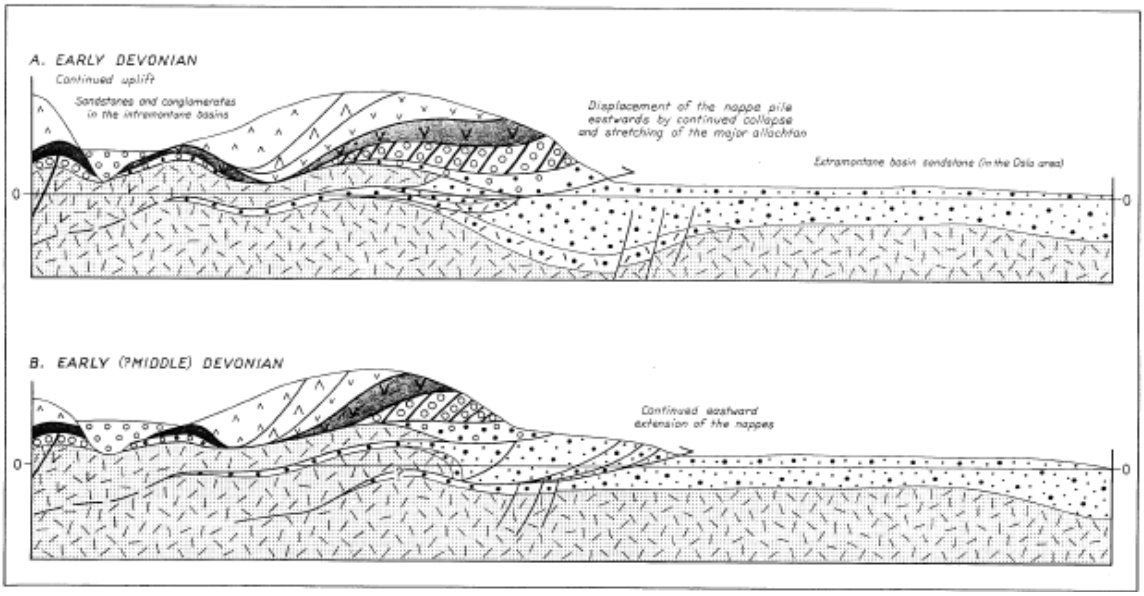

Figure 8: schematic geodynamic model at Early Devonian to Early (Middle) Devonian time (Gee, 1975). (a) Early Devonian time: translation of the Western Complex ceases and is followed by partial mobilization of the basement in the west and uplift. (b) Early (Middle) Devonian time: translation on the décollement of the parautochthon.

The most significant difference between the geodynamic model of Gee (1975) compared to the more recent models of Hacker and Gans (2005), Roberts (2002) and Brueckner and Van Roermund (2004) is that Gee (1975) did not include subduction in the mantle, but only a kind of décollement in principle responsible for the formation of the nappe structure. The roots of the nappes were thought to originate from sediments or slivers derived from the top of the basement. One of the main problems with this

model is the lack of explanation for the existence of the (U)HP rocks. In Gee's (1975) model, peridotites are coming from oceanic crust instead of the subcontinental mantle. So how can they contain (U)HP minerals? This question cannot be answered with this model. Thereby the rigid (thin) plates have endured a lot of stress that it is doubtful that the plates did not break.

4.2. Brueckner and Van Roermund (2004)

Brueckner and Van Roermund (2004) describe a multiple continental subduction/eduction model for the Scandinavian Caledonides called 'dunk tectonics'. Figure 9 is a tectonic map with the existence of active margins (plate tectonics) and the coupled ages to the different areas. The main difference with the tectonostratigraphic map of Gee (1985) (Fig. 1) is the incorporation of plate tectonics. Brueckner and Van Roermund (2004) state that the evolution of the Caledonides of Scandinavia included at least four major orogenic events; the two classic ones called the Finnmarkian and Scandian Orogenies, respectively 500 and 425-400 Ma. They also dated a third event in the SNC of N. Jämtland at around 454 Ma, called the Jämtlandian. All these orogenies occurred along the Baltoscandian margin. In contrast to the fourth event which occurred at the other side in the western Iapetus ocean (before closure) (Brueckner and Van Roermund, 2009). What must be kept in mind is that the break up of Rhodinia resulted also in several smaller fragments. These fragments (e.g. terranes) together with island arcs are interpreted as microcontinents situated between Baltica and Laurentia on the Iapetus Ocean. When the Iapetus Ocean was closing, these microcontinents collided with the adjacent continents resulting in an orogeny. The cause of these events is related to in continue closure of the Iapetus Ocean leading to continental subduction. Subduction of crustal slabs into the mantle subsequent leads to slab break-off of the oceanic crust followed by buoyancy-enhanced exhumation of the subducted continental crust towards the surface (called eduction; Fig. 10). Somewhere else another plate/continental fragment collides again, pushing the other masses further eastwards and continent further westwards and the model of Gee (1975) becomes applicable again. Therefore, in the east an accretionary terrane (slate belt) leads to thin skinned tectonics all in relatively low-grade rocks. However, this is not the case in Jämtland. Here, the Central Belt comes in too quickly if you compare the scale with other mountain fronts.

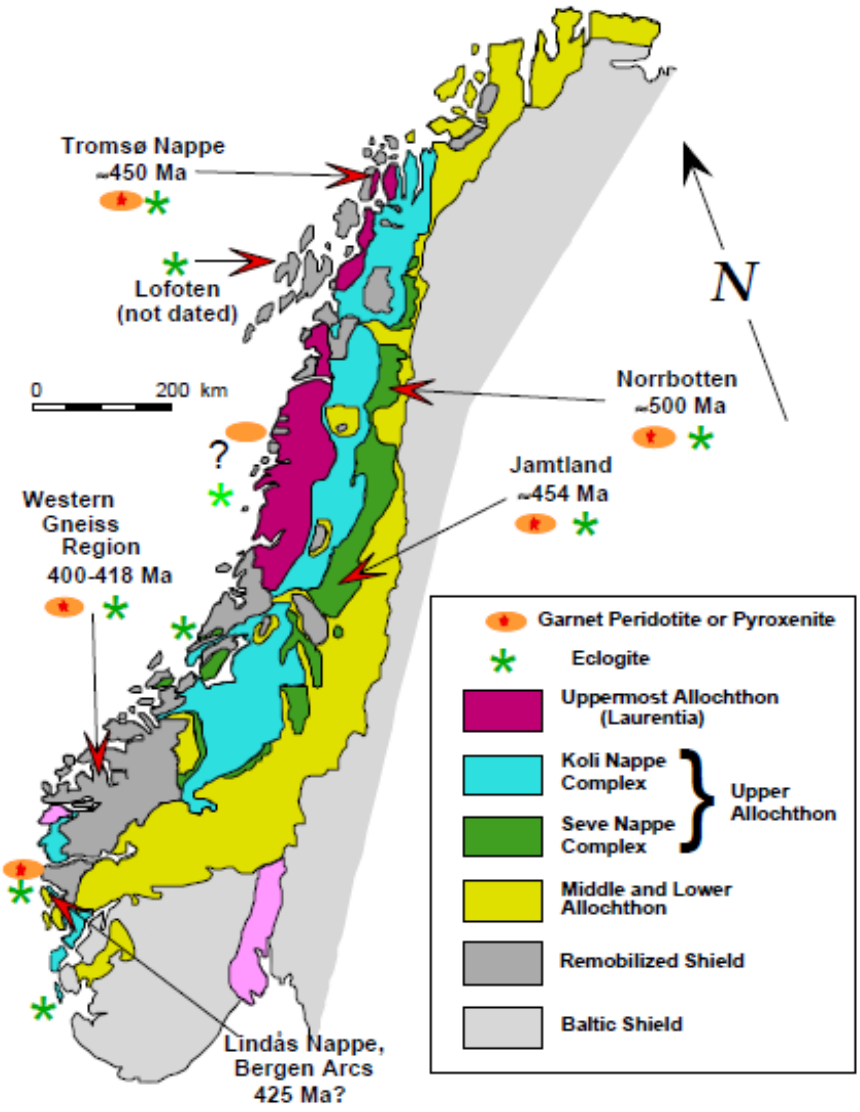

Figure 9: Tectonic map of the Scandinavian Caledonides illustrating the major Allochthonous complexes and locations of HP/UHP terranes, including mantle derived peridotite containing garnet-olivine assemblages (after Brueckner & Van Roermund, 2004; modified after Gee et al., 1985).

(U)HP metamorphic terranes are bounded by thrust faults at the base and low-angle normal detachments at the top. Garnet peridotite bodies are inserted from the overlying mantle wedge during subduction and/or eduction. The mechanism for achieving the subduction of crustal terranes appears to be through slab pull and/or possibly convective flow, but there is not the proper knowledge available yet. This pull force may be caused by the previous subducted oceanic plate that becomes metamorphosed into heavier rocks i.e. formation of denser minerals in the subducting slab. After the oceanic lithosphere breaks off (Wortel and Spakman, 2000; Fig. 11a), the crustal terranes/subducted continental crust returns to subcrustal levels. Buoyancy defines to what depth level within the crust. Subsequently different mechanisms may continue further thrusting (Fig. 11b). The motion all the way up again can be realized by (1) subsequent thrusting due to continued convergence, (2) extensional

collapse of an overthickened orogen, (3) ductile extrusion of subducted continental terrane between two bounding surfaces as these surfaces collapse together as scissors (Vannay and Grasemann, 2001). Finally, a combination of all these possibilities is most likely.

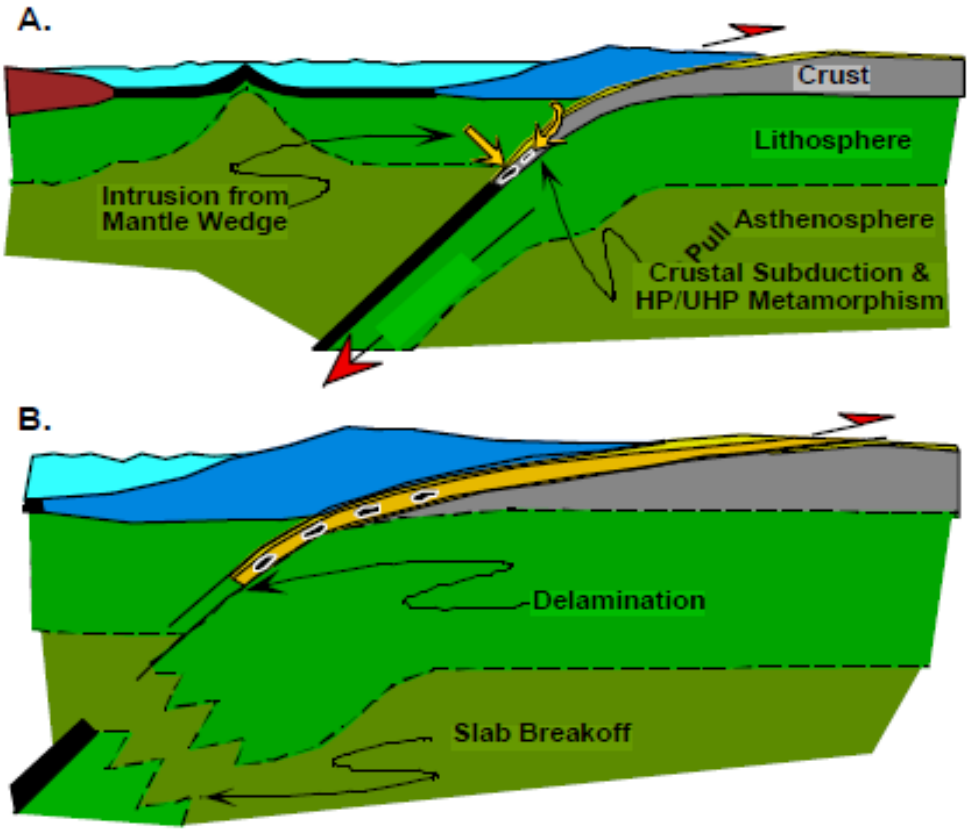

Figure 10: A simplified subduction/eduction model for an arc-continent collision (from Brueckner and Van Roermund (2004; modified after Chemanda et al (1996), Maruyama et al (1996), Matte (1998) and Brueckner (1998)). (a) Subduction of continental crust into the mantle where it endured HP/UHP conditions and was invaded by peridotite fragments from the mantle. (b) Its subsequent eduction out of the mantle. I.e. at the surface defines a (U)HP metamorphic terrane

Minimum P-T conditions for the Jämtland eclogites are 14-18 kbar and 550°- 780°C (Van Roermund, 1985). Suggesting shallower depths (<60 km) than for the Norbotten terrane (Brueckner and Van Roermund, 2004). The HP nappes in Jämtland are internally extremely deformed with abundant refolded isoclinal folds, sheath folds and mylonites (Van Roermund and Bakker, 1984). The terrane is relatively thin compared to the length of it, so extreme thinning perpendicular to the bounding detachment surfaces is suggested.

Based on detailed geochronology of the (U)HP terranes in the Scandinavian Caledoniden, three orogenic events have been illustrated in the model of Brueckner and Van Roermund (Figs. 11 and 12). Figure 11a illustrates the starting situation at the onset of the closure of the Iapetus Ocean with Laurentia in the west and Baltica in the east. Secondly, the model explains the position of fossil subduction zones in the nappe pile, which no other model has done yet. i.e. (U)HP belts (of different

age) indicate simply where subduction zones were positioned in the closing Iapetus Ocean. Figure 11a illustrates the main terranes and intercorrelated oceanic terranes including the basement, middle and lower Allochthons presented on A, the Seve Nappes presented partly on A and the rest on B, C and partly on D, the Köli Nappes on E and partly on D and F. The uppermost Allochthon is presented by G and partly with F. The Finnmarkian orogeny illustrated in figure 12B has occurred approximately 500 Ma. They assume the subduction of a microcontinent beneath the Virisen volcanic arc together with eclogite facies metamorphism and the introduction of subduction zone garnet peridotite of suboceanic affinity from the overlying mantle wedge. This resulted in the so called Virisen/Norbotten composite terrane (VNCT; Fig 11b). Dunk tectonics is basically a reconstruction of plate tectonic evolution based on the location of the (U)HP metamorphic terranes indicating the nappe pile.

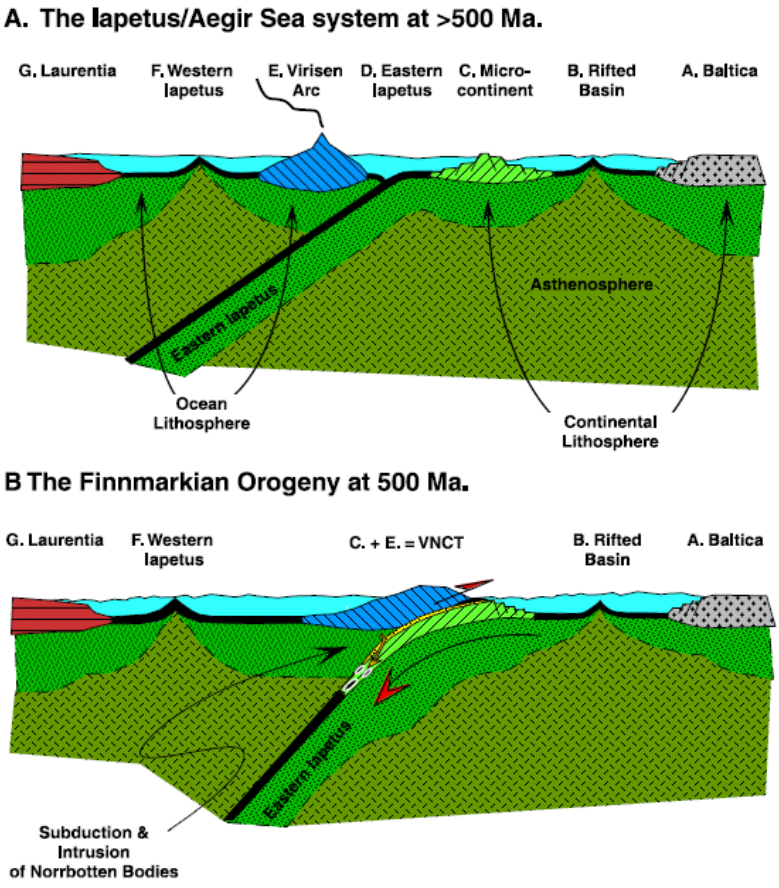

Figure 11: Subduction/eduction model from Brueckner and Van Roermund (2004) illustrating closure of the Iapetus Ocean followed by final continental collision. (a) Original configuration. (b) The Finnmarkian Orogeny (c) The Jämtlandian orogeny (d) exhumation of Jämtlandian. Note that Iapetus Ocean = Western Iapetus + Eastern Iapetus + rifted basins. (To be continued…)

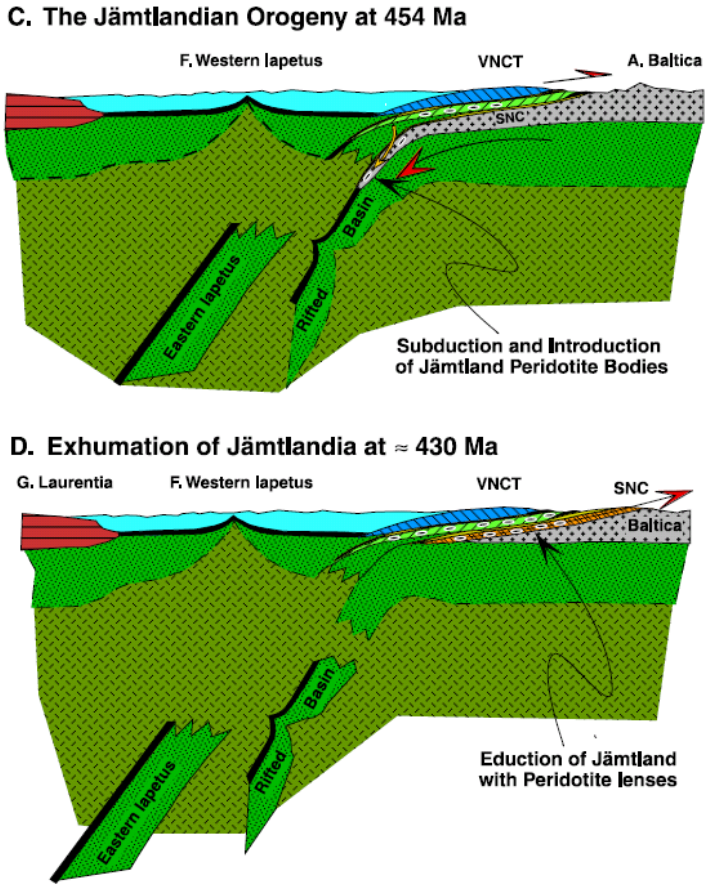

Figure 11: (…continued)

Rapid eduction of HP rocks lead to composite terrane accretion, including ophiolites and intrusive emplacement up to 455 Ma. The Finnmarkian orogeny subduction of oceanic crust (Eastern Iapetus) was followed by continental crust (Fig. 12a); this occurred until the western end of Baltica collided with VNCT what gave rise to the Jämtlandian orogen (~450 Ma, fig.11c). Again, rapid exhumation followed after slab break-off of the oceanic plate (Figs. 11c and d).

At the end of the Jämtlandian a major ocean called Western Iapetus, was still present along the western edge of VNCT. The closure of this ocean resulted in final collision between Baltica and Laurentia: the Scandian Orogeny (Fig. 12).

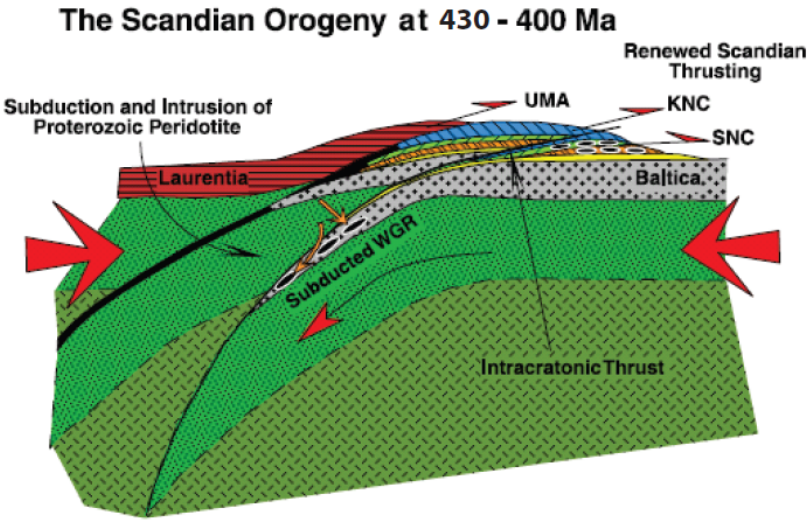

Figure 12: Subduction/eduction model for HP/UHP metamorphism during the collision between Laurentia and Baltica at the Scandian Orogeny at 425-400 Ma. (U)HP metamorphism as a result of intracratonic subduction during Scandian compression. Note that some previously formed (U)HP terranes could have been re-subducted into the mantle. (Brueckner and Van Roermund, 2004).

The model of Brueckner and Van Roermund (2004) explains (U)HP metamorphism, their ages and their exhumation, i.e. the geochronological characteristics of the different nappes.

4.3. Hacker and Gans (2005)

Hacker and Gans (2005) present a geodynamic model that can explain continental collision together with the creation of a single UHP terrane, as well as the petrology and thermochronology of nappes in the central Scandinavian Caledonides. They state that UHP metamorphism occurred in the late stages of continental collision, after the earlier stages of ophiolite emplacement and passive margin subduction. Nappe formation and nappe stacking however started at a much earlier stage ~480 Ma (Fig. 13a). The mechanism of the shortening (basically overthrusting without shortening in the mantle) is not explained here since there is no subduction illustrated in the early stages of their cartoons (Fig. 13). Therefore, the model of Hacker and Gans (2005) cannot explain Finnmarkian and Jämtlandian eclogite ages within the Scandinavian Caledonides.

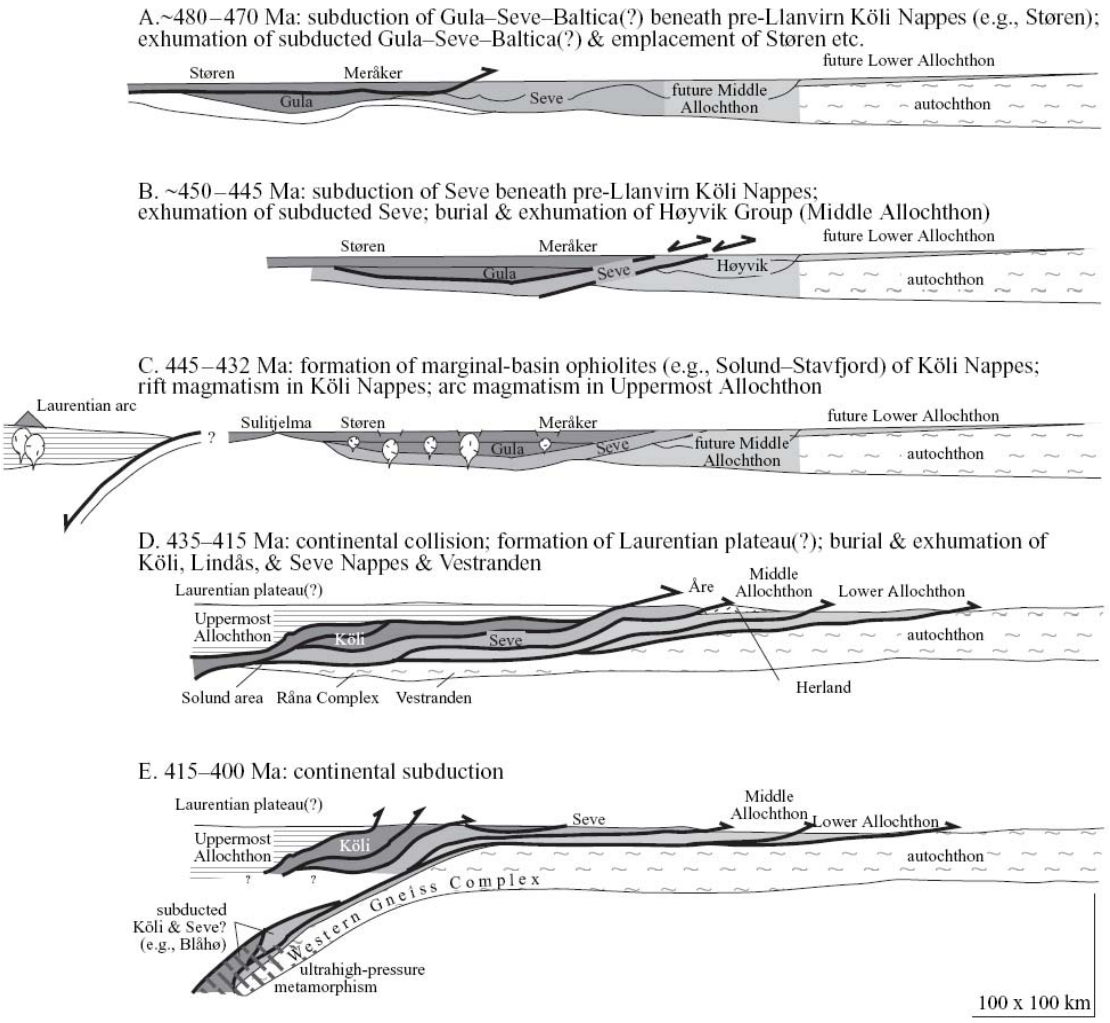

Figure 13: Evolutions of the Iapetus domain after Hacker and Gans (2005). (a) Subduction of the Gula Nappe – Seve Nappes – Baltica. In addition, exhumation of the subducted Gula-Seve-Baltica rocks as well as emplacement of the pre-Llanvirn portions of the Köli Nappes onto the Baltoscandian continental margin. (b) Subduction of the Seve Nappes beneath those parts of the Köli Nappes and exhumation of the Seve Nappes. (c) Formation of marginal-basin ophiolites of the Köli Nappes, rift magmatism in the Köli Nappes and arc magmatism in the Uppermost Allochthon. (d) Collision of the active margin of Laurentia, emplacement of the newly created arcs, marginal basins, and their basement onto the Seve Nappes, and telescoping of all structurally lower units. (e) Subduction of Baltica to ultrahigh-pressure depths.

Figure 13a represents an orogenic event called the Trondheim event (~480-470 Ma) with subduction (not clearly visible in their cartoon) of Gula-Seve-Baltica beneath the pre-Llanvirm Köli Nappes together with exhumation. Since there is no real subduction illustrated in their model the shortening of the crust but not the underlying mantle would be a big (space) problem in this model. Figure 13b illustrates an event called the Jämtlandian Orogeny at ca. 450-445 Ma, interpreted to be the orogenic successor of the Trondheim event. Subduction of the Seve Nappes beneath the pre-Llanvirn Köli Nappes coincided with reactivation of normal faults caused by rapid exhumation along these faults. Together these features indicate westward 'subduction' of the Seve Nappes beneath, perhaps the Köli Nappes, followed by thickening and heating. However the evidence for these assumptions is lacking.

The third event was an extensive magmatic episode at 445-432 Ma and includes the formation of new oceanic crust and intrusion of plutons and dikes throughout the Uppermost Allochthon and Köli Nappes (Fig. 13c). Figures 13d and 13e represent tectonic episodes that are directly related to (U)HP metamorphism in the Western Gneiss Region (WGR). It consists of continental collision which formed the Laurentian Plateau which coincided with the burial and exhumation of the Koli and Seve Nappes (435-415 Ma) it ended with continental subduction at 415-400 Ma.

The nappes prograde eastward which is permitted by diverse data that span the western to eastern edges of the Caledoniden Orogen. It began in the west with the emplacement of the Köli Nappes onto the Seve Nappes and the emplacement of the Uppermost Allochthon (part of Laurentia) onto the Köli-Seve-Baltica amalgam. They state that the combined uppermost Allochthon-Upper Allochthon-Middle Allochthon-Lower Allochthon stack subsequently reached its easternmost thermal influence on the Baltica margin around 420 Ma. The problem here is the UHP metamorphism occurred approximately 10 Myr later. The reason for this offset could be that the continental crust becomes denser than the mantle and sinks under its own weight to UHP depths. A second thought is that the continental crust is attached to the sinking oceanic lithosphere. A third option is that the continental crust is overlain by denser, sinking rocks which can push in fact the plate into the UHP terrain. Another solution could be the attachment of continental crust with a continental lithosphere.

The model of Hacker and Gans (2005) is technically an extract of Gee (1975) i.e. it adds only one single subduction zone. This assumption suggests that all (U)HP rocks in Scandinavia should have the same age which is a big problem. Another problem with this model is the thickness of the nappes. They are moved over each other without breaking. This is the same mechanical problem as in Gee's geodynamic model (1985). What is also lacking in the model of Hacker and Gans (2005) is explanation of the driving force of these plates.

4.4. Roberts (2002)

Roberts (2002) describes several aspects of the Scandinavian Caledonides. The most applicable here are the event chronology, palaeogeographic settings and likely modern analogues. Between the Late Cambrium and the Early Devonian, four major compressive/transpressive events occurred. Starting with the Finnmarkian (Late Cambrium, 542-510 Ma), then Trondheim (Early Arenig, 479-468 Ma), the Taconian (Mid-Late Ordovician, 472-444 Ma) and finally the Scandian (Early Devonian, 428-398 Ma) (Roberts, 2002). So far this is basically similar to Brueckner and Van Roermund (2004) although the Trondheim event is a bit earlier. Roberts (2002) state that Iapetus arcs and possibly adjacent microcontinents contracting/accreting along the margin of Baltica causing subduction scenarios that are responsible for the first two events. The Taconian event occurred along the margins of Laurentia,

but is again a tectonothermal event, caused by arc-accretion. The latest event (Scandian) during the Early Devonian (428-398 Ma) is describing the rapid subduction followed by rapid eduction of the Baltican margin beneath Laurentia. A possible fifth phase is the Solundian phase (380-360 Ma). This episode was occupied with orogenic collapse, widespread extension and Devonian basinal sedimentation with local upright folding. This is incorporated by others in their Scandian exhumation phase.

Tectonic events

The Finnmarkian event is the result from the collision of the Baltoscandian margin with an inferred magmatic arc, above the seaward-facing subduction zone. Figure 14 is a schematic overview of the Finnmarkian event (520-500 Ma). Here the eclogite-facies metamorphism has been reached during subduction of the continental margin/ocean transition zone. After subduction, rapid exhumation and emplacement of the Finnmarkian Nappes onto the Baltoscandian margin occurred.

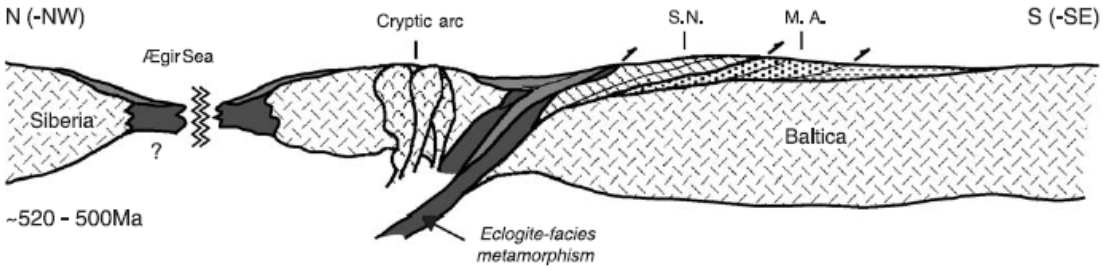

Figure 14: Schematic composite profile illustrating the Finnmarkian accretionary event in Late Cambrium time (~520-500 Ma). S.N. = Seve Nappe, M.A. Middle Allochthon (Roberts, 2002). Note: Siberia is indicated in the N (-NW).

The Trondheim event is characterized by deformation and metamorphism, including ophiolite obduction and blueschist metamorphic parageneses. Some plagiogranite dykes have been dated between 493-482 Ma with U-Pb zircon aging (Dunning, 1987). Figure 15 illustrates a schematic, composite profile of the Trondheim event.

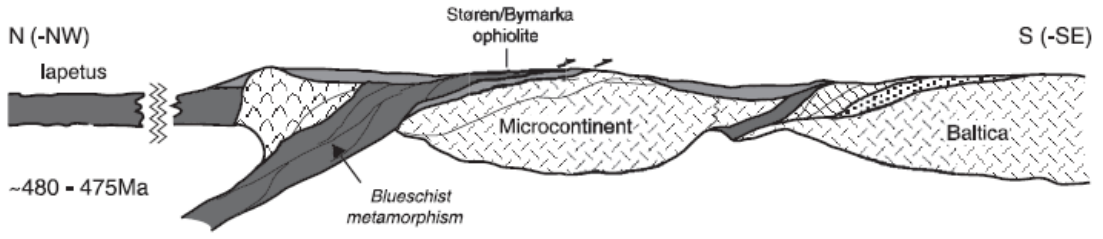

Figure 15: Schematic, composite profile illustrating the Trondheim event, in latest Tremadoc to Early Arenig time (~480– 475 Ma). After Roberts (2002). Again, oceanward subduction is inferred, down to at least blueschist-forming depths (Eide and Lardeaux, 2002).

The Taconian event (~470-450 Ma) describes subduction and accretion along the continental margin of Laurentia. Parts of these Laurentian shelf and peri-Laurentian arc complex terranes were later detached and retransported onto the nappes (Fig. 16). Proof for this event can be found in the

Uppermost Allochthon and in the most outboard Köli terranes (Roberts, 2002). Observed from these cartoons is the change in plates participating in the NW (first Siberia then Laurentia). This rotation of Baltica along his own axis is described by the model of Torsvik (Torsvik et al., 2005). His theory is under heavy attach.

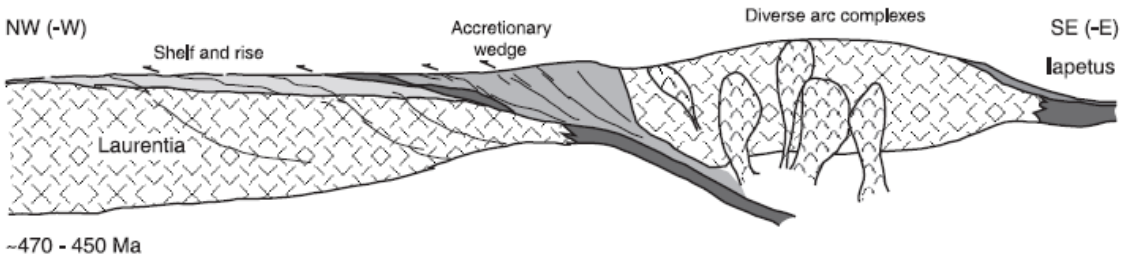

Figure 16: Schematic, composite profile showing the palaeotectonic situation during the Taconian event, in Mid to Late Ordovician time (~470– 450 Ma). After Roberts (2002). Subduction and accretion, including eclogite generation and ophiolite obduction, occurred along the continental margin of Laurentia. Note: Laurentia is indicated in the NW (-W)

The Scandian event caused an oblique collision between the plates Baltica and Laurentia (Terry et al., 2000). Here the Baltoscandian margin subducted underneath Laurentia. Terry et al., (2000) stated that this event was a very quick one. The duration was possibly less than 10 Myr, proven by monazite geochronology from UHP rocks in the Western Gneiss Region. All the Allochthons are affected by this event. In figure 17 can be seen that the Uppermost Allochthon is detached from Laurentia and transported upon the Iapetan terranes of the Upper Allochthon, above the Baltoscandian margin. The Scandian event caused major nappe emplacement, crustal overthickening and gradual imposition of an extensional and sinistral shear regime. It describes subduction of the Baltican margin and overlying volcanic assemblages and earlier nappes beneath the Laurentian plate. Rapid exhumation and ongoing thrusting caused emplacement of numerous thrust sheets onto Baltica and party above earlier nappes (Roberts, 2002; Fig. 17)

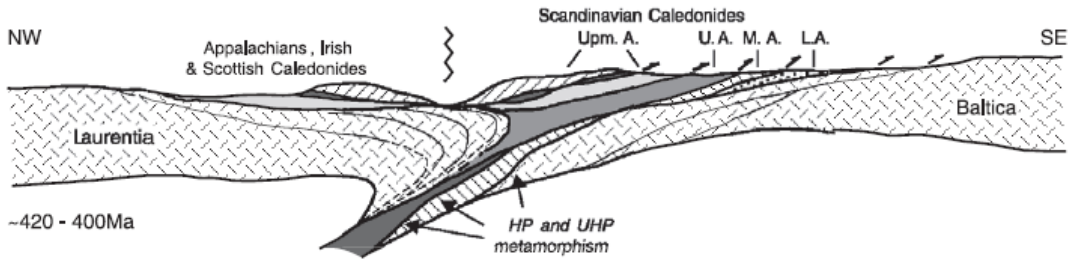

Figure 17: Schematic, composite profile illustrating the major Scandian, Baltica– Laurentia collisional event, in Mid Silurian to Early Devonian time (~420–400 Ma). After Roberts (2002). L.A., M.A., U.A. and Upm.A.—Lower, Middle, Upper and Uppermost Allochthons, respectively.

Late- to post-Scandian (Solundian) orogenic collapse of the Caledonides can be described by gravitational collapse under its own weight which caused late-stage extensional deformation

(Andersen, 1998). The Solundian involved low-angle, ductile detachments related to extensional shear (W to SW) and Early to Mid Devonian basinal sedimentation.

5. Monazites

Since the main part of this thesis is focussed on EMP monazite dating, this chapter will give a short introduction to monazites. Starting what they are and under what conditions monazite forms, what its crystal structure and chemistry is and what kind of chemical zoning do I find in them.

5.1. What are monazites and under what conditions do they form

The mineral monazite is present in several types of rocks like igneous, metamorphic and sedimentary rocks. Metamorphic monazites form at temperatures above 680 °C (Williams et al., 2007). This is the case for all rocks of the Central Belt of the SNC in N. Jämtland and S. Västerbotten, Central Sweden.
Monazite has become a powerful tool to determine the age of a metamorphic event the rocks endured. Monazite is a geochronometer that can preserve crystallization ages of the host rock through a long geological period of time (Williams et al., 2007). Monazite is a light rare earth element-bearing phosphate, (LREE)PO_4. The most import elements for the age determination are Uranium, Thorium and Lead. These radioactive elements are ^{238}U, ^{235}U and ^{232}Th which have small diffusion rates so they can retain the geological history (decay constant per 1 Ma of respectively: $1{,}55125 * 10^{-4}$, $9{,}8585 * 10^{-4}$ and $4{,}9475 * 10^{-5}$). The assumption that has been made is that there is no lead (Pb^{204}) present in the crystal structure after the formation of the monazite, i.e. al of the Pb (^{207}Pb and ^{206}Pb) is radiogenetic. So all the lead in the monazite is radioactive decay of Uranium and Thorium. Thereby, another assumption is made that all the Pb that has been formed, has to be preserved i.e. that there is no loss of the Pb to other minerals. In fact, under the particular circumstances it may record multiple recrystallization stages. This is possible if the second time the monazite endures intense metamorphism, new monazite will grow onto the existing monazite with (radioactive) elements that are set to the starting values. The pre-existing monazite may be undeformed and remains the timer that was set after the first metamorphic deformation. Gardes et al., (2006) state that the closure temperature at which solid-state diffusion of elements in the crystallographic lattice effectively ceases to be statistically

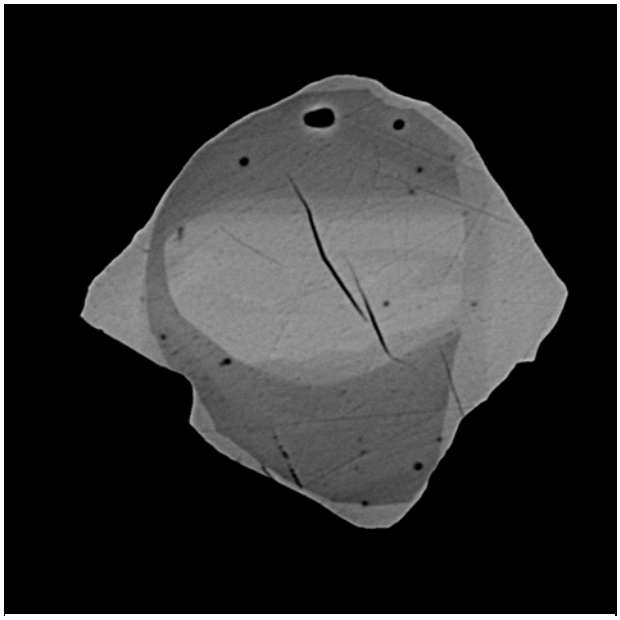

Figure 18: illustration of zoning in a sampled monazite from the Marsfjällen area, SNC. This monazite has a horizontal diameter of approximately 180 µm.

meaningful at the resolution of an analytical technique is reached at 800°C. However, the monazite system can apparently be fully or partially reset due to dissolution/precipitation or recrystallization processes at temperatures below 800°C (Williams et al., 2007). This might be the case with zoning. Zoning can be visualized under the microprobe revealing grey-level contrast within the monazite (Fig. 18).

A refinement of the technique together with an increase in the understanding of the formation conditions of monazites had led to significant increase of the use of monazites for geochronology over the past 15 years.

5.2. Crystal structure and chemistry

Monazite has a framework of nine-oxygen coordinated polyhedra and distorted PO_4 tetrahedra (Fig. 19a; Williams et al., 2007). It is a solid solution with the general formula $(LREE)PO_4$, where the LREE portion mainly consists of Ce, Nd and La. Most of the solid solutions are a mixture of monazite-(Ce), $(Ce,Nd,La)PO_4$ and two related minerals brabantite ($CaTh(PO_4)_2$) and huttonite ($ThSiO_4$)(Fig. 19b).

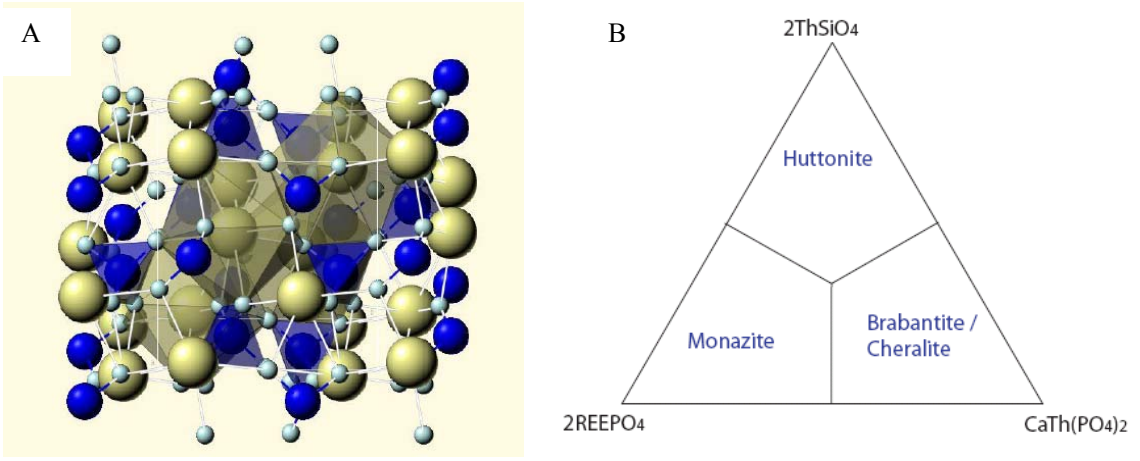

Figure 19: (a) Monazite structure. Blue spheres are P-atoms, yellow spheres are LREE-atoms and green spheres are O-atoms. The framework is made out of PO_4 tetrahedra with yellow 9-fold coordinated sites in between (webmineral.com). (b) Endmember diagram for the system monazite ($2REEPO_4$)-Brabantite/Cheralite ($CaTh(PO_4)_2$- Huttonite ($2ThSiO_4$) (modified after Linthout 2007).

The 4-fold coordinated sites are usually occupied by P^{5+}, but substitution by Si^{4+} is possible. Larger cations like Calcium, Thorium and Uranium can be captured in the 9-fold coordinated sites. This can be realized with the most common substitution:

$$2\ REE^{3+} \leftrightarrow Ca^{2+} + Th^{4+}$$

Another (coupled) substitution is:

$$P^{5+} + REE^{3+} \leftrightarrow Si^{4+} + Th^{4+}$$

The first reaction shifts the monazite to the brabantite end-member by incorporating additional Calcium and Thorium in the crystal lattice of monazite. The second reaction results in a shift towards the huttonite endmember, by substituting Thorium for a REE at the 9-fold coordinated site and silicon for phosphorus at the 4-fold coordinated site (Poitrasson et al., 1996).

Within the monazite, radioactive decay takes place of certain elements. ^{232}Th together with ^{238}U and ^{235}U will produce Lead (^{207}Pb and ^{206}Pb). The increase of total lead in the mineral is a function of monazite age and the original concentrations of Th and U (Williams et al., 2007). As said before, monazite can record multiple recrystallization stages or it can reset the formal recrystallization phase. Ayers et al., (1999) describes this process. They describe growth in an open system of individual monazite grains to larger grains, a process of finding the most energetically favourable position at a grain boundary. A growing monazite grain tries to keep up with a moving grain boundary, which requires recrystallization through dissolution and reprecipitation. This resets the geochronometer. In a closed system, the minimization surface energy is the driving force to determine whether the monazite tends to shrink or grow. During growth the same dissolution and precipitation process is happening which will reset the U-Th-Pb system (Ayers et al., 1999).

5.3. Types of zoning

Zoning is the result of (partly) dissolution of the monazite lattice (whether or not) enhanced by the presence of hydrothermal fluids. These fluids cause breakdown of the structure and enhance the formation of other related phases like apatite (Fig. 20). The formula of four most common apatite endmembers is $Ca_{10}(PO_4)_6(OH,F,Cl,Br)_2$. Apatite can be formed through incorporation of large amounts of Ca in the lattice structure. The REE are incorporated into other minerals that can be formed. For instance Allanite (from the epidote group) with a structural formula $Ca(Ce,La,Y,Ca,REE)Al_2(Fe^{2+},Fe^{3+})(SiO_4)(Si_2O_7)O(OH)$ and can be formed through complete

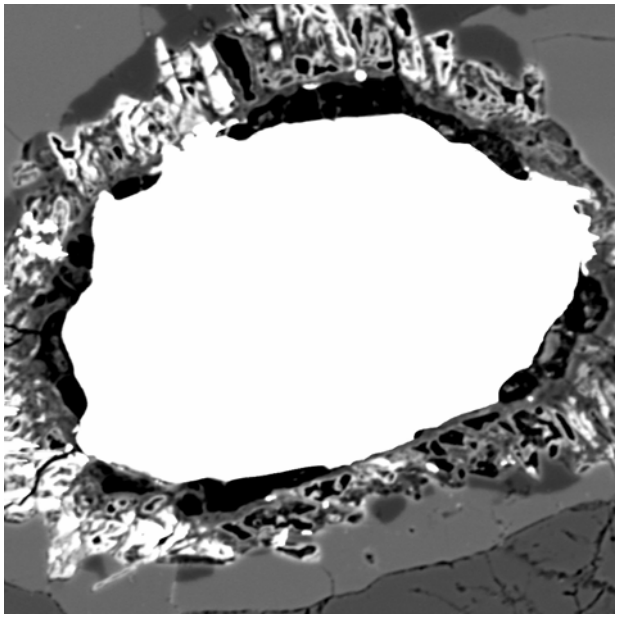

Figure 20: BSE image of a monazite breaking up into apetite. Horizontal diameter of the monazite is ~100 µm.

dissolution of the monazite (Ayers et al., 1999).

Formation of metamorphic monazite under lower amphibolite facies conditions, often involves breakdown of allanite. Secondary monazite seams grow around apatite or monazite rims nucleate along apatite grain boundaries (Krenn and Fringer, 2007). However, metamorphic monazite might also form through direct recrystallisation of an older monazite. This process is more common at higher metamorphic conditions as upper-amphibolite and granulite facies (McFarlane et al., 2005).

Zoning is often related to their growth history. Growth zoning is mainly defined by variations in Thorium content between the zones, resulting from substitution of the huttonite- and brabantite endmembers of monazite (Ayers et al., 1999). Several variations of zoning are described and illustrated below.

- Concentrical zoning: reflecting the composition of the melt and the equilibrium composition of the crystallizing monazite (Williams et al., 2007). Representing igneous growth of the monazite (Ayers et al., 1999; Fig. 18).
- Sector zoning: element preferentially crystallize onto one crystal face rather than another (Fig.21a; Williams et al., 2007).
- Veining: alteration of the composition along (former) cracks (Fig. 21b). This may be caused by hydrothermal alteration of monazite (Poitrasson et al., 1996).
- Patchy zoning: the result of in situ hydrothermal alteration of pre-existing monazite (Ayers et al., 1999) (Fig. 22).
- Intergrowth type of zoning (Zhu and O'nions, 1999). Formation during primary monazite growth by the intergrowth of two different monazite crystals with contrasting Thorium contents (Fig. 23).

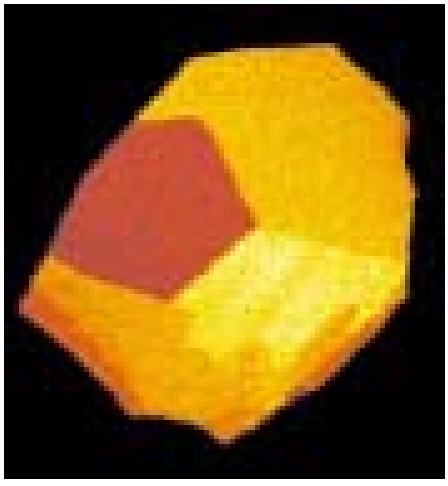

Figure 21a: X-ray image of sector zoning (Williams et al., 2007).

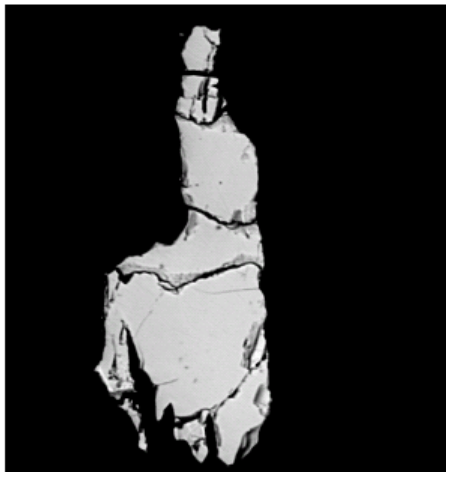

Figure 21b: BSE image of Veining. Length monazite ~100 µm

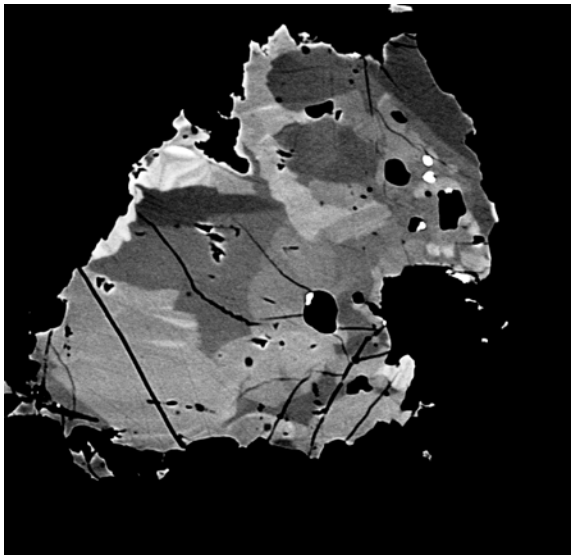

Figure 22: BSE image of Patchy zoning. Diagonal length of ~220 µm.

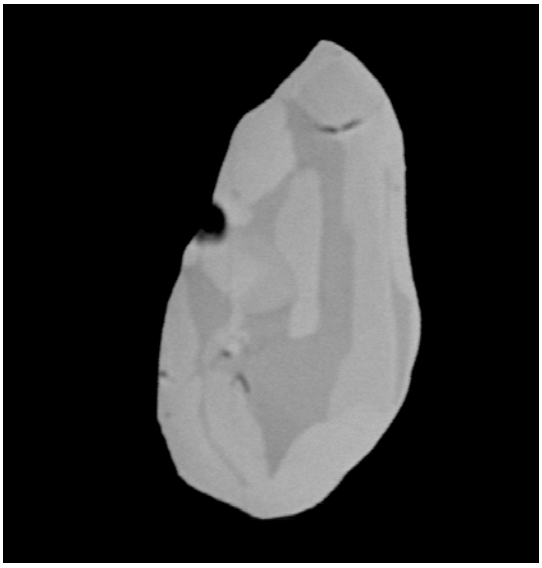

Figure 23: BSE image of the intergrowth type of zoning. Length monazite ~100 µm

6. Results

6.1. Field Observations

Figure 24: Photographs made in the fieldwork area. (a) Northern part of the fieldwork area. From left to right: MSc student Michiel Gademan, Dr. Herman L.M. Van Roermund, MSc student Matthijs Hogerwerf (author of this MSc thesis). (b) Mountain Kittelfjäll consisting of kyanite-K-feldspar rocks. (c) Outcrop of kyanite-K-feldspar rocks near Kittelfjäll. (d-e) Outcrop of kyanite-K-feldspar rocks near Marsliden. (f) HP rocks near Jarpetjäkke (southern part of the fieldwork area).

Figure 24 shows a selection of photographs made in the fieldwork area. Figures 24a-e are taken in the northern part, where kyanite-K-feldspar rocks were sampled. Figure 23f is taken in the southern part, where the HP gneisses of the Avardo unit have been sampled. These photographs illustrate the situation and environmental circumstances to what the rocks are exposed. All rocks are heavily affected by physical and chemical weathering. Most of the physical weathering these rocks endured is caused by freezing and thawing and intense polishing by formal ice caps. Therefore, good exposures of the representative rocks can be found mostly on the top of the mountains. In addition, some large peridotite bodies are found within these rocks (see figure 25a). Other features visible are boudinage (Fig. 25b) and folds on centimetre scale (Fig. 25c).

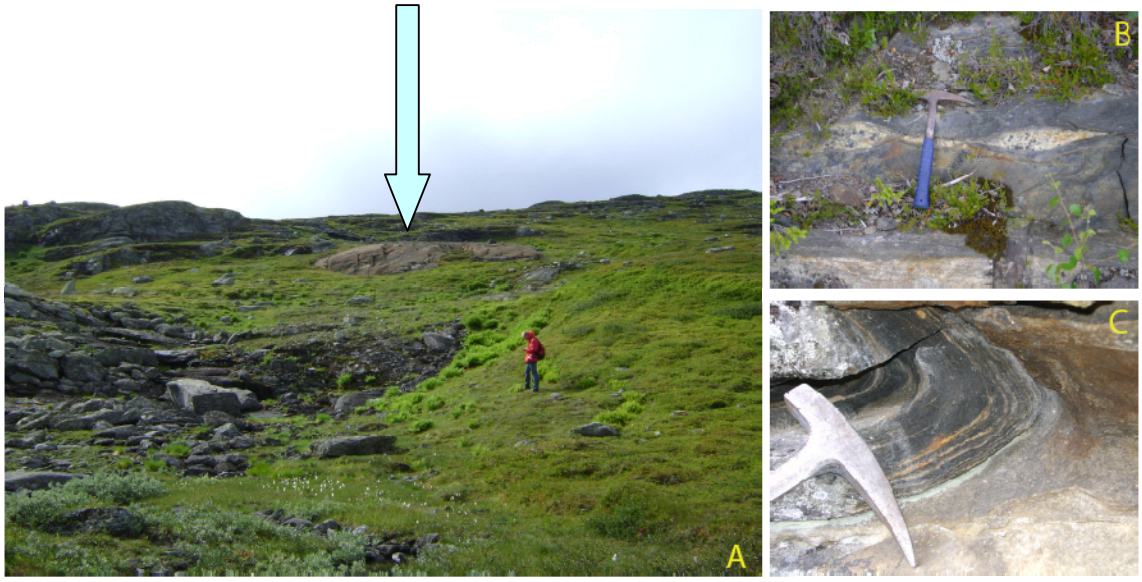

Figure 25: (a) Illustration of a peridotite body near Jarpetjäkke (southern part of the fieldwork area). Body indicated with arrow. (b) Illustration of boudinage in gneisses in the northern part of the fieldwork area. (c) Illustration of folding on centimeter scale in gneisses in the northern part of the fieldwork area.

Figure 26a is showing an equal area plot of all foliation orientations measured from the sampled rocks of the northern part of the fieldwork area. These (n=20) kyanite-k-feldspar rocks have a dominant dip to the west with an average angle of 30^{o}. The average strike is approximately 21^{0} (021/30W)

The southern part of the fieldwork area, where the Avardo gneiss and Sjouten unit are sampled, are showing a less straight forward equal area plot (Fig. 26b). The dominant dip is to the west with an average angle of 24^{o}. The average strike of rocks that are dipping to the west is 48^{o} (048/24W). The average strike of rocks that are dipping to the east is approximately 87^{o} with an average dip of 26^{o} (087/26E). Overall, these rocks are subhorizontal with a dipping direction to the west.

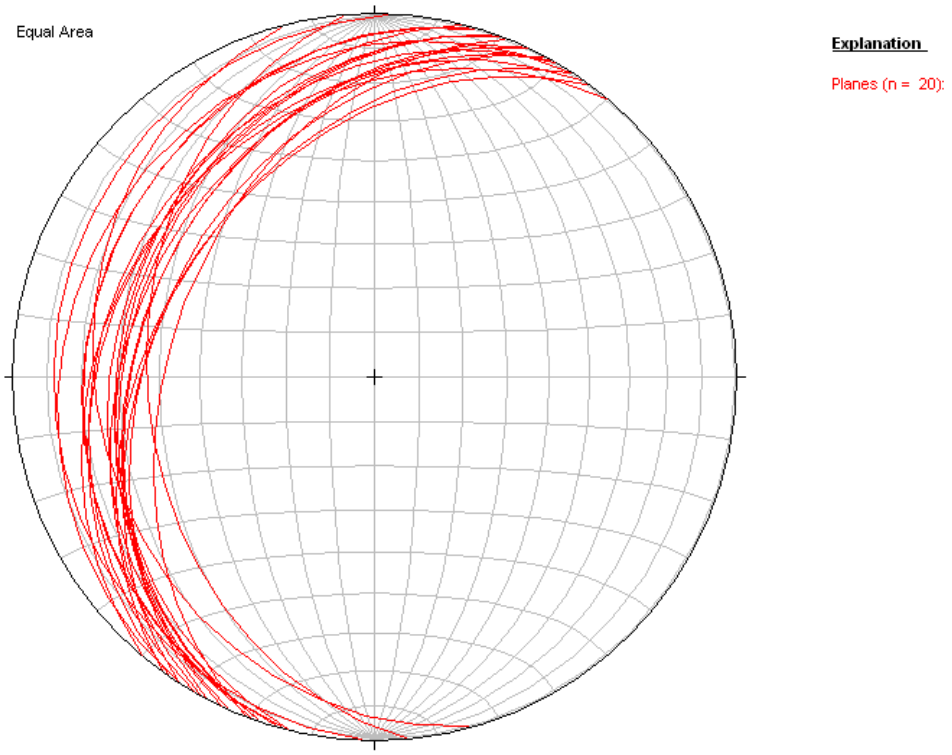

Figure 26a: Equal area plot of strike and dip measurements of the kyanite-k-feldspar rocks in the northern part of the fieldwork area in a lower hemisphere projection (software from http://gcmd.nasa.gov/records/StereoNet.html). The average strike dip is 021/30W.

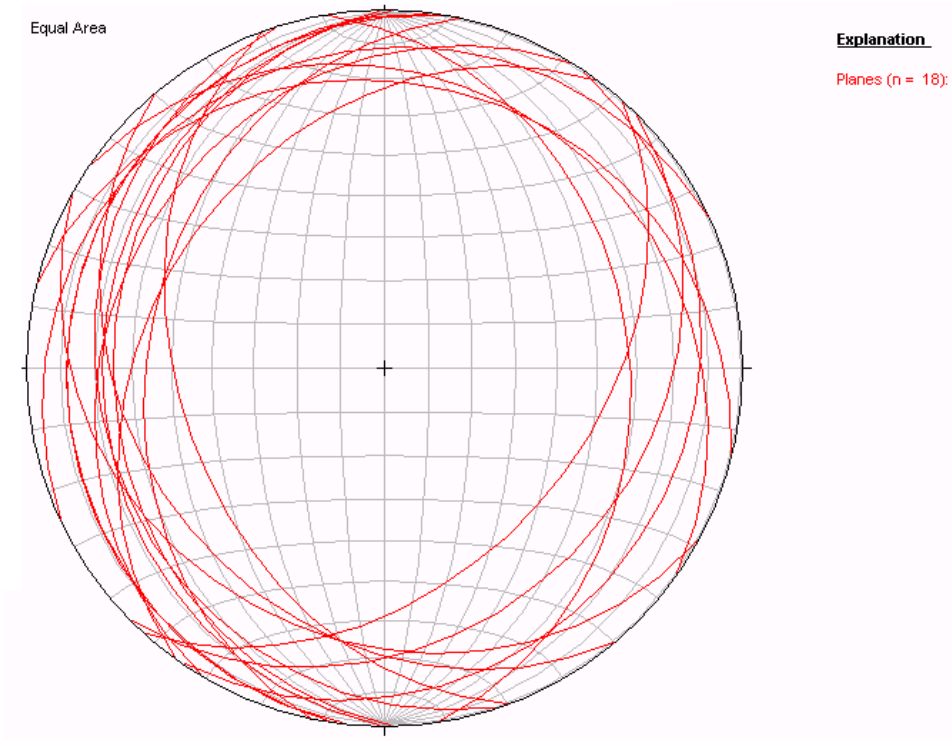

Figure 26b: Equal area plot of strike and dip measurements of the HP rocks in the southern part of the fieldwork area in a lower hemisphere projection (software from http://gcmd.nasa.gov/records/StereoNet.html). Average strike dip is 048/24W and 087/26E.

6.2. Microstructure and Mineral assemblage

The microstructure of rocks is an illustrative tool that reflects the structural metamorphic conditions it endured and sometimes even chronologically if there are multiple stages of metamorphism/deformation. All thin sections made of the Marsfjället and HP gneisses are shown in appendix 11.3.1-11.3.26 (Marsfjället gneiss) and 11.4.1-11.4.27 (Avardo and Sjouten). All thin sections are investigated under the optical microscope as well as with the EMP (BSE imaging). The Marsfjället and HP gneisses are very similar in their mineral assemblage (Fig. 27). The dominant minerals that are found in the thin section of the Marsfjället and HP rocks are quartz, garnet, k-feldspar, kyanite, biotite, muscovite and plagioclase. Garnets found in the thin sections are relative small if they are present in the mylonite bands (Fig. 27c); however garnets can be relatively big when they are present outside deformed bands (Fig. 27d-g). There is less biotite and muscovite in the Marsfjället gneiss and more plagioclase, K-feldspar and kyanite than in the HP gneiss. In both gneisses garnets are found, varying in size from several tens of microns to several millimeters (Fig. 27). Biotite is mostly present in mylonite zones. Within these mylonite zones biotite shows elongated minerals up to the size of a few hundreds of microns. Muscovite is comparable with the biotite, but it seems that there is another type of muscovite in the rocks that is relatively undeformed (Appendix 11.4.13). These muscovites are clearly overprinting the surrounding minerals. Most of the time plagioclase and k-feldspar are relatively undeformed and may be up to multiple hundreds of micros in size (Appendix 11.3.15 and 11.3.19). Kyanite is somewhat smaller than plagioclase and k-feldspar, but is also not strongly deformed and sometimes even intact (Appendix 11.3.26). These large kyanite crystals are only found in the Marsfjället gneiss. The most dominant mineral found in both gneisses is quartz. Quartz is present as very large minerals (up to millimeter scale) (Appendix 11.3.7) but also as very small grains in mylonite bands. In smaller proportions and sizes (< 5 vol %), rutile (TiO_2), hematite (Fe_2O_3), magnetite (Fe_3O_4), apatite ($Ca_{10}(PO_4)_6(OH,F,Cl,Br)_2$) and monazite ($(LREE)PO_4$) are present. The monazite grains found within the HP unit are slightly smaller than the monazite grains found with the Marsfjället gneiss.

Almost all gneisses contain mylonite bands indicative for dynamic recrystallization (Figs. 27a-c, h-i). What can be observed here is that mylonite bands consists of biotite, two feldspars and quartz. These elongated mylonite bands have a dominant direction over the whole thin section. All garnets however are showing intense deformation (Fig. 27f)

Another important feature that can be observed is the deformation lamellae in the plagioclase. The plagioclase forms at high PT conditions and during cooling plagioclase tends to break down. Another observed effect of the deformation is twinning. The kyanite has lined up inclusions of for instance

quartz what might indicate a second generation of growth of minerals. In figure 27b muscovite is lined up within the mylonite zone, while other thin sections are showing more intact muscovites. The same elongated structure is observed in these minerals and might be overprinting an older foliation as can be seen in figure 27h. Images 27h and 27i are taken from the HP rocks in the southern part of the fieldwork area. These rocks are slightly more deformed but show the same mineral assemblage, with the same mylonite bands.

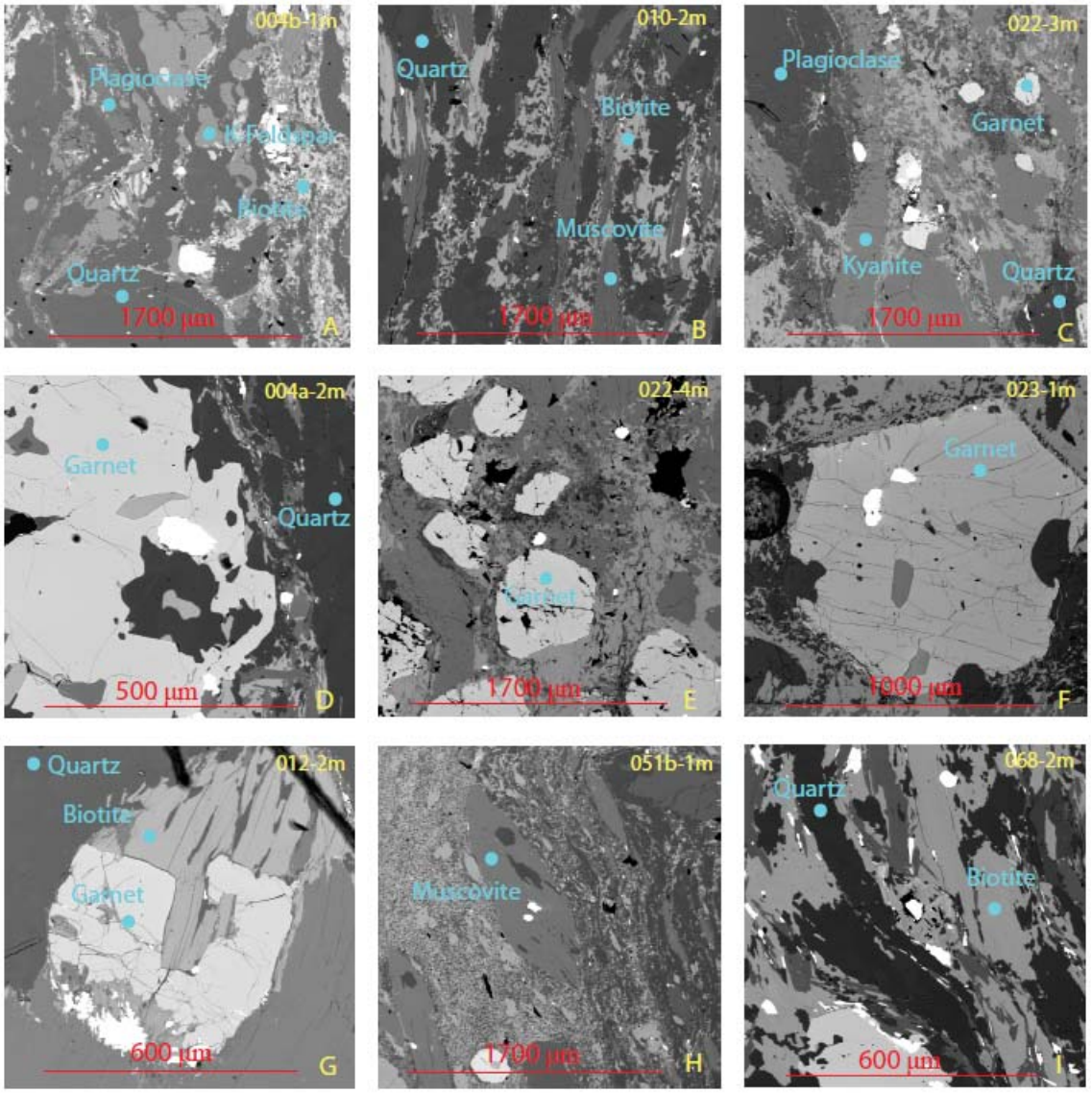

Figure 27: illustration of BSE images of several thin sections. (a-c) Images of gneisses from the northern part of the fieldwork area where elongated bands are present consisting dominantly of quartz, biotite and feldspars. (d-g) Images of garnets in thin sections taken from rocks of the northern part of the fieldwork area. (h-i) illustration of the microstructure of thin section from rocks of the southern part of the fieldwork area (HP rocks)

The monazites of the Marsfjällen gneiss that have been found and dated are present in kyanite, k-feldspar, plagioclase, garnet, biotite, muscovite, quartz or a combination of these minerals. This

indicates the close relationship between the growth of the monazite versus the metamorphic minerals/grade.

Monazites of the HP rocks are only found in biotite, muscovite, quartz or a combination of all the listed minerals in table 2 (except for kyanite). This has been summarized in table 2. What is not shown in this table are the monazites that have been found that are not dated. Some of these monazites have been fully situated within a garnet (sample 052d), but have never been dated since the monazite was too small or too deformed. Nevertheless this indicates again that there is a close relationship between the growth of the monazite versus the metamorphic minerals/grade.

	Kyanite	K-feldspar	Plagioclase	Garnet	Biotite	Muscovite	Quartz	Combination
Marsfjället	002-6	002-3 022-1 026-1	023-4	010-3 022-2	012-4 023-2	010-2 012-2	002-1 004b-1 027-1	004a-1 004a-2 004b-3 012-1 015-2 015-3 017-2 017-3 026-3 027-3
HP	-	-	-	-	052-4 064-3	051b-1 051b-4 052-1 068-4	052c-2	037d-1 052c-1 061-1 064-1 064-4 068-3

Table 2: The 'host' minerals of the dated monazites. BSE images of each sample number can be found in Appendix 11.3 and 11.4.

6.3. Monazite ages

Monazites have been identified and measured with the use of the EMP. The equipment has been calibrated with the use of a standard, which was a monazite with a known age of 1125 Ma. This monazite standard has been measured before, between and after each session of approximately five monazites. Incorrect outcoming ages are already filtered out. This filtering has been done by (1) checking the outcoming data for a total compound of approximately 100%, if not the measurement is wrong. (2) (Abrupt) significant differences in certain elements compared to the same element in other point measurements, and (3) checking afterwards with BSE imaging to look if the spots are on the right positions in the monazite and are not burned.

All results of the monazite age dating can be found in the digital Appendix added.

6.3.1 Standard

The result of measurements of the standard is shown in figure 28a, where the average age of 373 point measurements is 1132 Ma. The known age is 1125 Ma, so this outcome is less than 1% deviation (0.6%). This is a good indication of the initial calibration level of the microprobe. Calibration is accepted when the mean is 1125 +/- 10 Ma. In a bar-diagram, it can be seen that two distinctive peaks are visible at the age periods of 1115-1135 Ma and 1135-1155 Ma (Fig. 28b). Out of the diagram in Figure 28c, something can be said over the accuracy of the result of the point measurements in PbO vs. ThO_2*. R^2 and y are representing respectively the measure of goodness-of-fit of linear regression and steepness of the drawn red line which intersects with the origin. R^2 is 0,9997, which is perfect. T, T(0) and t are respectively representing: age according to the natural trendline (1132,7 Ma), age according to the trendline forced to go to 0,0 (1129,7 Ma) and the mean age (1132,7 Ma). These numbers are perfectly matching with each other.

The data points are approximately situated on the intersection line with the origin. This indicates that the primary assumption that there is no ^{204}Pb present in the crystals after growth of the monazite. This goes hand in hand with the assumption that Pb loss during the existence of the monazite can be neglected.

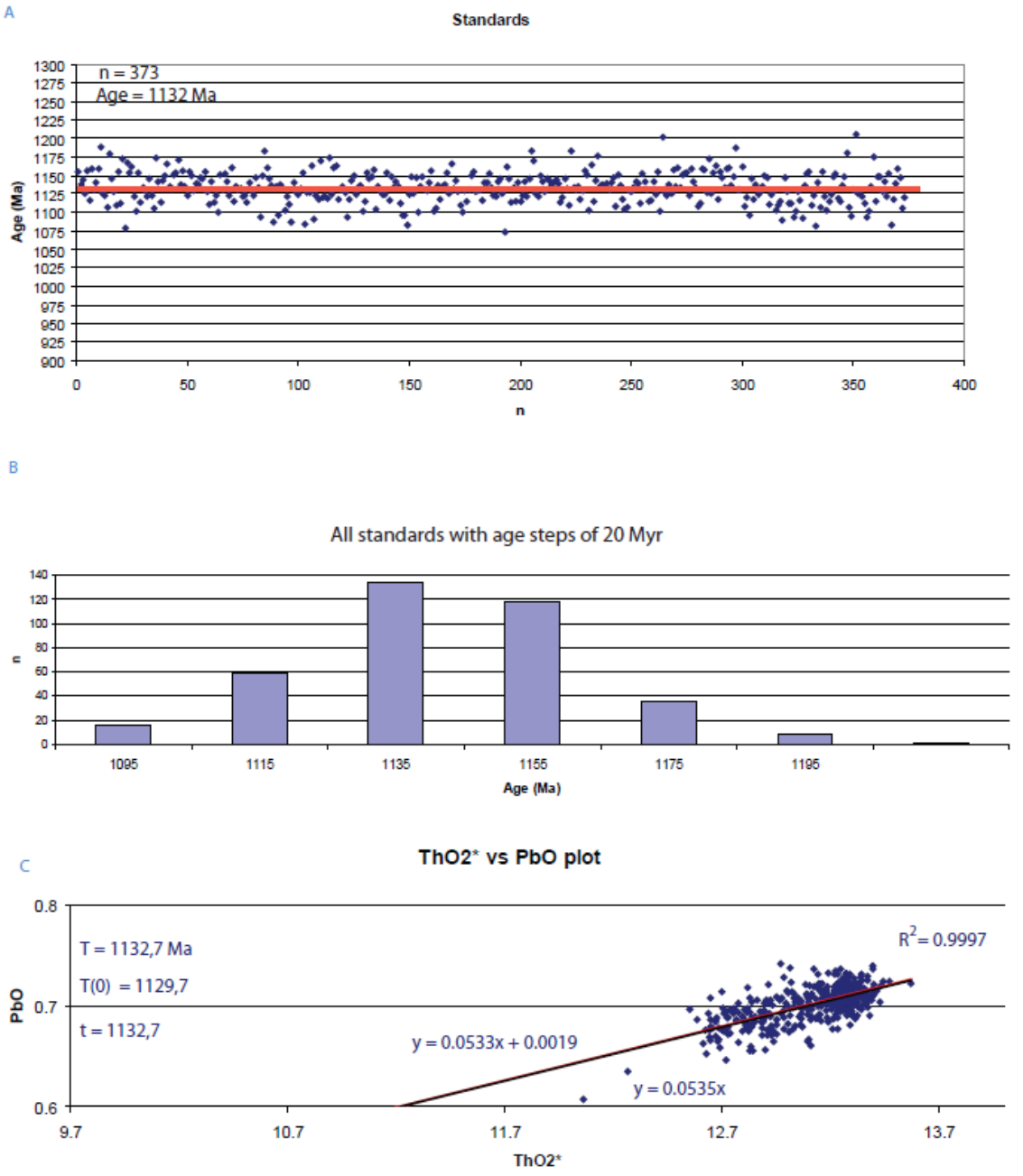

Figure 28: (a) Simultaneous EMP age-results of measurements on a monazite standard with known age (1125 Ma). The average age over 373 point measurements is 1132 Ma. (b) Bar-diagram of all 373 point measurements of the reference monazite. (c) The accuracy of the results can be checked by this ThO_2* versus PbO plot. R^2 of the drawn red line which intersects with the origin is 0,9997. T, T(0) and t are respectively 1132,7, 1129,7 and 1132,7 Ma.

6.3.2 Marsfjället Gneiss / Northern part

On the Marsfjället gneiss, in the Northern part of the fieldwork area (Figs. 2 and 6), 393 point measurements have been measured on 22 different monazites dispersed in 11 different rock samples. The average outcoming age is 502.8 Ma (Fig. 29a), with a range of 620-400 Ma (95% of the data points) or 460-540 (50% of the data points). In a bar plot with age intervals of 20 Myr the peak (n=56)

has an approximately corresponding age of 500-480 Ma (Fig. 29b). However, another peak of 55 point measurements has an age between 560-540 Ma. Nevertheless the bars between these peaks are at least based on >40 counts. Figure 29c illustrates the ThO_2^* versus PbO plot, where the red line is intersecting with the origin. Almost all the points are in line with the intersection line, which indicates that the data is accurate enough, since the assumption was that there was no PbO at the start of the formation of the monazites. R^2 is therefore quite high (0,9756). T, T(0) and t are respectively 505,0, 497,3 and 502,8 Ma. These numbers are again perfectly matching with each other. Therefore this data seems to represent only one deformation phase.

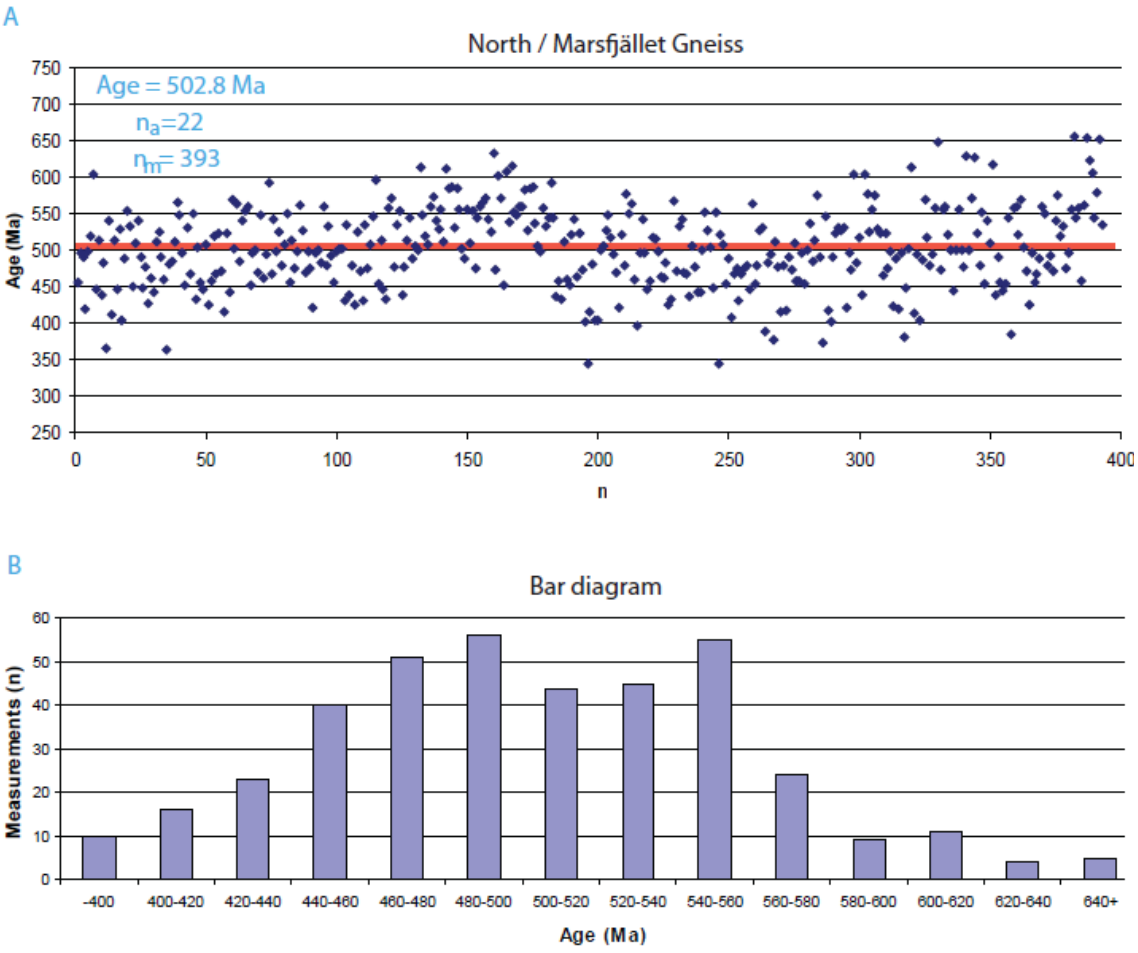

Figure 29: (a) The 393 point measurements are taken on the 22 different monazites within the samples of the northern part of the fieldwork area. The average age is 502.8 Ma. (b) A bar plot of the same measurements with time intervals of 20 Myr. (c) next page.

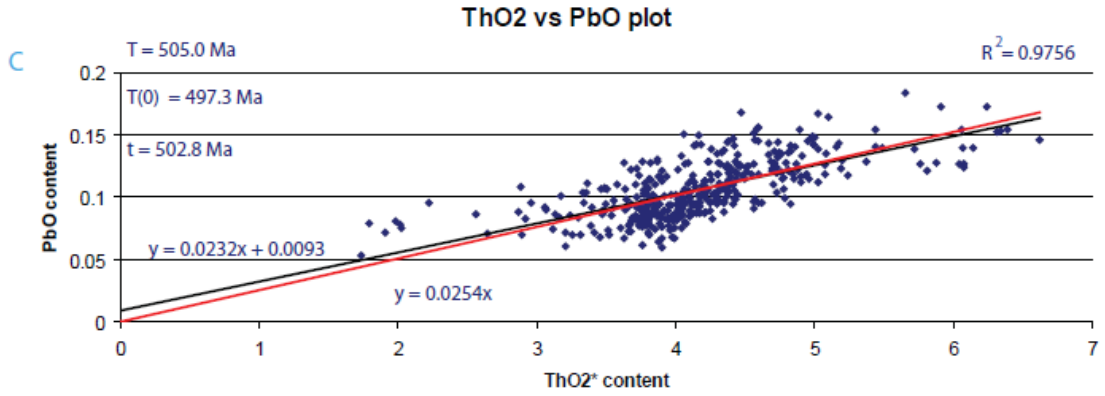

Figure 39: (c) In this plot the ThO_2* vs. PbO has been plotted to illustrate the accuracy of the data. n_a is the number of different monazites that have been measured on n_m, which is the number of point measurements. R^2 of the drawn red line which intersects with the origin is 0,9756. T, T(0) and t are respectively 505,0, 497,3 and 502,8 Ma.

6.3.3 Avardo gneiss

The HP units in the southern part of the fieldwork area (Fig. 2 and Appendix 11.2.3) have also been dated. However, only monazites have been found in the Avardo gneiss and not in the Sjouten unit. The outcoming age is slightly older with an average age of ~513 Ma (Fig. 30a). This age has been based upon 153 point measurements on 12 different monazites dispersed in seven different rock samples. The spacing is approximately the same as for the measurements of the Marsfjället gneiss (Fig. 30b). The ThO_2^* versus PbO plot (Fig. 30c) indicates again that the results are quite reliable with an R^2 of 0,9783. T, T(0) and t are respectively 507,3, 490,6 and 512,7 Ma. These numbers are nicely matching with each other and with the Marsfjället gneiss.

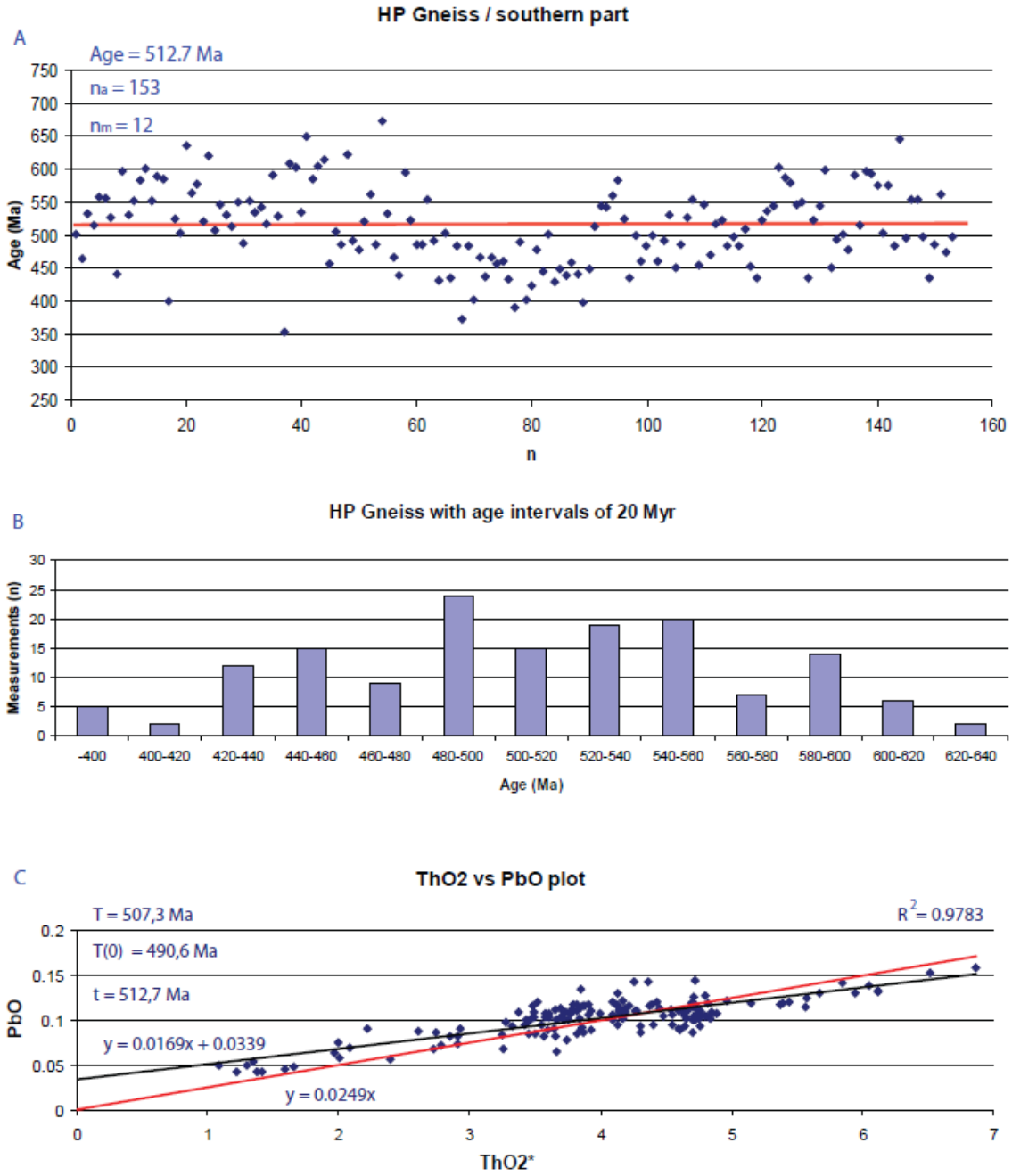

Figure 30: Data representing the HP gneiss in the southern part of the fieldwork area. (a) 157 point measurements are done on 12 different monazites in 7 different rock samples. The average outcoming age is ~524 Ma. (b) A bar plot of the same measurements with time intervals of 20 Myr. (c) In this plot the ThO_2* vs. PbO has been plotted to illustrate the accuracy of the data. n_a is the number of different monazites that have been measured on n_m, which is the number of point measurements. R^2 of the drawn red line which intersects with the origin is 0,9783. T, T(0) and t are respectively 507,3, 490,6 and 512,7 Ma.

6.4. Detailed features of dated monazites

Monazite 09Z-017-3 is illustrated in figure 31. This monazite has a diameter of approximately 140 µm. Eighteen spot analyses have been done on this monazite. The calculated age of each spot is presented next to the spot. Clearly visible in figure 31 is the zoning of the monazite. The dark part has an average age of 488.7 Ma and the lighter part on the right side of the monazite has an average of 460.6 Ma. Another monazite is illustrated in figure 32. This monazite has approximately the same size (140 µm) and shows also a special zoning pattern. These different reflecting colours can be separated into at least 4 possible different grey levels, which are all measured. L1 and L2 are representing the inner part of the monazite with an average age of 470 Ma. If you divide these lines into dark and light reflectance the average age changed to 435 Ma for the darker part and 500 Ma for the lighter part. The intermediate reflectance here, L3, is somewhat smaller but nevertheless has the oldest average age of 508 Ma. The outer parts of this monazite with very light reflectance, is measured with L4, L5 and 2P and the average age is 478 Ma. In the case of monazite 17-3 the darker reflectance is ~30 Myr older than the lighter part, however, in monazite 15-2 the darker reflectance is much younger than the lighter part (435 vs. 500 Ma).

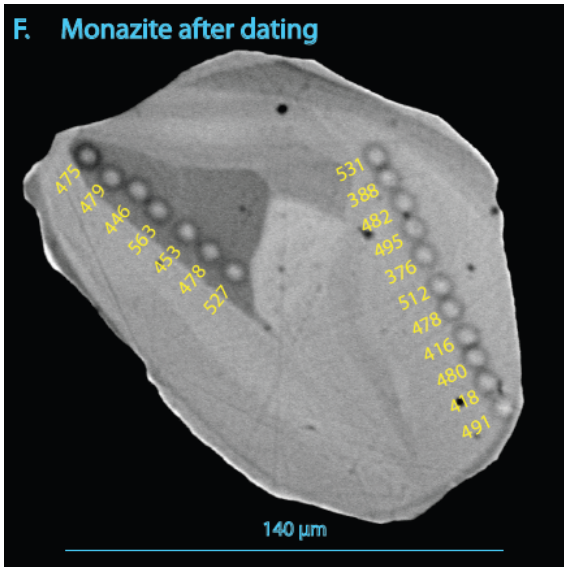

Figure 31: Monazite 17-3 (Appendix 11.3.17). Indicating 18 different spot analysis along two different linescans. The Dark reflectance with 7 point measurements have an average age of ~489 Ma. The relatively light reflectance with 11 point measurements have an average age of ~461 ma

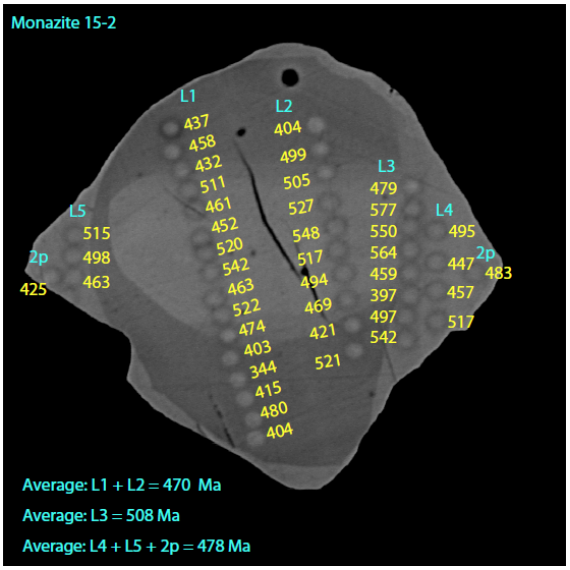

Figure 32: Monazite 15-2 (140 µm)(Appendix 11.3.15). Indicating 43 point measurements on 5 different linescans and two loose points. L1 + L2 (26 point measurements) give an average age of 470 Ma. L3 (8 point measurements) give an average outcome of 508 Ma. L4 + L5 + 2p give an outcome of 478 on 9 point measurements.

Monazite ages are determined with the contents of PbO, ThO_2 and UO_2. The standard that has been used has mean values of respectively 0.700, 12.608 and 0.497; the Marsfjället rocks 0.106, 3.833 and

0.332; the Avardo rocks 0.102, 3.654, 0.310. The variations of these contents for the Marsfjället and Avardo gneisses are illustrated in figure 33.

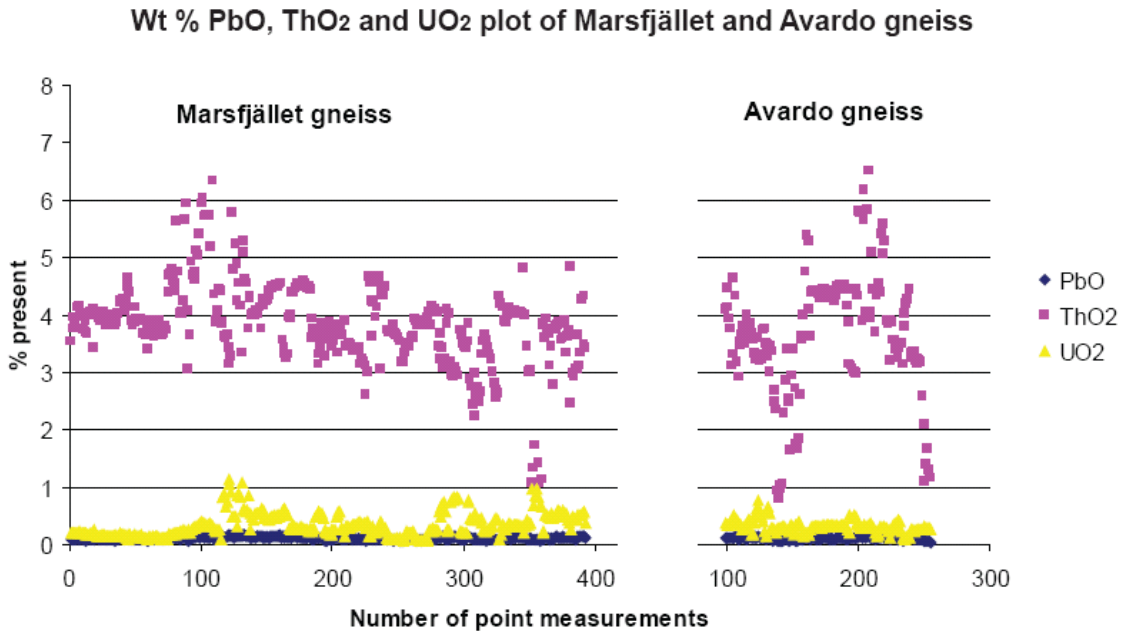

Figure 33: Wt% of PbO, ThO_2 and UO_2 plots of the monazites from the Marsfjället and Avardo gneiss. Average values of these contents are respectively 0.106 (PbO), 3.833 (ThO_2) and 0.332 (UO_2) for the Marsfjället gneiss; and 0.102, 3.654 and 0.310 for the Avardo Gneiss.

These percentages are not consistent in explaining the grey level variations. The backscatter coefficient (η*) is determining whether the reflectance will be relatively light or dark. The higher η* is, the lighter the image of the monazite. An increase in η* can be explained by a decrease of Th^{4+}, a decrease in Ca^{2+} and an increase in REE. These are formed according to the reaction given earlier is this script: $2\ REE^{3+} \leftrightarrow Ca^{2+} + Th^{4+}$. This is exactly what was found in the analysed monazites (Fig. 34). Backscattered coefficients, calculated using monazite analyses are plotted in figure 34. The following formulas were used to calculate the backscatter coefficient:

$$\eta^* = \Sigma c_j * \eta_j$$
$$Z^* = \Sigma c_j * Z_j$$
$$\eta = -0.0254 + 0.0162 * Z - 1.86 * 10^{-4} * Z^2 \text{ (Where Z is } Z^*\text{)}$$

Where: Cj = normalised oxide wt%, η* = backscatter coefficient, Z* = (atomic mass cation/total mass oxides)* (atomic number cation) + (Atomic mass anion/total mass oxides)/atomic number anion.
Full calculations can be seen in the digital Appendix Backscatter coefficient.xls.

Age, Phosphor content and Silica content do not influence the backscatter coefficient and thereby the grey level variations.

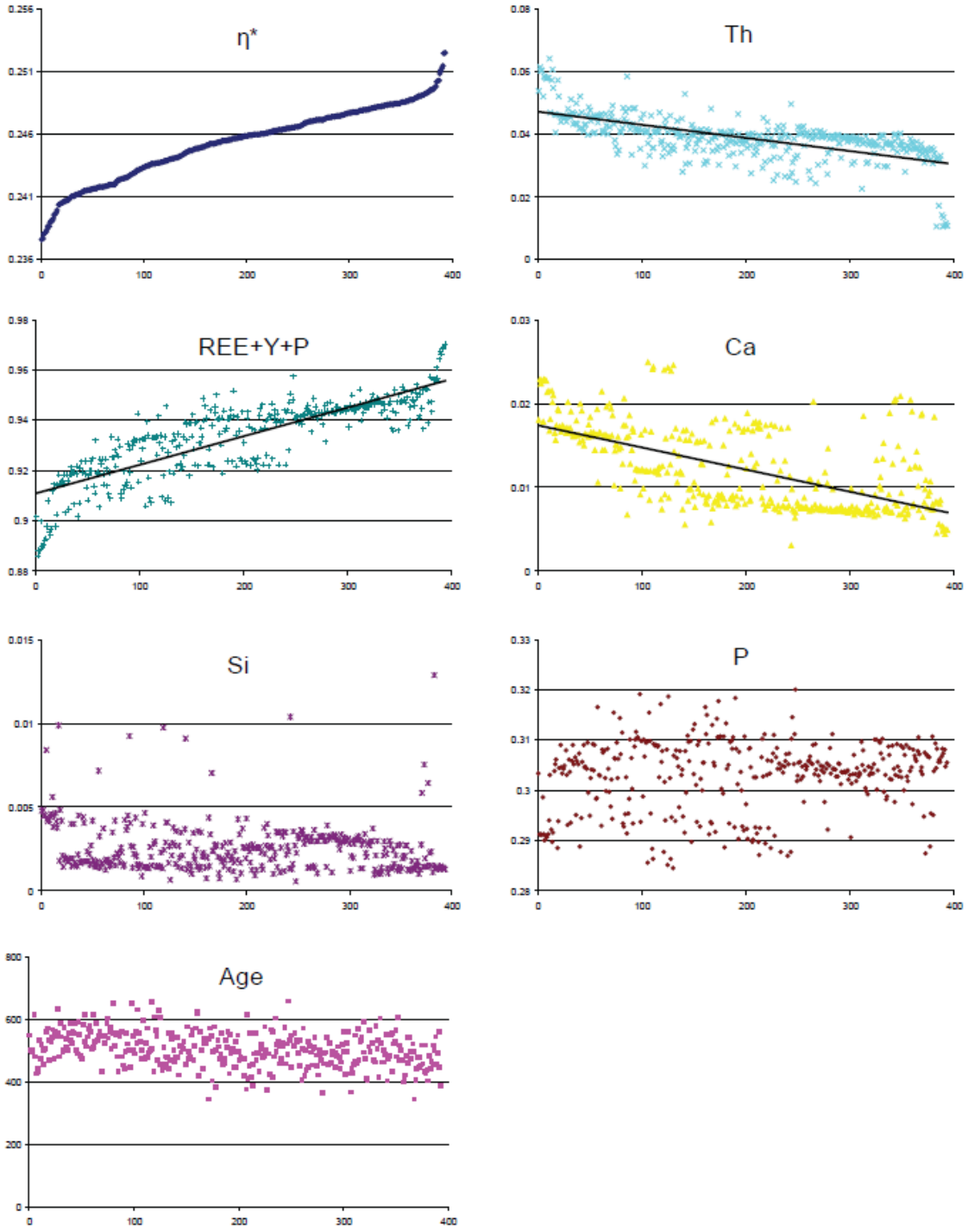

Figure 34: Diagram of calculated backscatter coefficients of all analysed monazites from the Marsfjället gneiss ranked from low to high backscatter coefficient (from 1 to 350). The accompanied values of Th, REE+Y+P, Ca, Si, P and Age are plotted in the other diagrams. All the horizontal-axes are number of point measurements (1-350). The vertical-axes are describing the content (in %) for Th, REE+Y+P, Ca, Si, P and Ma for the calculated age.

6.5. Bulk rock chemistry

X-ray fluorescence (XRF) has been used to determine the bulk rock composition of rock samples. Representative rock samples of the Marsfjället gneiss have been used for the XRF (004a and 015) (Fig. 6). The outcoming bulk rock compositions are used as input data for the computer program Theriak-Domino to calculate the PT conditions. These data is also used to make the ACF-'AKF diagrams. The XRF results are shown in table 3.

	SiO2	Al2O3	TiO2	Fe2O3	MnO	CaO	MgO	Na2O	K2O	P2O5	S	Total
	%	%	%	%	%	%	%	%	%	%	%	%
Sample 4	77,41	10,54	0,62	3,16	0,04	0,99	0,88	1,51	3,46	0,07	-0,05	98,63
Sample 15	73,98	12,26	0,71	4,82	0,09	0,91	1,40	2,01	3,06	0,04	-0,05	99,22
	As	Cu	Pb	Zn	Ni	Cr	V	Sn	Sr	Ba	Rb	Ga
	ppm	ppm	ppm	ppm	ppm	ppm	ppm	ppm	ppm	ppm	ppm	ppm
Sample 4	-0,81	32,92	16,85	62,39	20,43	40,75	56,97	5,12	179,38	724,68	124,13	14,96
Sample 15	0,73	9,42	18,67	159,76	18,99	77,91	71,61	6,69	148,10	830,47	89,13	17,73
	Zr	Nb	Y	Sc	La	Nd	Th	U				
	ppm	ppm	ppm	ppm	ppm	ppm	ppm	ppm				
	348,20	12,51	24,84	6,67	26,14	15,93	6,93	1,50				
	324,32	20,56	25,83	8,34	40,21	15,38	9,55	1,67				
	Si	Al	Ti	Fe3+	Mn	Ca	Mg	Na	K	P	S	
	%	%	%	%	%	%	%	%	%	%	%	
Sample 4	36,18	5,58	0,37	2,21	0,03	0,71	0,53	1,12	2,87	0,03	-0,05	
Sample 15	34,58	6,49	0,43	3,37	0,07	0,65	0,85	1,49	2,54	0,02	-0,05	

Table 3: XRF data for samples 4a and 15. (The full result of the XRF data can be found in digital Appendix: raw XRF data.xls)

The sum of the oxides (based on all $Fe^{2+} = Fe^{3+}$) is 98.63 and 99.22 for respectively the rock samples 4a and 15. Both samples are lookalikes and both have over 70 wt% of SiO_2 (77 and 74 wt%). The rest of the rock mainly consists of the following oxides: Al_2O_3 (~11 wt%), TiO_2 (0.6 and 0.7 wt%), Fe_2O_3 (3.2 and 4.8 wt%), MnO (0.0 and 0.1 wt%), CaO (1.0 and 0.9 wt%), MgO (0.9 and 1.4 wt%), Na_2O (1.5 and 2.0 wt%), K_2O (3.5 and 3.1 wt%) and P_2O_5 (0.1 and 0.0 wt%). Data of the minor and REE are given in ppm. Data of larger and more abundant elements is also given in separate element percentages. Estimations of Fe^{2+} and Fe^{3+} in mineral analysis can be difficult. However, most of the time it is allowed to assume that Fe-total is Fe^{2+} (Bucher and Frey, 2002), so the Fe^{3+} given in the XRF data must be multiplied with 0.899 to get Fe^{2+} (Bucher and Frey, 2002).

The XRF data has been converted to independent element data that has been used as input for the computer program Theriak-Domino. The recalculations can be seen in Appendices 11.6.1 and 11.6.2.

6.6. ACF – A'KF diagrams

Metamorphic facies presented in triangular endmember diagrams give the possibility for quantitative evaluation of metamorphic conditions. Each metamorphic facies includes all bulk rock compositions and their stable mineral assemblages. In order to describe a metamorphic facies and to compare them with others, the use of the combined ACF and A'KF diagrams is an outcome. The result (based on XRF data) is shown in figure 35, in which the evaluation of the bulk rock chemical components of a metamorphic rock and its mineral assemblage, or the approximation of its protolith composition can be done as well as the evaluation of the metamorphic facies conditions. The next formulas, after Kornprobst (2002), have been used to pinpoint the locations of the bulk rock chemical compositions of samples 4a and 15 in ACF-A'KF diagrams.

ACF diagram: $A = (Al_2O_3 + Fe_2O_3) – (Na_2O + K_2O)$

$C = CaO – 3.3\ P_2O_5$

$F = FeO + MgO + MnO$

A'KF diagram: $A' = (Al_2O_3 + Fe_2O_3) – (Na_2O + K_2O + CaO)$

$K = K_2O$

$F = FeO + MgO + MnO$

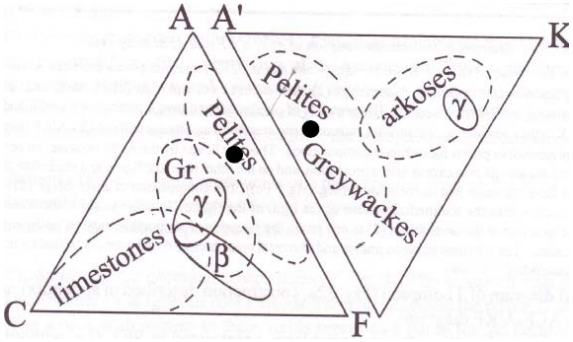

Figure 35: ACF-A'KF diagrams showing the compositional fields of the principal sedimentary and igneous rocks on the ACF-A'KF diagrams: γ = granitoids, Arkoses, Pelites, Gr = greywackes β = basalts and andesites (J. Kornprobst, 2002). The black dot indicates of where samples 4a and 15 plot.

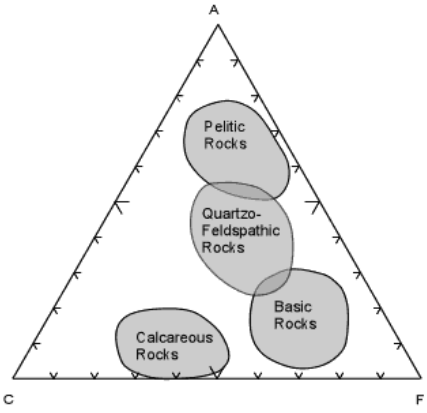

Figure 36: Triangular plot in metamorphic petrology showing different types of rocks in an ACF diagram. Pelitic, Quartzo-Feldspathic, Basic and Calcareous rocks (Nelson, 2000).

According to Kornprobst (2002) bulk rock chemical composition of samples 4a and 15 plot in the pelites field of the ACF-A'KF diagram (Fig. 35). According to Nelson (2000) the bulk rock chemical composition of samples 4a and 15 plot between the boundary of politic and quartzo-feldspatic rocks.

6.7. PT conditions

To obtain the PT conditions of the Marsfjället gneiss, again samples 4a and 15 are used as representative samples. Samples 4a and 15 contain the following stable minerals: garnet, K-feldspar, plagioclase, kyanite, biotite, muscovite, rutile and quartz. The challenge is to find a field in the PT diagram that corresponds with these minerals. To do this, the computer program Theriak-Domino has been used (THERIAK-DOMINO Vers. 20.03.07 User's Guide *Christian de Capitani Konstantin Petrakakis)*. Input data for the computer program Theriak and Domino is the bulk rock composition. The data from the XRF has been recalculated to ratios of the following elements: Si, Ti, Al, Fe, Mg, Ca, Na, K and Mn (Appendices 11.6.1 and 11.6.2). Oxygen and hydrogen must be added in a way that there is no single oxygen or hydrogen molecule left over, so that they will combine to H_2O. The program makes it possible to calculate 106 different minerals with the given elements. These minerals are listed in the Appendix 11.7 together with there requested elements. In this Appendix, the minerals of interest are highlighted. What is important to know about this computer program is that the program can make pseudo sections of PT plots i.e. best representative lines in PT space based upon the input data (Fig. 37).

6.7.1 Program Theriak-Domino

Theriak is a program that calculates the equilibrium assemblage for a given bulk composition with data from a thermodynamic database. The strategy of Theriak is a linear programming method designed to produce the correct answer even in extremely complex, non-ideal systems. Domino is a program that calculates almost any type of equilibrium assemblage phase diagram. The user defines two independent variables that may be P, T and activity of a component or a pseudo-binary system. The calculation may be a phase diagram, mapping the stable assemblages, isopleths of mineral compositions, isolines for amounts, densities, volumes of single phases or rock bulk parameters and much more. The Theriak-Domino software is relatively fast compared to other software and is a useful tool to find a stability field in a PT diagram for the given bulk rock composition. In this way, using EMP mineral analyses and optical microscopy, the exact location in the PT diagram can be reconstructed.

6.7.2 PT plots

PT plots have been made for two rocks of the Marsfjället gneiss (sample 04a and 15). The result for sample 4a is shown in figure 37. What can be observed is that the PT stability field lies between pressures of 12500 and 16000 bar (12.5 – 16.0 kbar) and temperatures of 600 and 850 ^{o}C. Within this field, the following minerals are stabile: garnet, 2-feldspars (plagioclase and K-feldspar), biotite, white mica, hematite, rutile, α-quartz and kyanite.

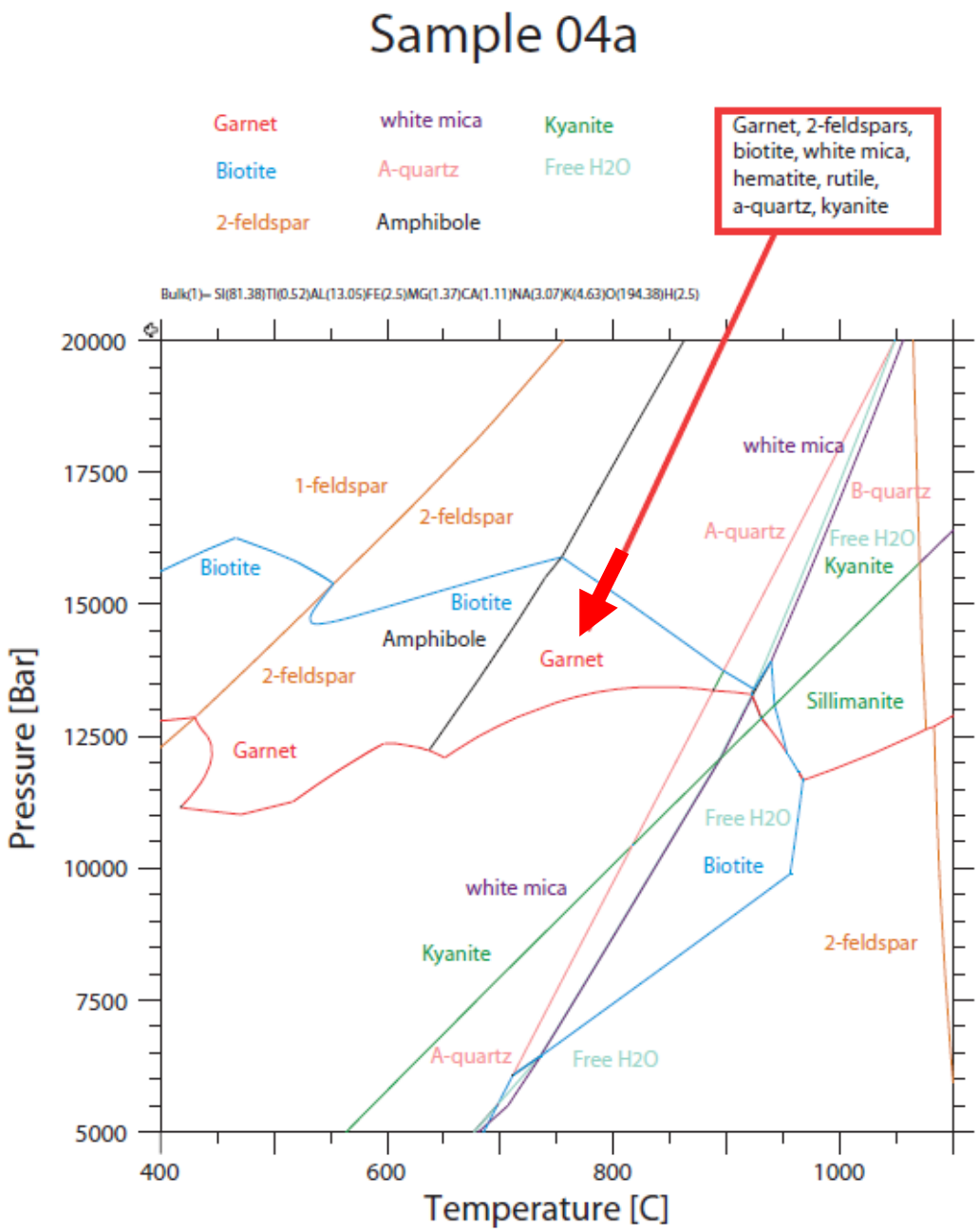

Figure 37: Pseudosections of sample 04a. The stability field (highlighted by the red arrow) of sample 4a with the next minerals present: garnet, white mica, kyanite, biotite, (α-)quartz, (1- and 2-) feldspar, amphibole and free H_2O. The individual stability fields for each mineral are given lines with different colours. Crossing these lines would result in mineral "IN" or mineral "OUT". Fields are indicated with mineral names that are placed within the stability field of that specific mineral. The stability field of 2-feldspar is consisting of plagioclase and k-feldspar, while the 1-feldspar stability field is representing k-feldspar on the left side and plagioclase on the right side. Note: the input data is given in the text above the diagram. This has been based on the (same ratios) data calculated in Appendix 11.6.1.

The result for sample 15 is almost similar to that of sample 4a (Fig. 38). The boundaries of the perfect stability field, where all minerals present in the samples are possible to form, are pressures between 12.5 and 17.0 kbar and temperatures between 550 and 850 ^{o}C.

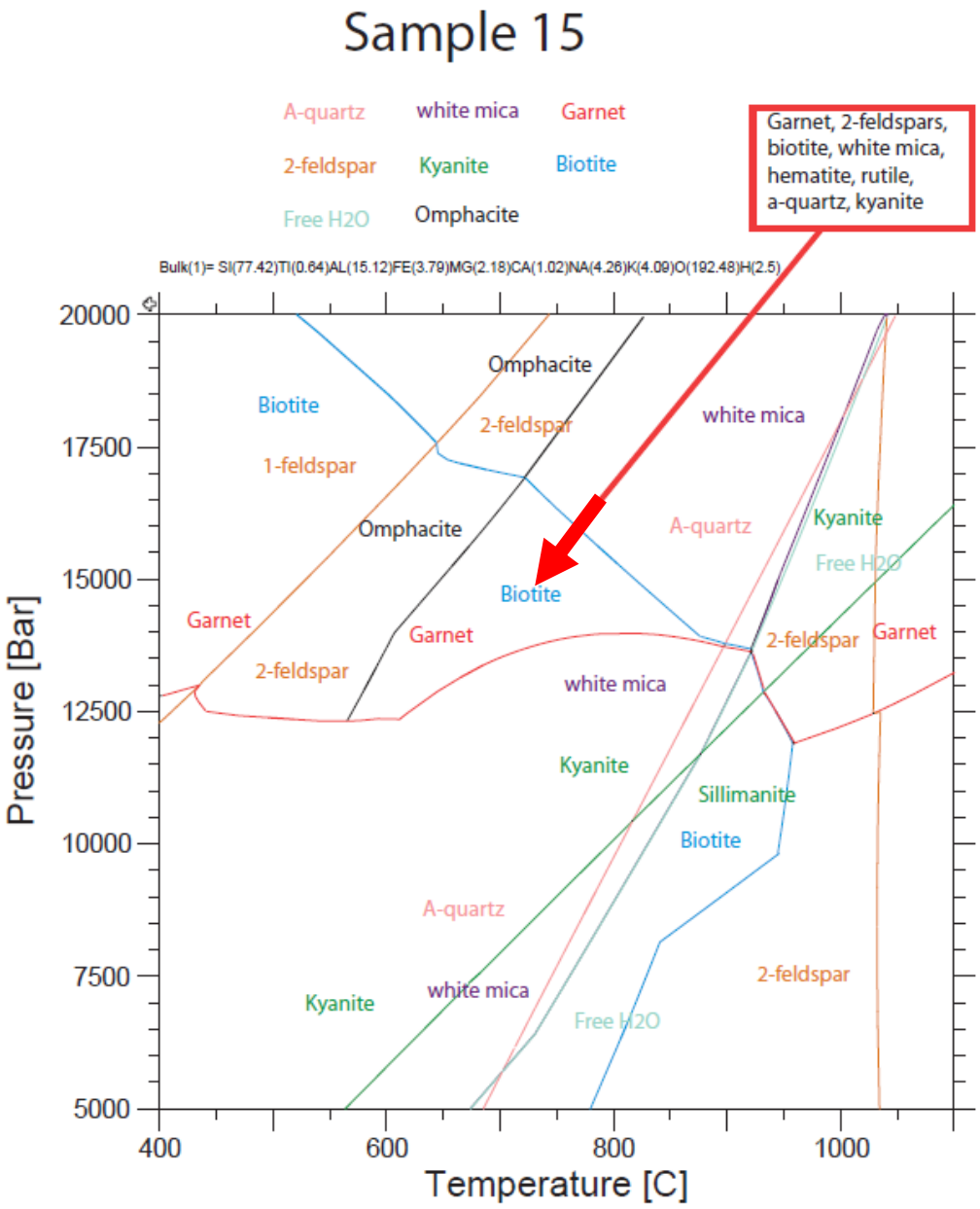

Figure 38: Pseudosections of sample 15. The stability field of sample 4a (highlighted by the red arrow) illustrates the minerals present: garnet, white mica, kyanite, biotite, (α-)quartz, (1- and 2-) feldspar, rutile and hematite. The individual stability fields for each mineral are given lines with different colours. Crossing these lines would result in mineral "IN" or mineral "OUT". Fields are indicated with mineral names that are placed within the stability field of that specific mineral. The stability field of 2-feldspar is consisting of plagioclase and k-feldspar, while the 1-feldspar stability field is representing k-feldspar on the left side and plagioclase on the right side. Note: the input data is given in the text above the diagram. This has been based on the (same ratios) data calculated in Appendix 11.6.2.

An important feature is the melting curve which is represented with the free water stability field. In this field the free water is present in the form of steam. Slightly different between these pseudo sections of samples 4a and 15 is the stability field of biotite, which seems a bit larger for sample 15. The rest of the reaction lines are approximately the same.

6.7.3 PT discussion

The program Theriak-Domino requires a certain amount of oxygen (O) and hydrogen (H) to 'produce' minerals. The trick is to get the minerals filled up and the remaining O and H are then used to form H_2O. It is not allowed to have separate O or H atoms left over. However, certain minerals are using H while other minerals don't. The list of minerals that can be formed are present in appendix (11.6), and the most important ones are highlighted. These are:

- Kyanite: $SiAl_2O_5$
- Quartz: SiO_2
- Rutile: TiO_2
- Garnet: $Si_3Al_2(Ca/Fe/Mg)_3O_{12}$
- K-feldspar: Si_3AlKO_8
- White Mica: $Si_3Al_3KH_2O_{12}$
- (second) feldspar → Albite/Anortite: Si_3AlNaO_8 / $Si_2Al_2CaO_8$
- Biotite (phlogopite/annite): $Si_3Al(Mg/Fe)_3KH_2O_{12}$
- Magnetite: Fe_3O_4
- Hematite: Fe_2O_3
- Water: H_2O

What is interesting here is the difference concerning the use of O and H. If you for instance have relatively high O content, so there is no O_2 left over, then the H_2O- in and out line is shifted to the right compared to relatively low O content (see figure 39a and 39b). The reason for this is the increase of the biotite-area together with the decrease of the garnet-area. Since H_2O is using a ratio OH → 1:2, and biotite (OH group) is using a ratio of OH → 1:1, the use of OH is in favor. Therefore less water and more biotite will be formed. The extra added O in the bulk rock has now been compensated.

Biotite uses the following elements: $Si_3Al(Mg/Fe)_3KH_2O_{12}$. If the amount of biotite is higher, less Fe and Mg will be available for the other minerals to form. Garnet ($Si_3Al_2(Ca/Fe/Mg)_3O_{12}$) is one of the minerals that suffers from this uptake of Fe and Mg and will release it from the mineral structure. Therefore the garnet-area decreases and the biotite area increases. In the same situation with high O content, hematite is present in the whole PT diagram, while magnetite is absent in the whole PT diagram. Hematite (Fe_2O_3) uses Fe^{2+} while magnetite (Fe_3O_4) uses some Fe^{3+}. The fact that the hematite area increase with the increase of oxygen can simply be explained by the fact that hematite uses 1.5 O per 1 Fe, while magnetite uses 1.33 O per 1 Fe. The preference for the formation of magnetite instead of hematite is visible in the case were there is a minimum amount of Oxygen available.

Another important parameter here is the solidus line. The solidus is represented by the free H_2O line in the diagram. On the right sight of the line free water can be present in the form of steam (although in very small portions); while on the left side no free water can be formed. According to Bucher and Frey (2002), the combination of free water and white mica as well as biotite is not common. In fact these areas shouldn't overlap that much since biotite and muscovite build in OH groups in there structure and in that way uses the water. To see what happens if you increase the H_2O content, additional water has been added to the original bulk content with the exact ratio of 1 O and 2 H. The result is visible in figure 39c and 39d. Figure 39d, where almost no water molecules are present, is almost the same except for the kyanite and biotite stability fields. The kyanite field decreases and the biotite field increases. If you add 20 molecules of water to the system, the whole PT diagram is changed. First of all the free water can be found anywhere in the diagram. Second, the white mica is more present in the form of the formation of a second white mica in the upper left part of the plot. Third, the biotite, which has approximately the same area, shows difference in the form of a 'gap' within the field. Fourth, the kyanite field has decreased dramatically. It can now only be found in the upper right corner of the diagram. Fifth, the 2-feldspar stability field has also decreased dramatically. There isn't even a 1-feldspar stability field in some parts of the diagram. And finally the garnet stability field has been shifted up to higher pressures and temperatures. The alpha-beta quartz stability fields stay unchanged.

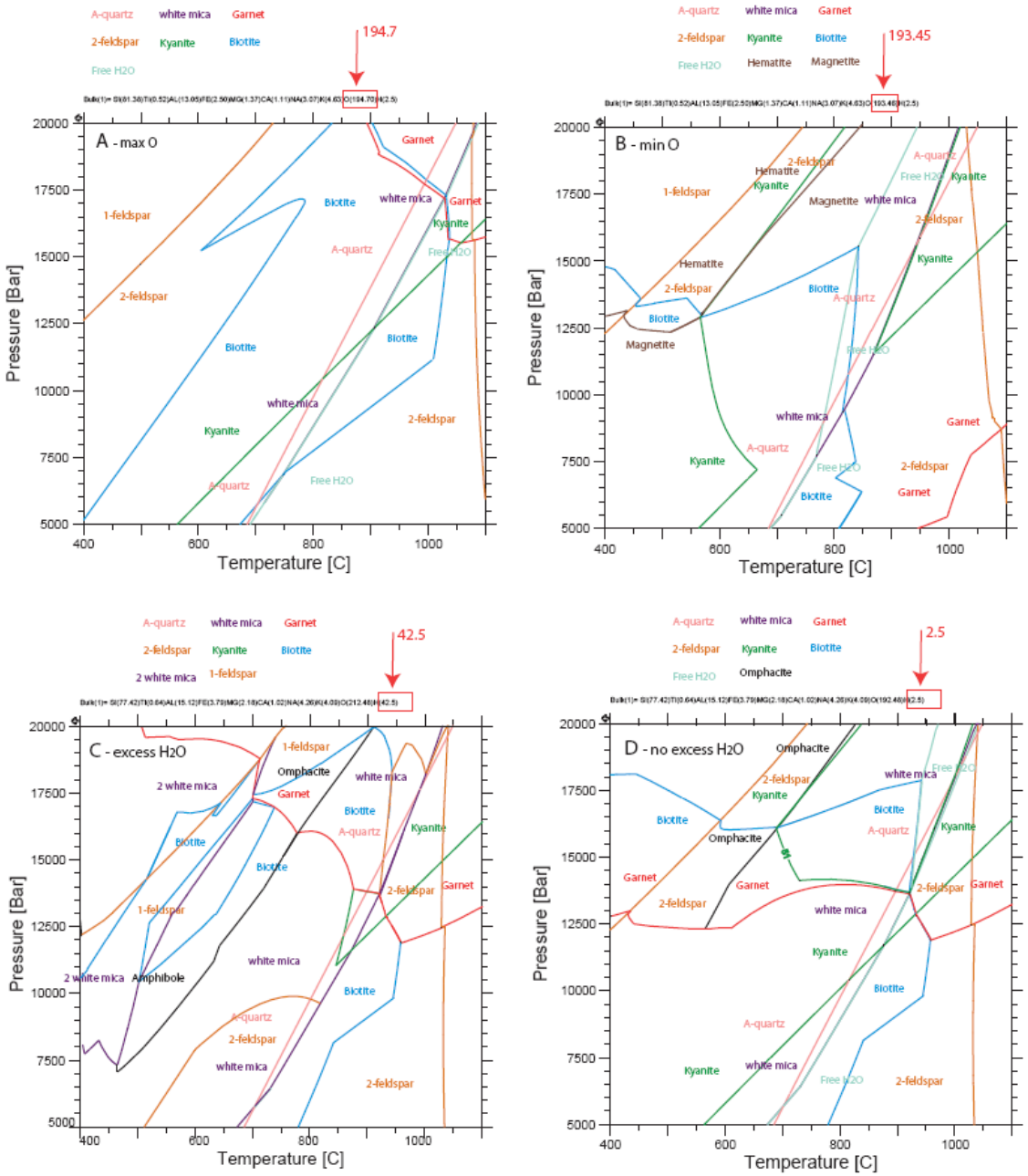

Figure 39: Pseudosections illustrating the factors O and H input, as well as H_2O. (a-b) Figures a and b are pseudo sections of sample 4a, where the difference in O content is illustrated. Figure a illustrates a maximum of oxygen content, while figure b illustrates a minimum of oxygen content. (c-d) figures c and d are pseudo sections with different H_2O content in sample 15. Figure c illustrates a possibility where the excess of water causes all the assemblages to be 'wet'. Figure d illustrates the dry version, where the water is only available on the right side of the free water line.

6.8. EMP Mineral analysis

6.8.1 Location for EMP mineral analysis in thin sections

Images of the thin sections of sample 4a and 15 are illustrated in figures 40 and 41. The photos of figures 40 and 41 have been made with the use of a cross-polarized filter, so that the different minerals can be identified better. Figures 40 and 41 also include the locations of the minerals that are used for EMP mineral analysis. These locations are illustrated in BSE images in figures 42 and 43

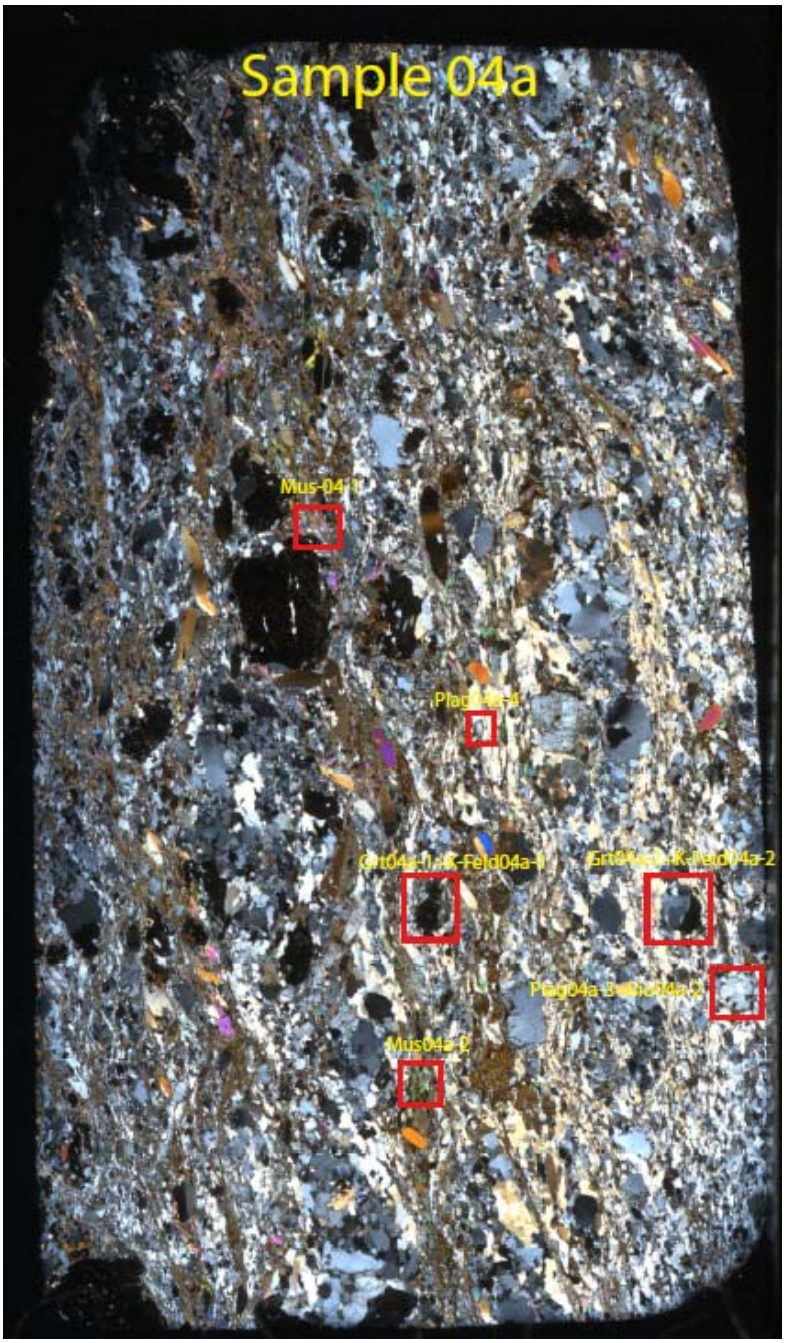

Figure 40: Cross-polarized light image of the thin section of sample 4a. Indicating the location of the minerals that have been used for the mineral analysis.

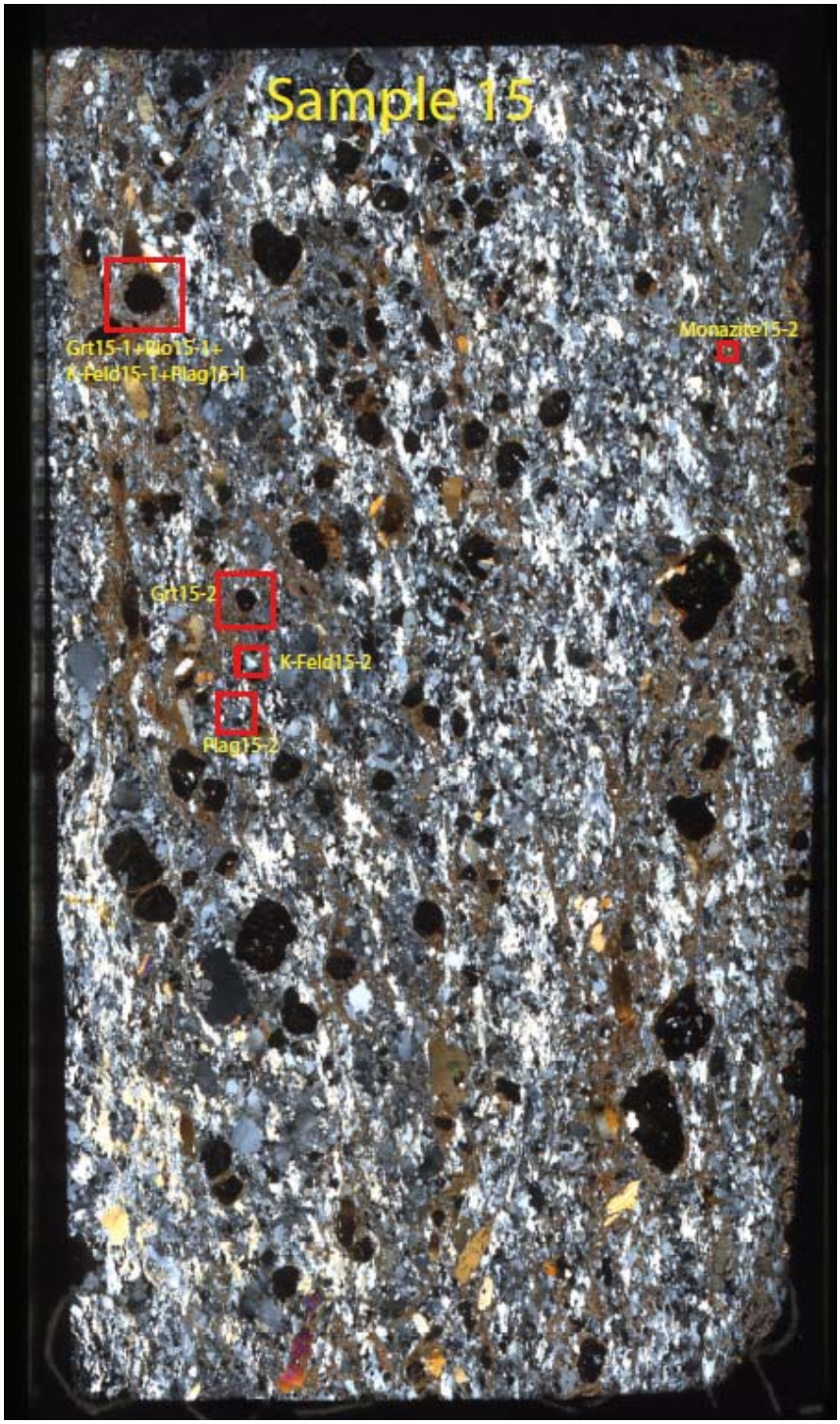

Figure 41: Cross-polarized light image of the thin section of sample 15. Indicating the location of the minerals that have been used for the mineral analysis.

Figure 42 and 43 are indicating the more specific location of the linescans that have been made on minerals of sample 4a and 15. Two garnets, two k-feldspars and two plagioclases in each thin section have been measured, as well as one biotite. In addition two muscovite minerals have been measured of sample 4a.

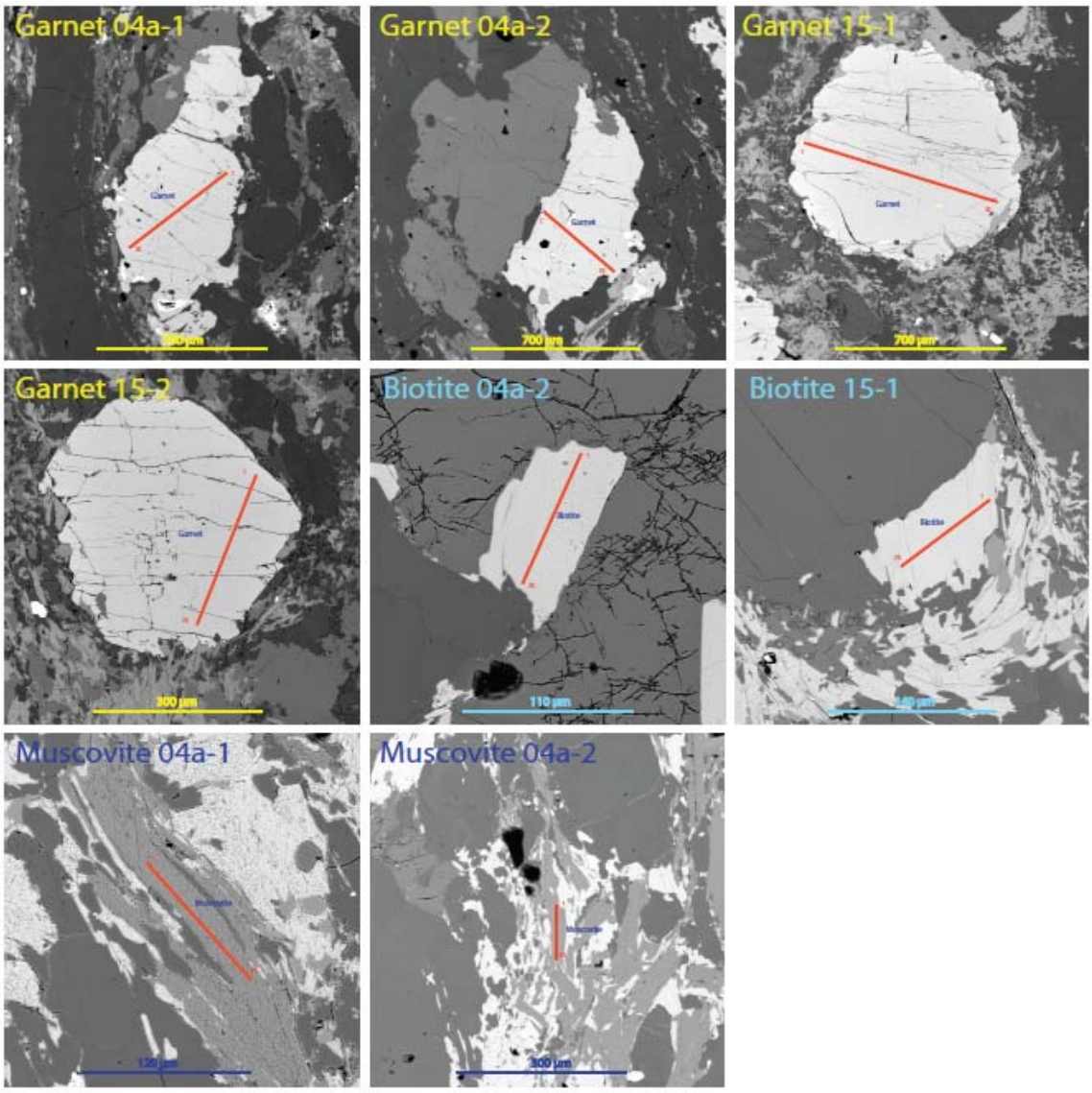

Figure 42: Location of the linescans made on garnets, biotites and muscovites in samples 4a and 15. Locations of BSE images are indicated in figures 40 and 41.

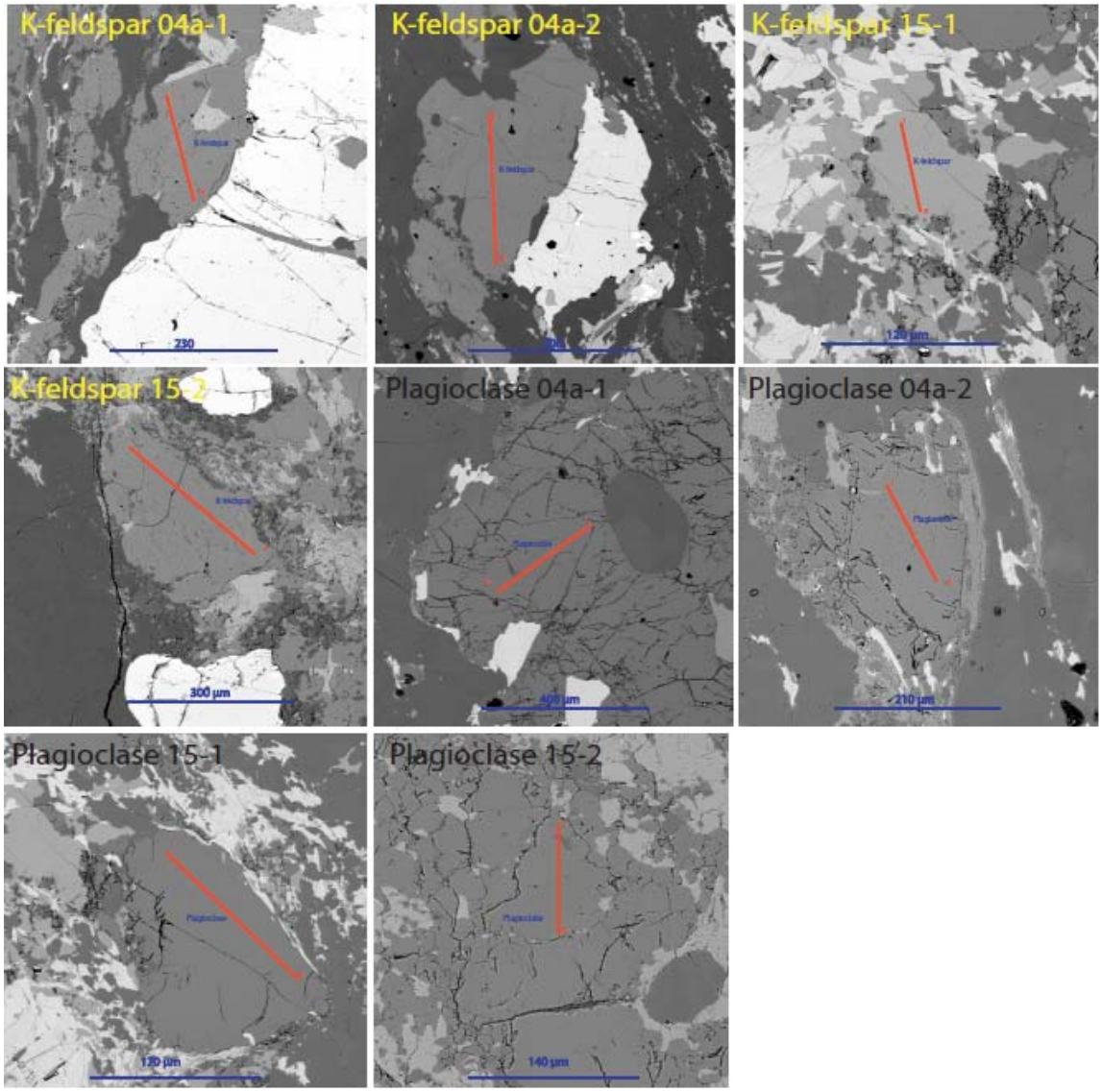

Figure 43: Location of the linescans made on k-feldspars and plagioclase in samples 4a and 15. Locations of BSE images are indicated in figures 40 and 41.

6.8.2 *EMP mineral analysis results*

The results of the mineral analysis are given in digital Appendix EMP.xls. In addition element oxides wt% ranges as well as endmember compositions are graphically illustrated in figures 44-53.

Figures 44 and 45 are graphs illustrating the element-oxide wt % and endmember compositions of garnets from samples 4a and 15. Dominant element-oxides are presented in the graph, while the element-oxides close the value of zero are left out. Silica-oxide is the most dominant element-oxide in these garnets with an average content of approximately 37 %, followed by iron-oxide (31%), aluminum-oxide (21%), magnesium-oxide (4-7%), calcium-oxide (2-4%) and manganese-oxide (1-2%). The dominant endmember of all garnets is Almandine with an average content of approximately 70%, followed by pyrope (18-26%) and grossular (6-11%).

What can be observed from figure 44 as well as from figure 45 is the zoning of garnets 15-1 and 15-2. In the centre of these garnets, FeO content is slightly lower while the SiO_2 and MgO contents are slightly higher compared to rim values (Fig. 45). This results in less almandine and more pyrope-rich in the garnet cores. Another difference between the garnets of samples 04a and 15, besides the zoning, is the higher content of magnesium-oxide paired with a lower content of CaO, in sample 15. The latter is interpreted to be due to bulk rock chemical differences.

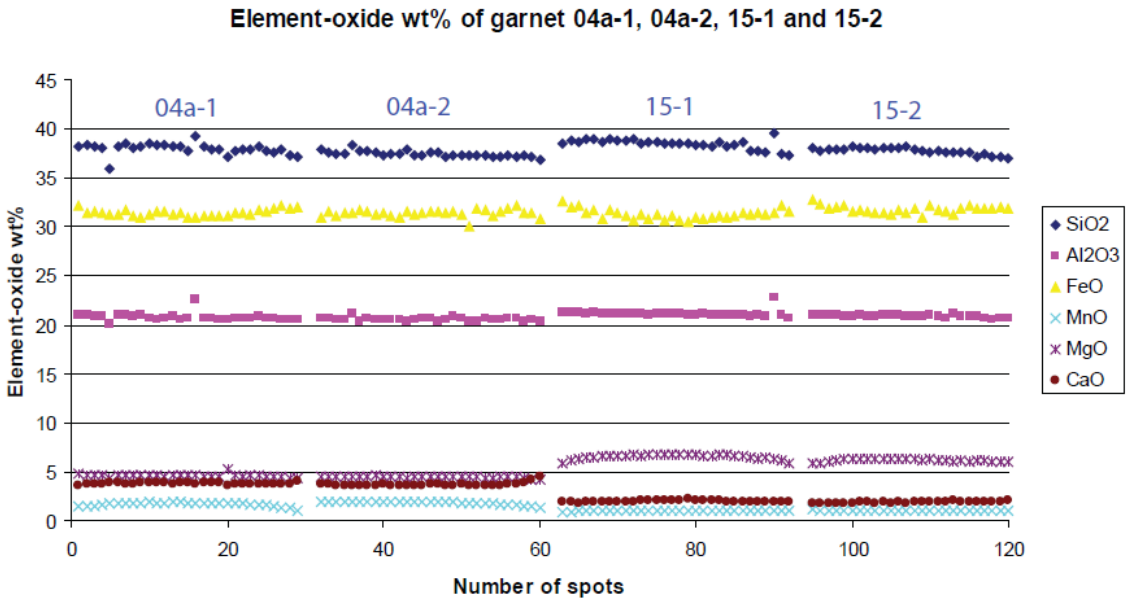

Figure 44: Element-oxide wt % of garnet 04a-1, 04a-2, 15-1 and 15-2. SiO_2, Al_2O_3, FeO, MnO, MgO and CaO are shown in the figure. Na_2O, TiO_2 and Cr_2O_3 are left out of the graph since there content approaches zero. Location linescans indicated in figure 42.

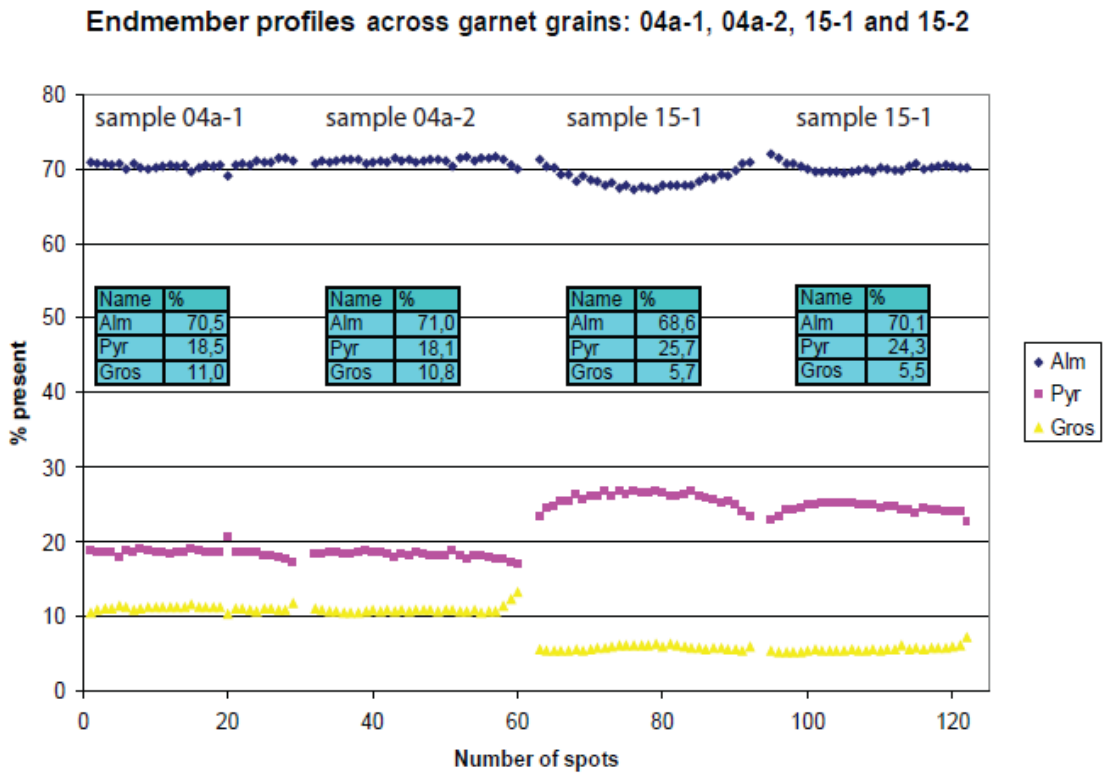

Figure 45: Endmember profiles across garnet grains 04a-1, 04a-2, 15-1 and 15-2. Location linescans indicated in figure 42.

Figures 46 and 47 are graphs illustrating the element-oxides and endmember compositions of biotite from samples 4a and 15. Dominant element-oxides are presented in the graph of figure 46. Silica-oxide is again the most dominant element-oxide in the biotite with an average content of approximately 35%, followed by iron-oxide (17-20%), aluminum-oxide (16-17%), potassium-oxide (10%), magnesium-oxide (8-10%) and titanium-oxide (5%). The dominant endmember of the biotite is different per sample. In sample 4a approximately 56% is Annite and 44% is Phlogopetite. In sample 15 phlogopite is slightly higher with 51% and 49% Annite. No zoning within these biotite samples have been observed. Difference between the biotite from sample 04a and 15 is the Fe/Mg ratio what is causing the difference in the endmember graph (Fig. 47). The latter is interpreted to be due to bulk rock chemical differences.

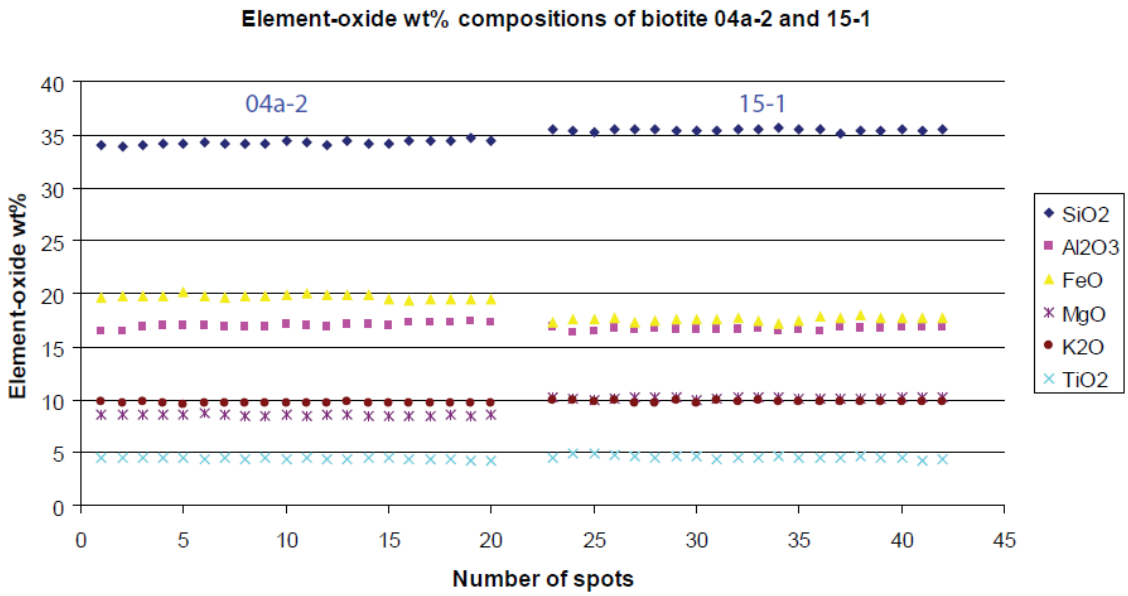

Figure 46: Element-oxide wt% of biotite 04a-2 and 15-1. SiO_2, Al_2O_3, FeO, MgO, K_2O and TiO_2 are shown in the figure. MnO, CaO, Na_2O and Cr_2O_3 are left out of the graph since there content is approaching zero. Location linescans indicated in figure 42.

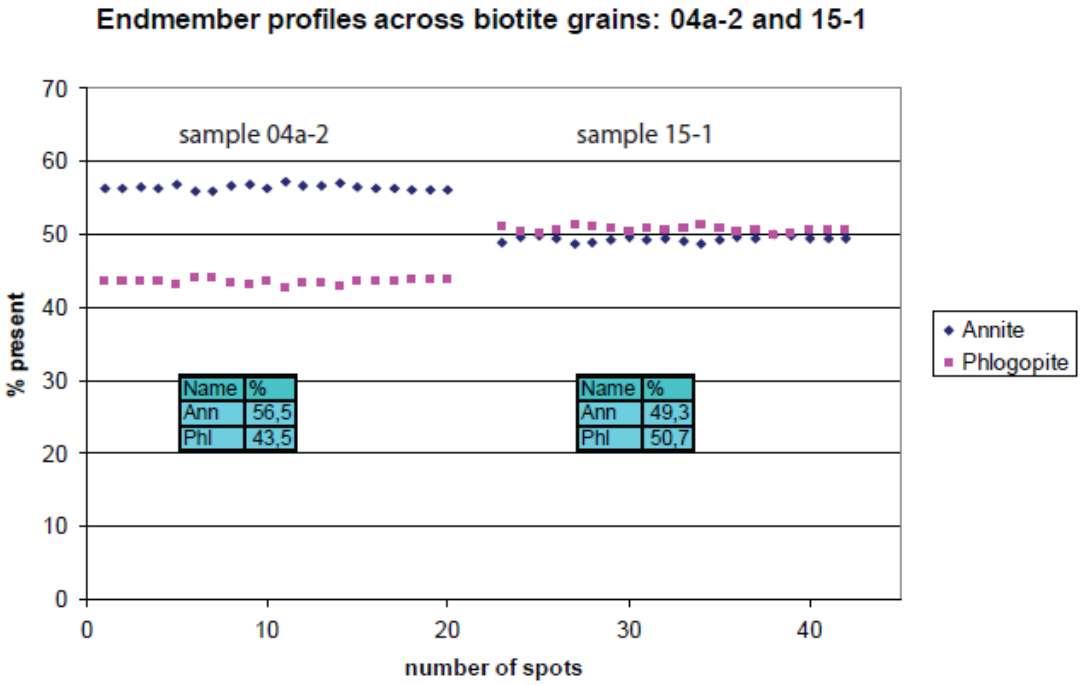

Figure 47: Endmember profiles across biotite grains 04a-2 and 15-1. Location linescans indicated in figure 42.

Figures 48 and 49 are graphs illustrating the element-oxide and endmember compositions of white mica from samples 4a. Silica-oxide is the most dominant element with an average content of approximately 47%, followed by aluminum-oxide (34%), potassium-oxide (7-8%), iron-oxide (4%), titanium-oxide (3%) and magnesium-oxide (2%). The dominant endmember of the white

mica is muscovite (43-50%), followed by Fe-celadonite (28-29%), Mg-celadonite (18-22%) and paragonite (4-5%). No zoning within these white mica minerals was observed.

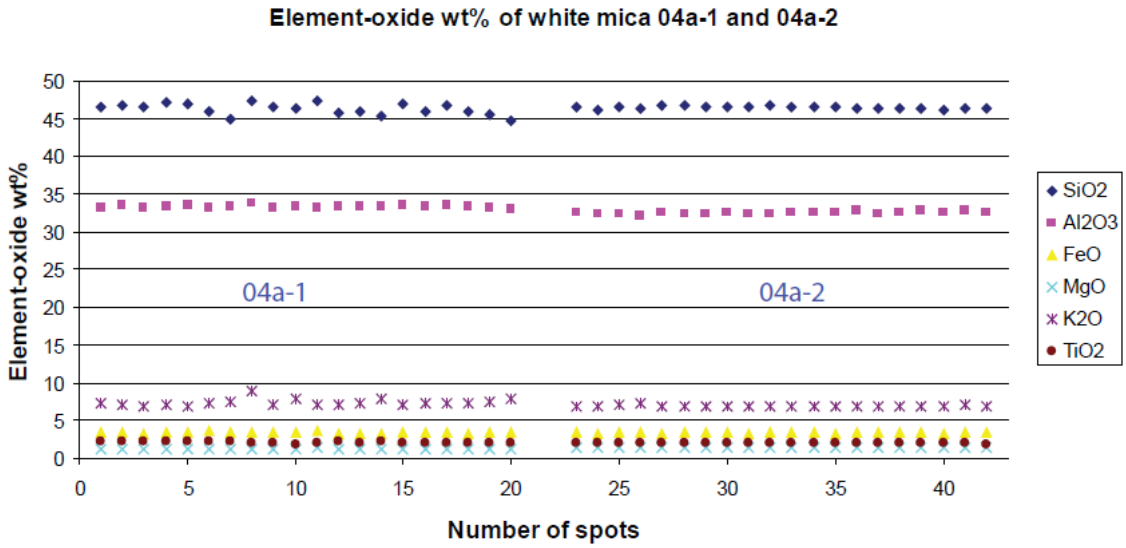

Figure 48: Element oxide wt% of white mica 04a-1 and 04a-2. SiO_2, Al_2O_3, FeO, MgO, K_2O and TiO_2 are shown in the figure. MnO, CaO, Na_2O and Cr_2O_3 are left out of the graph since there content approaches zero. Location linescans indicated in figure 42.

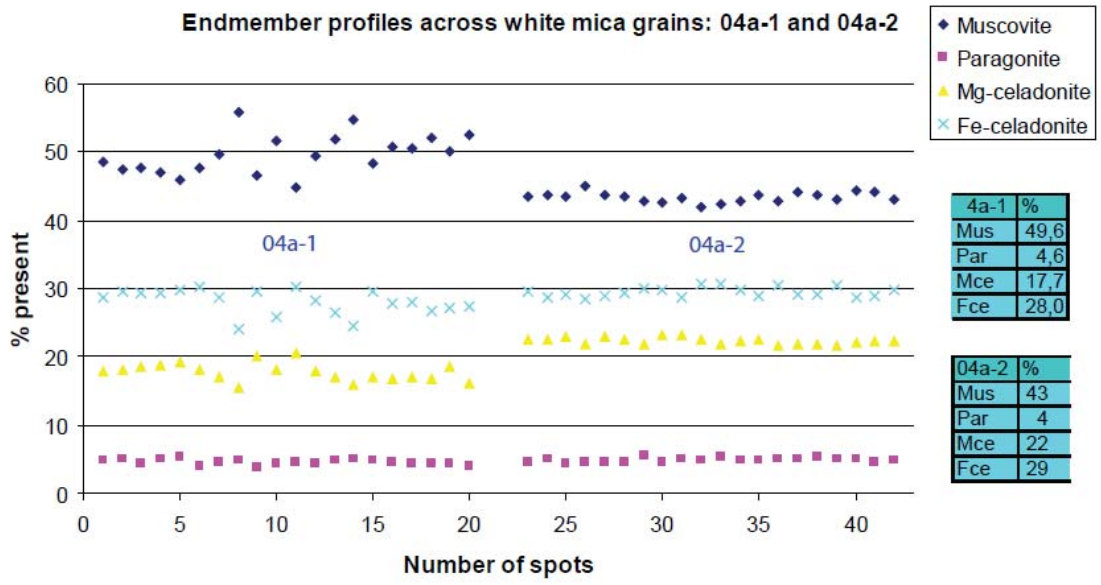

Figure 49: Endmember profiles across white mica grains 04a-1 and 04a-2. Location linescans indicated in figure 42.

Figures 50 and 51 are graphs illustrating the element-oxide and endmember compositions of plagioclase from samples 4a and 15. Silica-oxide is again the most dominant element-oxide with an average content of approximately 57-62%, followed by aluminum-oxide (25%). Smaller contents of the element-oxides calcium-oxide, potassium-oxide and sodium-oxide differ per linescan (0-9%). The dominant endmember of the plagioclase is Albite (59-76%), followed by Anorthite (24-40%) and k-feldspar (1%). Some zoning can be observed in the plagioclases of

sample 15. In here the albite content is lower (approximately 3%) and the anorthite content is higher (approximately 3%) near the core of the minerals. Also a significant difference can be observed between these separate samples. Sample 4a has smaller differences between the two most abundant minerals present; Albite and anorthite. This is in agreement with the bulk rock chemistry.

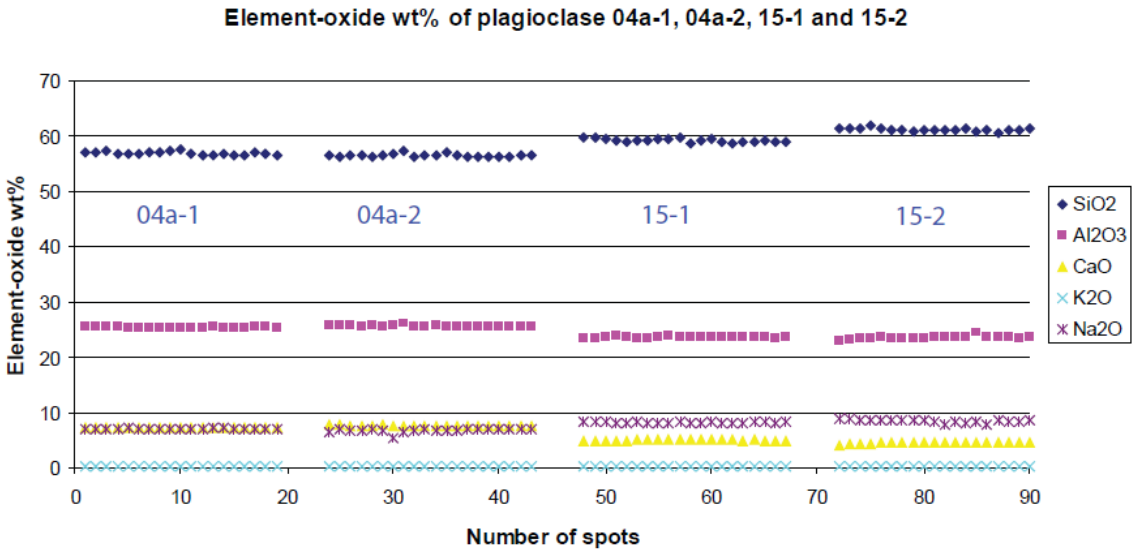

Figure 50: Element oxides wt% of plagioclase 04a-1, 04a-2, 15-1 and 15-2. SiO_2, Al_2O_3, CaO, K_2O and Na_2O are shown in the figure. FeO, MgO, MnO, TiO_2 and Cr_2O_3 are left out of the graph since there content approaches zero. Location linescans indicated in figure 43.

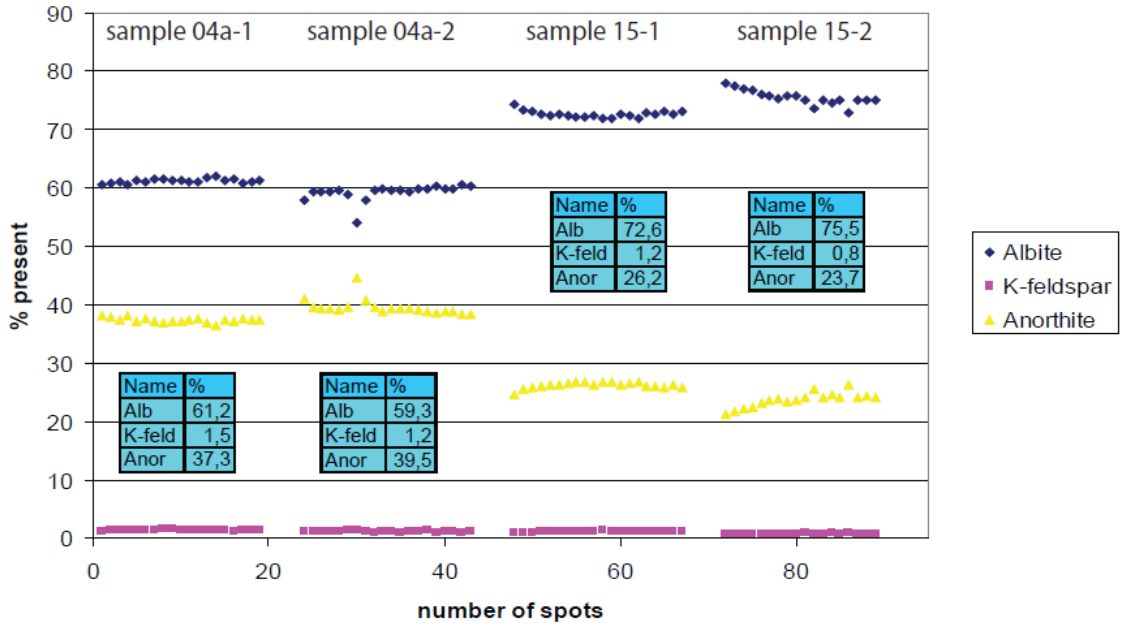

Figure 51: Endmember profiles across plagioclase grains 04a-1, 04a-2, 15-1 and 15-2. Location linescans indicated in figure 43.

Figures 52 and 53 are graphs illustrating the element and endmember compositions of K-feldspars from samples 4a and 15. Silica is the most dominant element with an average content of approximately 60-63 %, followed by aluminum (19%) and potassium (15%). Smaller contents of the elements calcium and sodium are quite small (<2%). The dominant endmember of the K-feldspar is K-feldspar (86-90%), followed by albite (10-14%) and anorthite (<1%). No zoning can be observed in the plagioclases.

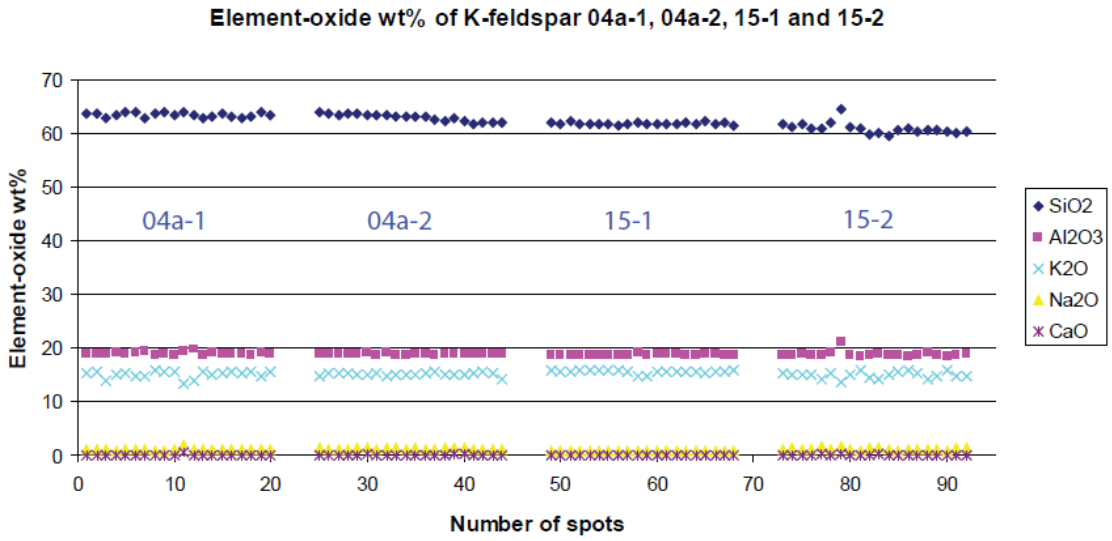

Figure 52: Element oxide wt% of k-feldspar 04a-1, 04a-2, 15-1 and 15-2. SiO_2, Al_2O_3, CaO, K_2O and Na_2O are shown in the figure. FeO, MgO, MnO, TiO_2 and Cr_2O_3 are left out of the graph since there content approaches zero. Location linescans indicated in figure 43.

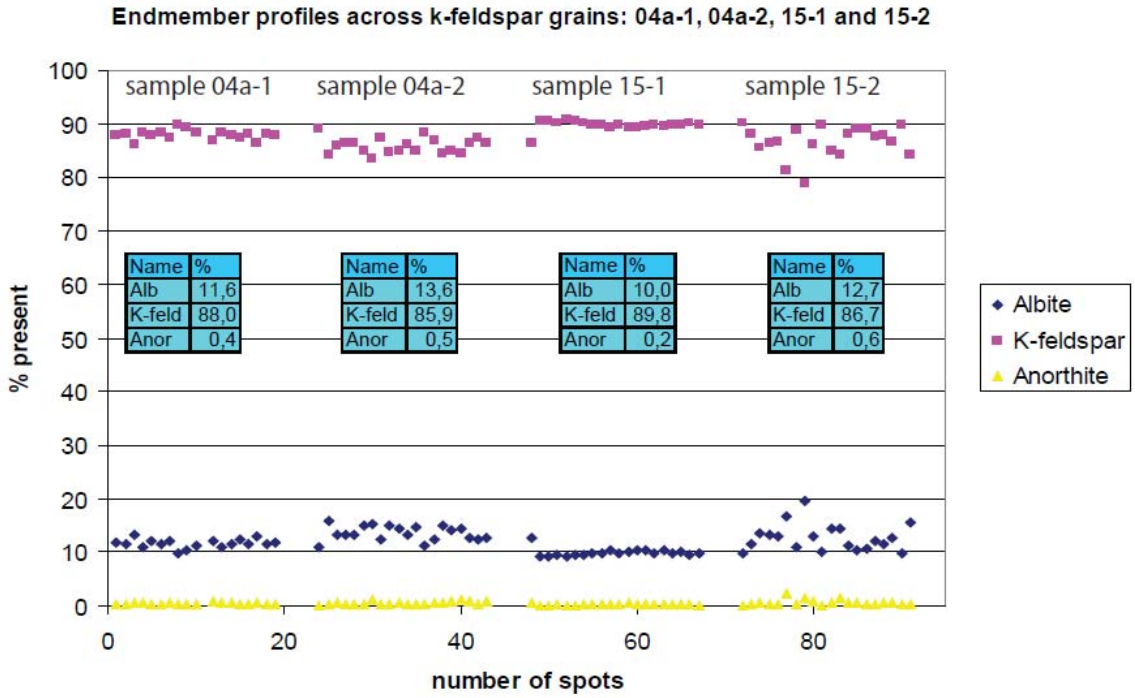

Name	%
Alb	11,6
K-feld	88,0
Anor	0,4

Name	%
Alb	13,6
K-feld	85,9
Anor	0,5

Name	%
Alb	10,0
K-feld	89,8
Anor	0,2

Name	%
Alb	12,7
K-feld	86,7
Anor	0,6

Figure 53: Endmember profiles across k-feldspar grains 04a-1, 04a-2, 15-1 and 15-2. Location linescans indicated in figure 43.

6.8.3 Endmember diagram according to Theriak-Domino

The computer program Theriak-Domino is also used to determine the growth conditions for each separate mineral. Unfortunately the Theriak-Domino is not very useful in this matter. The pseudo-sections illustrating the PT stability fields have already been made calculated out of the bulk rock chemical compositions (Figs. 37 and 38); however in figure 54 the exact endmember composition of each solid solution is shown. The PT stability field found for the whole rock had temperature boundaries between 550 to 850 ^{o}C and pressure boundaries of 12.5 to 17.5 kbar (Figs. 37 and 38). Figures 54a-b shows the chemical composition of the garnet expressed in endmembers Almandine, Grossular and Pyrope. Averages found with the use of EMP are 71% Almandine, 18% Pyrope and 11% Grossular for sample 4a. For sample 15 these values are respectively 69%, 25% and 6%. Interpreting the trend of the figure, these samples would have PT conditions of less than 400 ^{o}C and pressure of 12 kbar.

The same has been done for the feldspars (Figs. 54c-d), with an average endmember composition for samples 4a and 15 of 60-75% albite, 23-40% anorthite and 1-2% k-feldspar for the plagioclase; and 86-90% k-feldspar, 10-14% albite and 0-1% anorthite for the k-feldspar. Since the program uses two feldspars (k-feldspar and plagioclase), this figure illustrates the lines of k-feldspar content of the plagioclase, and the albite and anorthite content of the k-feldspar. The PT positions would again fall out of the figure. The white mica has been subdivided into 4 different endmembers; muscovite, paragonite, Fe-celadonite and Mg-celadonite (Figs. 54e-f). The average compositions determined by the EMP are respectively: 43-50%, 5%, 28-30% and 18-22%. However this composition can again not be found in the figure. The biotite minerals with the endmembers annite and phlogopite (57-50% / 43-50%) are very different from what it should be according to the program Theriak-Domino.

What can be obtained from these plots is the trend of the endmembers that are present. For the garnet counts that there are vertical parameters lines (thermometer) where the grossular and almandine content decrease while the pyrope content increases with increasing temperatures. The feldspars are also showing vertical parameter lines with an increase in plagioclase as second feldspar. Above approximately 1100 ^{o}C the K-feldspar disappears and there is only plagioclase left. Feldspar thermometers are based on ternary solution models that take into account the K content in plagioclase and the Ca content in alkali feldspars (Elkins and Grove, 1990). Exsolution of Ab-rich plagioclase from the alkali feldspar and of K-rich feldspar from plagioclase upon cooling is a common phenomenon, and it is essential that exsolved grains are reintegrated to obtain the compositions of the original feldspars (Bucher and Frey, 2002).

The white mica shows horizontal parameter lines for the most dominant endmember which indicates that it can be used as a barometer. Muscovite is the most dominant endmember. Its relative volume wt% increases during decompression while the amount of dissolved Mg-celadonite compound decreases. Biotite shows no significant change in endmember composition.

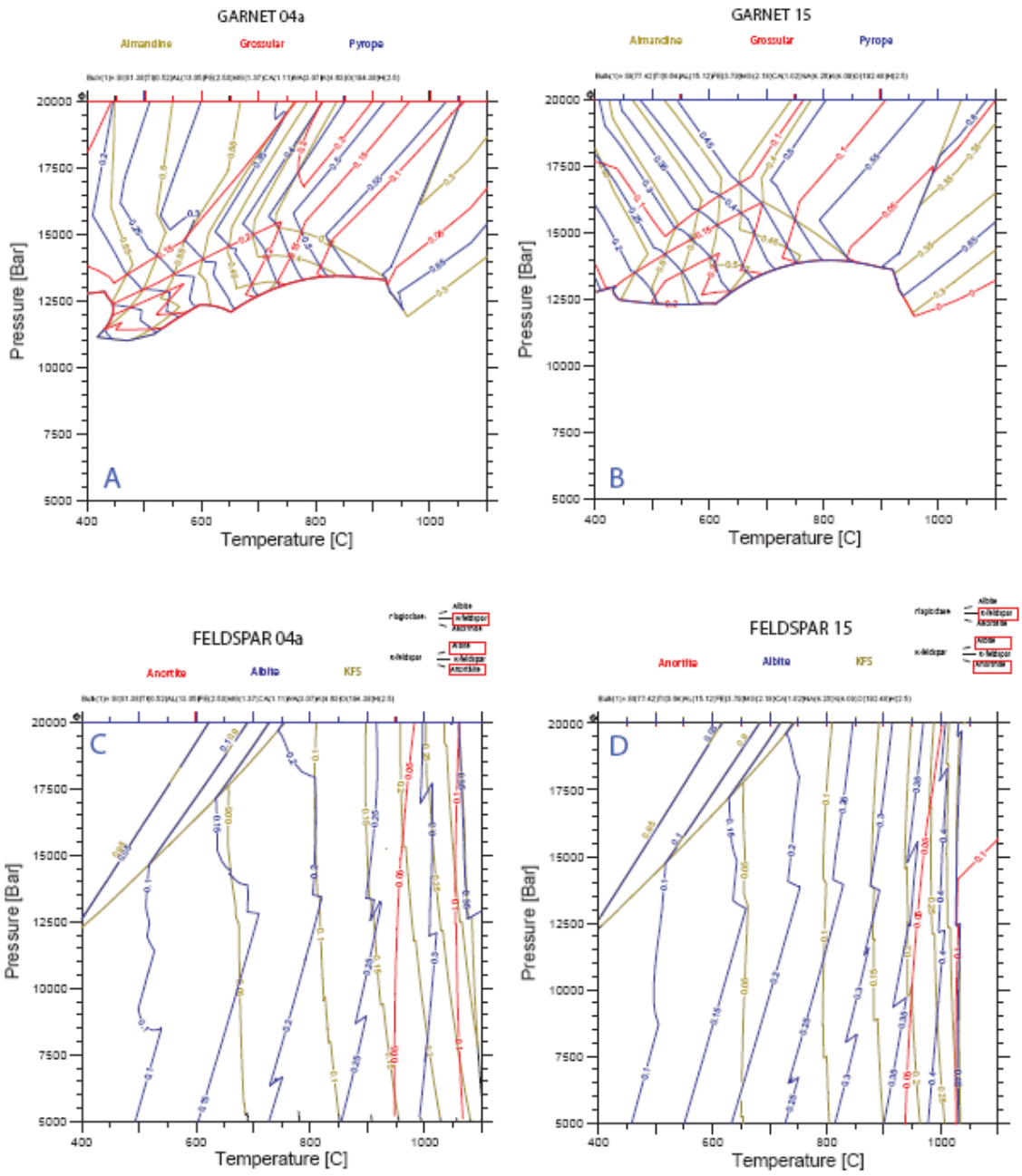

Figure 54: Pseudosections illustrating the PT conditions at which various endmember compositions of garnet (A+B), feldspar (C+D), white mica (E+F) and biotite (G+H) are stable in the two gneiss samples 04 and 15. To be continued…

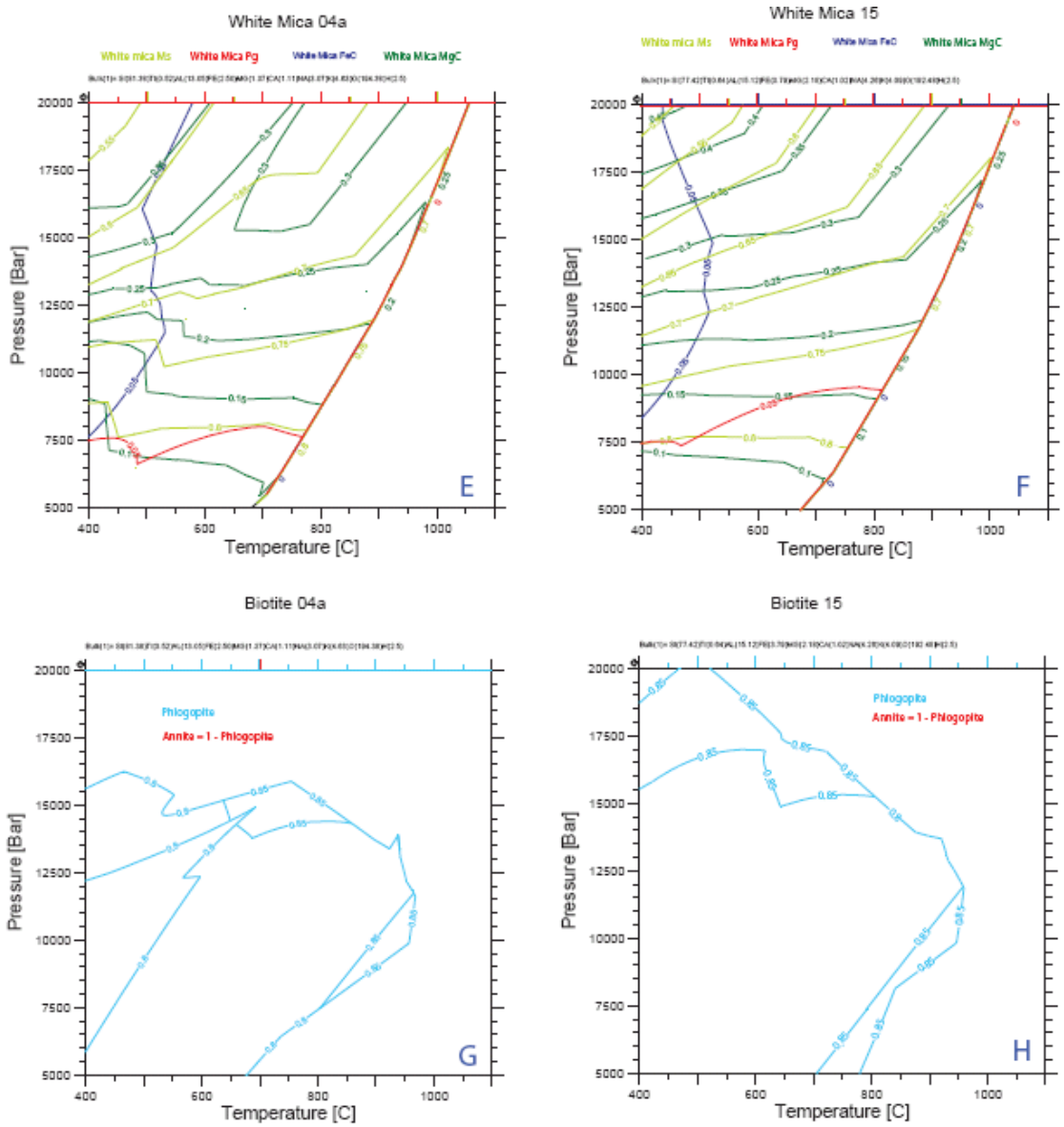

Figure 54 (continued): Pseudosections (e-h)

6.9. Svartsjöbäcken schist

The Svartsjöbäcken schist belongs to the Western Belt of the SNC (sample 24 in fig. 6 and Appendix 11.6.2). There is no tectonic contact between the Central and Western Belt and it is therefore very interesting to know the age of these rocks. Two rocks have been taken at Fatmomakke (phyllites). The metamorphic grade is low amphibolite facies to mid amphibolite facies. Field observations are best shown in figures 55a-d. Figure 55 gives an overview of the good exposure of the Svartsjöbäcken schist near Fatmomakke, as well as the layered structure of the schist, the locally abundant garnets that are present and foliation and folding of the rocks.

Figure 55: Field observations of the Svartsjöbäcken schist. (a) Overview of good exposures of the schist. (b) Illustration of the layered structure of the schist. (c) Illustration of the garnets growing on top of the schist. (d) Illustration of the isoclinal folds of the schist.

The lineation found in these rocks is very developed and shows an orientation of 113/12W. Fold-axes are perpendicular to the transport direction expressed by the lineation. The garnets present in these rocks show growth during folding. Around these garnets a ring of biotite is formed. This indicates the transition of garnet into biotite under lower pressure and temperature conditions. In the field these rocks are shiny, which is indicative for the presence of secondary muscovite. These may form because of the original high Al content in the bulk rock composition.

A more detailed BSE image of the microstructure of the Svartsjöbäcken schist can be seen in figure 56. The Svartsjöbäcken schist mainly consists of quartz, feldspars (k-feldspar and plagioclase), garnet, biotite and muscovite.

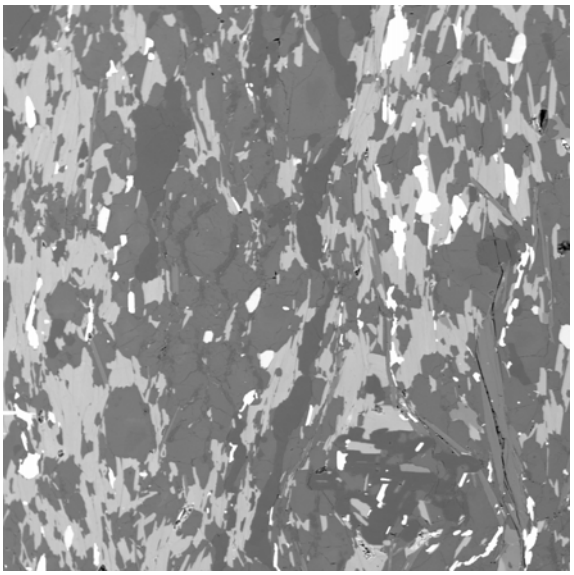

Figure 56: BSE image of the microstructure of the Svartsjöbäcken schist. Horizontal length BSE image is ~1700 µm. (Appendix 11.5)

The monazites that are found within these rocks are very small but big enough to do 19 point measurements on eight different monazites in two different rock samples of the Svartsjöbäcken schist. The average age is ~488 Ma (Fig. 57). The dated monazites with their accompanied age and location within the thin sections can be found in Appendix 11.5 and digital Appendix Svartsjobacken.xls. In there, the calculations of r^2 (0,992) is indicated.

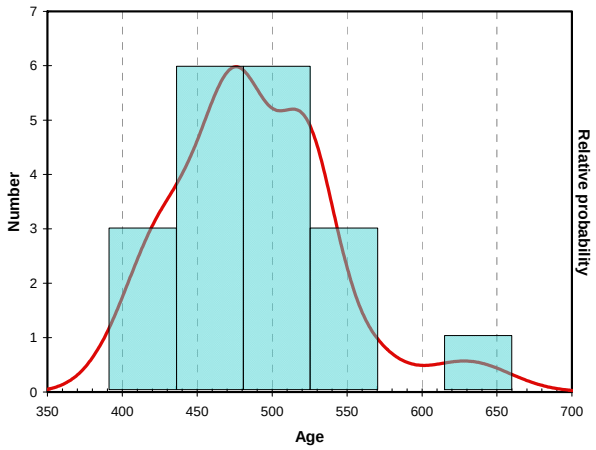

Figure 57: Bar diagram of 19 point measurements on 8 different monazites from two samples of the Svartsjöbäcken schist. The average age is approximately 488 Ma.

7. Discussion

7.1. Age determination

Isotopic age dating methods like for instance U-Pb zircon (Dunning, 1987), K-Ar (Sturt et al., 1978), Rb-Sr (Sturt et al., 1978), ^{40}Ar-^{39}Ar (Mørk et al., 1988) and Sm-Nd dating (Mørk et al., 1988) have been performed in the area. This project has been based upon EMP monazite dating. Montel et al., (1996) describes the pros and cons of the monazite age dating method. Disadvantages of this age dating method are mainly related to the presence of the mineral monazite in the rocks. Not all rocks contain the mineral monazite, such as calcium rich rocks like mafic and intermediate rocks and metabasites or mafic greywackes. These rocks often do contain zircon and biotite for measurements of U-Pb and Rb-Sr. Another disadvantage of the monazite age dating method is the measuring limit for relatively low Pb contents. If the Pb content is low, measurements are difficult and less precise. However, if there is abundant Pb in the monazites, the precision is said to have a variance in +/- 30-50 Myr. Thereby, two important assumptions must be made concerning the Pb content. First is that there was no initial ^{204}Pb present at the formation stage of the monazite; and second that there was no leakage of Pb after the formation. Advantages on the other hand are that if you make the number of measurements large enough, the deviation will decrease. The correctness of the ages can also be checked by comparison with a standard. This is a monazite with a known age that can be used to calibrate the EMP. Another advantage of this dating method is that it is non-destructive. You can perform a measurement repeatedly on the same monazite. The spatial distribution is also quite low; only five μm for a single point measurement, which means that at least 30 measurements can be done on a monazite of 150 μm in length. Another advantage of this technique is that you know the petrographical position of the dated crystal within the microstructure, because you work with polished thin sections. In this way, different outcoming ages might be explained better.

7.1.1 Reliability results

The reliability of age determination of the monazites is a very important issue. Partly the reliability can be checked with the measurements of the standard monazite with a known age of 1125 Ma. The result was an average age of 1132 Ma based on over 373 point measurements taken before, between, and after the measurements of two separate monazites of the SNC. These measurements of the standard have a deviation below 10 Myr that is acceptable for the initial calibration level of the microprobe. Therefore, the reliability of the age of the Marsfjället gneiss of 502,8 Ma of 393 point measurements is good with only a deviation of +/- 3 Myr (the same 0.6% used as for the standard). Calculations of the isochron plots strengthen these results with an r^2 of 0,9756. According to the same isochron plots, T (age according to the natural trendline) is also fitting quite nicely with an age of 505,0 Ma. T(0) is slightly lower with an age of 497,3. If you use the standard deviation as a range for

the outcoming ages, the + / - would be much larger (44.1 Ma). This indicates that 68.2 % lies between 459 and 547 Ma. 96% would fall between 415-591 Ma. These percentages are indicative for a normal distribution curve.

The age of the Avardo gneiss is slightly older with an average age of 512,7 +/- 3 Ma. This has been based on 153 data points. This number is only half of the point measurements done on the Marsfjället gneiss, but quite a lot. Therefore, indicators for the precision like r^2, T and T(0) are also quite reliable. If you use the standard deviation as a range for the outcoming ages, the + / - would again be much larger (49 Ma). This indicates that 68.2 % lies between 464 and 562 Ma. 96% would fall between 415-611 Ma. These percentages are indicative for a normal distribution curve.

A very important aspect for calculating the ages of the monazite is the correctness of the measurements of Thorium, Uranium and Lead. These elements form the basis of the monazite age dating method. Variability in Pb content affects the outcoming ages the most. If all the Lead contents are increased with 0.01 % mass concentration, the average outcoming age would not be 504.4 Ma, but would be 551 Ma, which is a deviation of almost 10%. If this 0.01% deviation in the mass concentration is added to the Th and U content, the average outcoming ages would be 501.8 Ma and 499.4 Ma respectively, which is less than 1%. This already indicates the dominancy in the measured Pb content compared to Th and U. This is a huge disadvantage of the monazite age dating method. However, the number of measurements has counter attacked this disadvantage. The Marsfjället gneiss in the northern part has been based on 393 point measurements. The HP gneiss is based on 153 point measurements.

With an r^2 of 0,9756 and 0,9783 together with the resemblance of T, T(0) and t which are respectively 505,0, 497,3 and 502,8 Ma for the Marsfjället gneiss and 507,3, 490,6 and 512,7 Ma for the HP gneiss, an assumption can be made that this strong match seems to represent only one deformation phase. Also the slightly younger T(0) of the HP gneiss may be correlated to the slightly smaller monazite grains within the HP gneiss compared to the Marsfjället gneiss.

7.1.2 What is already known / comparison outcoming ages

Sturt et al., (1978) introduced the Finnmarkian phase as an early Caledonian (540-490) phase of extensive thrusting. The Finnmarkian event involved the outermost Baltoscandian margin, comprising the basal Upper Allochthon, Seve-Kalak superterrane and some parts of the Middle Allochthon. This is considered the current interpretation not applicable anymore, but the Finnmarkian still retains for mid-Cambrium to Early Ordovician deformation and metamorphism of the Baltoscandian margin and in the exotic terranes. Therefore the outcoming age of 502,8 Ma is referred to as Finnmarkian.

This project is the first one that dates monazites taken from the Central Belt of the Seve Nappes in North Jämtland and South Västerbotten. However, other dating methods have been used in this area and have different outcoming ages (Table 4). Roberts (2003), Gee (1985), Brueckner and v. Roermund (2004) all dated the rocks to be 454 Ma or less. This is suggesting Jämtlandian in contrast with the Finnmarkian age found in this project. Others like Andreasson (1994) found ages of intrusive dikes of 573-460 Ma.

Mørk (1988) and Dallmeyer (1991) used ^{40}Ar-^{39}Ar and Sm-Nd dating of peaking in eclogite facies, provided ages of 505 Ma. This suggests that the 502,8 Ma found in this thesis for the central part of the SNC in northern Jämtland and southern Västerbotten is supporting this outcome. However, these ages are from north Norway and Sweden. The Trondheim event may be correlated with the Finnmarkian but the timing is different; U-Pb zircon ages of 493-482 Ma (Dunning, 1987). The Taconian event 470-450 Ma and the Scandian Event are approximately 420-400 Ma. Williams and Claesson (1987) dated the Seve Nappes on 440-425 Ma. Hacker and Gans (2005) already dated the Finnmarkian event what produced high-pressure metamorphism in the Seve Nappes in Norbotten at 503 Ma.

Age	Reference
<454 Ma	Roberts (2003), Gee (1985), Brueckner and v. Roermund (2004)
573-460 Ma	Andreasson (1994)
505 Ma	Mørk (1988), Dallmeyer (1991)
493-482 Ma	Dunning (1987)
440-425 Ma	Williams and Claesson (1987)
503 Ma	Hacker and Gans (2005)
502,8 Ma	This MSc thesis

Table 4: Overview of the known ages according to their method and author.

What can be said about these different ages is that the range is quite large. Therefore, the Finnmarkian age found does fit with some ages. However, it is also quite different from for instance the Sm-Nd ages of Brueckner and Van Roermund (2004). Some of this date is simply not accurate enough anymore or have to be revised (for instance ages based on ^{40}Ar-^{39}Ar dating).

7.2. PT conditions

Metamorphic age determinations as well as determination of formal PT conditions of rocks of the SNC are essential for making a (new) geodynamic model for the formation of the Caledonides. First some principal aspects of (U)HP metamorphism will be discussed. This will be done with the use of a PT diagram to illustrate an overview of possible PT-t paths and PT stability fields. This will be followed by projecting these principals to the data that has been obtained in this master thesis. Finally, a comparison with other relevant projects/interpretations will be made to strengthen the results.

7.2.1 (U)HP conditions

Where do the terms HP and UHP come from? Ernst and Liou (2008) state that HP conditions are reached when the PT conditions exceed the lithostatic pressures, which are defined by the aragonite-calcite polymorphic transition curve (Fig. 58). Beyond the HP field, you can find the UHP field, which is defined above the quartz-coesite line (except for low temperatures). Figure 58 also illustrates apparent subduction PT-t paths for continental subduction and collision and oceanic plate subduction. What can be observed is that the oceanic plate subduction reaches maximum PT condition of 10 kbar and 300 °C and stays in the greenschist and blueschist facies. On the other hand, continental subduction and collision could reach maximum PT conditions of almost 30 kbar and 700 °C and reaches the dry eclogite facies.

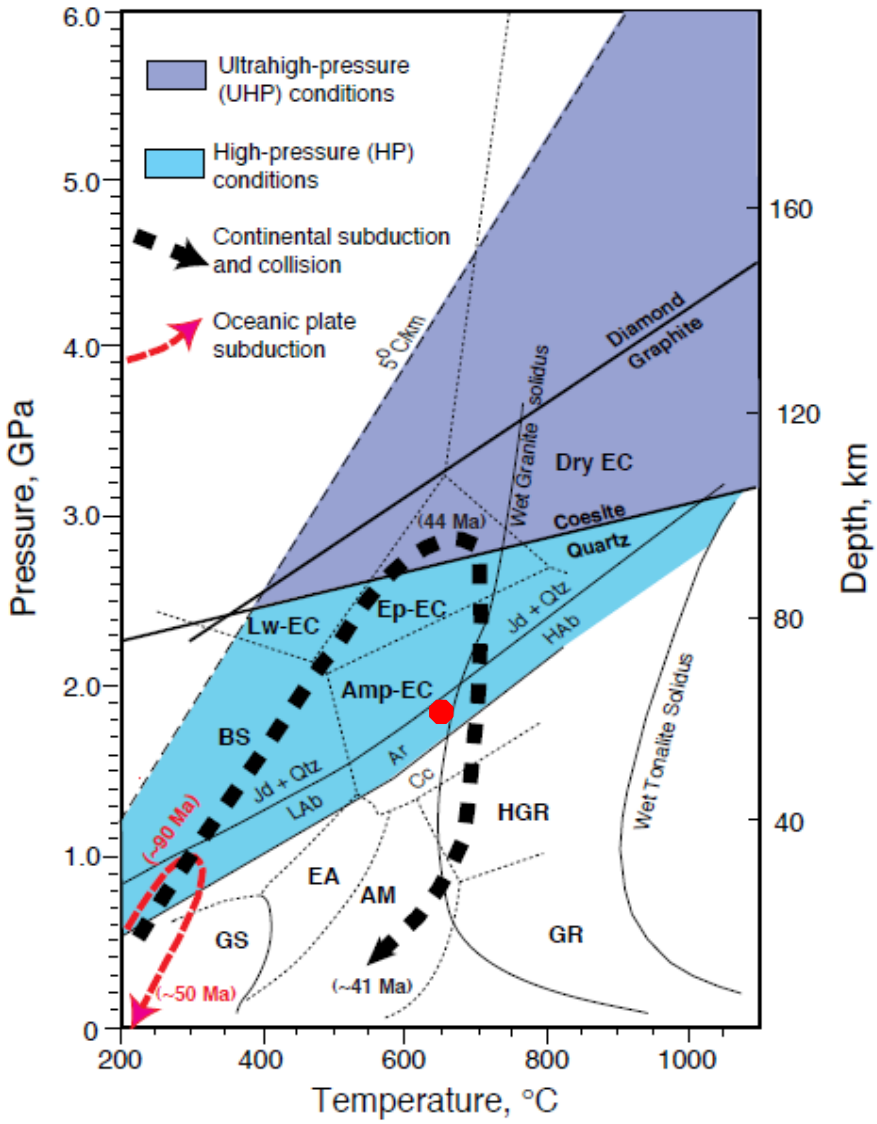

Figure 58 (previous page): Apparent subduction PT-t paths followed by exhumation to mid crustal levels for (a) Eocene continental collision of UHP imbricate thrust sheets and (b) oceanic plate subduction. A low subduction zone geothermal gradient of 5 ^{o}C/km is shown for reference. Mineral abbreviations: Ar = aragonite; Cc = calcite; Jd = jadeite; Qtz = quartz; LAb = low albite; and HAb = high albite. Metamorphic-facies abbreviations: AM = amphibolite; Amp-EC = amphibolite-eclogite; BS = blueschist; EA = epidote amphibolite; EC = eclogite; Ep-EC = epidote-eclogite; GR = sillimanite-granulite; GS = greenschist; HGR = kyanite-granulite; Lw-EC = lawsonite-eclogite; and Px-Hf = pyroxene hornfels (Taken from Ernst and Liou., 2008). The red dot at approximately 17 kbar and 650 ^{o}C indicates the metamorphic PT conditions of the Marsfjället gneiss.

Although there is much known concerning (U)HP conditions, there are still some unsolved problems. (U)HP conditions are related to differential circulation within the earth's dynamic lithosphere-astenosphere system: cold, dense oceanic crust descend into a hotter mantle at rates exceeding those of thermal re-equilibration by conductive heat transport (Ernst and Liou, 2008). This means you have relatively low temperatures at high pressures. Prograde P-T trajectories of subducted rocks are maintained during decompression and ascent because warmed at depth, UHP complexes cool slowly due to their low thermal conductivities. The important question what is applicable here is what is the duration of (U)HP metamorphism? The answer according to Ernst and Liou (2008) is that most of the time this period is relatively short. It may vary from 2-5 Myr up to 15-20 Myr. Hacker et al (2007) state that coastal Norway has endured (U)HP metamorphism of 15-20 Myr. The exhumation rate of (U)HP complexes is, according to Ernst et al (1998), depending on the strength of the subducted lithospheric materials, extents of deep-seated devolatilization, and rates of recrystallization. Average rates are approximately 10mm/year over at least 5 Myr (Carswell et al., 2003a; 2003b).

Exhumation rates are closely linked to slab break-off. Slab break-off is described by von Blanckenburg and Davies (1995), which allows relatively low dense continental crust attached to relatively dense oceanic crust to break apart and consequently pushed back up to the surface due to buoyancy forces. This decoupling and exhumation of collisional complexes may be enhanced as the crust warms in the upper mantle, weakens and becomes more ductile (Stockhert and Renner 1998). Densities of the oceanic crust (~3.0 g/cm3) and continental crust (~2.7 g/cm3) are sufficiently buoyant to overcome frictional resistance of the denser surrounding material; anhydrous mantle (~3.2 g/cm3), basaltic eclogite (~3.6 g/cm3); eclogite felsic gneiss (~3.0 g/cm3) and garnet peridotite (~3.3 g/cm3). Thus all (>90%) documented HP-UHP complexes consist dominantly of low-density rock types (Ernst, 2001). This goes hand in hand with cooling and decompressing of the (U)HP complexes since rocks have a low thermal conductivity. (U)HP rocks stay relatively warm during rapid exhumation and therefore mineralogical overprinting of typical granulite-, amphibolite-, and greenschist-facies conditions is ad hence (Ernst and Liou, 2008). However, (1) if the rocks are very dry the cooling would be faster. Another explanation could be (2) the thickness of the plates. If the plates are relatively thin, the cooling rate of these plates is bigger. Alternatively, a third possibility could be (3) the occurrence of extensional faulting against the overlying, cooler hanging wall. A combination of these

cooling factors is also possible (Ernst and Liou, 2008). This way the overprinting of typical greenschist-facies will not occur. This might be the case for the SNC rocks. There only seems to be a possible overprint of muscovite, but for almost all samples the peak metamorphic assemblages are preserved.

The retrograded (U)HP slabs often cease there exhumation at middle levels of the continental crust (Ernst and Liou, 2008). Several drivers can promote the last part of the exhumation up to the surface. Crustal contraction of low-density crustal underplating. Causing continuing isostatic compensation and erosion. The continental lithosphere has a lower subduction angle after the slab break-off that can account for the late-stage doming (Ernst et al., 1997). A third exhumation mechanism is antithetic faulting, which is typical for compressional orogens, whereby collapse of overlying crust enhances erosional removal (Ring and Brandon, 1994). Rapid uplift of diapiric bodies of continental crust gradually warm and soften the overthickened crust and causes the felsic crust to loose strength. It becomes buoyant and rises and therefore may be responsible for the last stages of exhumation of UHP terranes (Zeitler et al., 2001). A combination of these factors is also possible.

7.2.2 Water

A very important aspect is the presence of water in the rocks. A mineralogy that corresponds to a maximum hydrated state implies saturation of fluids. During a metamorphic event the following reaction will occur:

Hydrous assemblage → less hydrous or anhydrous assemblage + H_2O.

This is the dehydration process which takes place during prograde metamorphism. The clue here is the release of H_2O. This H_2O is in a gas phase, so H_2O is present in the form of 'steam' (above critical point). Steam is, in contrast to solid minerals, a very compressible phase and its volume is strongly dependent on PT conditions (Bucher and Frey, 2002). At low temperatures liquid water is denser than 'steam', but with increasing temperatures this difference becomes zero at the critical point. At temperatures above the critical point the H_2O phase is therefore a supercritical fluid phase or simply a fluid. This critical phase is at 374^{o}C and 217 bar (Bucher and Frey, 2002). The origin of water within metamorphic rocks has several causes. The first one is relic formation waters of sedimentary rocks. Second, dehydration water from originally stored H_2O in hydrous minerals. Third, meteoric water. Fourth, magmatic water released from solidifying magmas (Bucher and Frey, 2002). In the case of the Scandinavian Caledoniden the meteoric water can be neglected, but not much is known about the other three possibilities. Some of the low density fluids produced during prograde dehydration is transported away from the site of production through interconnected pore space and lost by the system. If the

production of H_2O is higher than the loss (for instance if the porosity of the rocks is low), the local pore pressure increases. The transport of H_2O can then be enhanced by hydraulic fracturing. The speed of this process can be described by the difference in density. The surrounding rocks have pressures of approximately 3 g/cm^3, while the produced fluids have densities of around 0.82 g/cm^3 (Bucher and Frey, 2002). A Fluid inclusion is off course a different situation. Here the fluids can't escape from the rocks.

PT-t paths have different positions of peak temperatures and peak pressures. This means that maximum pressure and maximum temperature will be generally diachronous. This means sedimentary rock formation in which apparently similar material varies in age from place to place. In the field we found these assemblages of peak metamorphism, but how is it possible that these assemblages didn't get (fully) overprinted to a low-grade assemblage on the way back to the surface? This is because low-grade rocks often contain large amounts of hydrates and are affected by dehydration reactions during the prograde part of the metamorphic cycle (Bucher and Frey, 2002). Dehydration of the rock will continue until the tangent point of the p-T path and last active dehydration reaction is reached (least hydrated state). At this point the rock contains a prograde assemblage in equilibrium with an aqueous fluid phase saturating the mineral grain boundaries and filling the pore spaces. This amount is in the order of 0.2 vol%. After that the reactions will consume water again and form hydrates from anhydrous minerals. This 2 vol% H_2O will produce 1,5 vol% biotite. This small amount of water will be used up pretty quickly which will lead to no free fluid. This prevents the mineralogy of the rock to adjust to changing PT conditions. On top of that is the catalytic property of H_2O in the rock. Chemical reactions need this to proceed. So, metamorphic rocks represent the PT conditions corresponding to the least hydrated state (Bucher and Frey, 2002). Retrograde metamorphism is very common in metamorphic rocks, but they do not succeed to complete. Late deformation events can cause the 'intrusion' of water again (shear zones). Isolated inclusions in refractory minerals such as garnet may preserve minerals from before the subduction (Bucher and Frey, 2002). Since we are talking of a whole plate subduction, different depths and temperatures will be reached since the rocks are on different positions. The presence of water causes a lowering of the melting temperatures of transformed, partly hydrated oceanic crust, the upper mantle wedge, and/or lower crustal protoliths at astenospheric depths along and above a sinking oceanic plate (Ernst and Liou, 2008). However, closure of a relatively small ocean basin, only generates minor volumes of hydrous intermediate and silicic melts (Ernst and Liou, 2008). This is consistent in case of the Caledoniden Orogeny. Blueschists and eclogites who carry these hydrous phases occur in several subduction terranes with typical low temperatures. In these rocks, H_2O may be carried to great upper-mantle depths under metamorphic field gradients of approximately 5 ^oC/km. However, white mica and biotite remain stable to pressures exceeding 30 kbar for typical subduction-zone geothermal gradients of 10 °C/km, especially in the absence of a separate H_2O phase (Luth, 1997). Thus, on descent to depths of 120–160

km, mica-rich quartzofeldspathic rocks fail to evolve significant amounts of H_2O and transform incompletely, to stable UHP assemblages. This is again consistent with what can be obtained from the computer program Theriak-Domino. Free H_2O against biotite and white mica only share a minor field according to the results of the pseudo sections made (Figs. 37 and 38). Transportation of H_2O into the deep Earth and its corporation in grain-boundary melts would drastically lower the solidus temperatures and viscosities, promoting more rapid mantle circulation, overturn and enhance plate and plume tectonic processes (Ernst and Liou, 2008). These in turn would facilitate devolatilization of the mantle. So gasses are reintroduced into the mantle primarily through the subduction and progressive devolatilization of descending lithospheric plates (Litasov and Ohtani, 2003).

The pseudo sections that are made for the Marsfjället rocks, with the program Theriak-Domino, imply PT conditions between 12.5 and 16-17 kbar and temperatures between 550-600 and 850 ^oC (Figs. 37 and 38). This would suggest the rocks were situated in the kyanite-granulite or possibly the amphibolite eclogite facies in the HP field. These conditions can only be reached during continental subduction and collision. This fits with what is already known about the Scandinavian Caledoniden.

7.2.3 Microstructure and mineral assemblages

The two samples measured with the use of XRF are taken from the Marsfjället gneiss in the northern part of the fieldwork area. According to the bulk rock chemistry, the most common element-oxide in these rocks is SiO_2 (quartz), followed by Al_2O_3, FeO, K_2O, Na_2O, MgO, CaO, TiO_2, MnO and P_2O_5. These results of the XRF can be seen back in the microstructure of all the samples (Appendices 11.3 and 11.4). The most dominant mineral is quartz, followed by garnet, feldspars (k-feldspar and plagioclase), kyanite, biotite and white mica. In smaller amounts some rutile and magnetite/hematite is detected. These representative bulk rock compositions are according to the ACF-'AKF diagrams part of the pelites and quartzofeldspatic rock fields (Figs. 35 and 36). This is conforming of what is known about the Scandinavian Caledoniden. Under the optical microscope and with BSE imaging, some dynamic recrystallization of biotite, feldspar and quartz is observed. Dynamic recrystallization is the result of intense strain. Some white micas are also present in these foliated zones, but some rocks do not contain any. These 'intact' white micas are most likely an overprint of the retrograde path that the rocks have undergone. Another indication for a possible second deformation event are the inlined inclusion trails in some kyanite grains. Exsolution lamelle in plagioclase is indicative for unmixing during cooling.

The monazites within the rocks are enclosed in individual or multiple minerals. Host minerals for the monazites of the Marsfjället gneiss are kyanite, k-feldspar, plagioclase, garnet, biotite, muscovite and quartz or a combination of these minerals (Appendix 11.3). For the Avardo gneiss, the host minerals

are dominantly biotite, muscovite and quartz, but also in garnet (Appendix 11.4). This indicates a close relation between monazite growth and growth of mineral parageneses that gave rise to HP conditions.

There has no significant age difference between different host minerals of the monazite been found. This is another indication that the ages of the monazites are the same ages as of the mineral paragenese. Therefore, the ages found can only be coupled to one deformation phase/event.

7.2.4 EMP mineral analysis

Mineral analyses have been done on several of the most dominant minerals present in the collected samples: garnet, biotite, white mica, plagioclase and K-feldspar. Zoning has been detected in the garnet, where there is less Mg and more Fe in the rims of the garnets, and in the plagioclase, where there is less Ca and more Na in the outer parts of the mineral grain. This zoning is interpreted to be the result of retrograde metamorphism after subduction occurred. Therefore, the magnesium and calcium released from the garnet and plagioclase might be used for the formation of other minerals formed at lower pressure and temperatures. What is most disappointing is the disagreement with the endmember diagrams obtained with the computer program Theriak-Domino. The data obtained by the microprobe cannot be plotted into endmember diagrams obtained with the computer program Theriak-Domino.

7.2.5 Obtained PT conditions compared to what is already known

Hacker and Gans (2005) have calculated PT conditions for the Seve Nappes of ~645 ^{o}C and 10 kbar to 745 ^{o}C and 13 kbar. These PT conditions correspond quite nicely with the PT conditions found with the computer program Theriak-Domino (pressures between 12.5 and 16-17 kbar and temperatures between 550-600 and 850 ^{o}C).

7.3. Conceptional model

7.3.1 Peridotite bodies

In most subduction zones of continental and oceanic crust, small lenses of garnet peridotite are included. These rocks have been found in the fieldwork area and give inside information on mineralogy, bulk-rock composition, and geochemical evolution of the mantle beneath and/or overlying subduction zones (Fig. 25a). Garnet peridotites are described by multiple authors (Brueckner., 1998; Zhang et al., 2000; Brueckner et al., 2003a; Carswell et al., 2003b; Brueckner and Van Roermund., 2004, 2008; Van Roermund., 2009) and play a key factor in the construction of a geodynamic model of the Scandinavian Orogeny. Garnet peridotites include mantle-derived and crust-hosted mafic-ultramafic cumulates (Brueckner, 1998; Zhang et al., 2000; Brueckner et al., 2003a; Carswell et al., 2003b; Brueckner and Van Roermund, 2004, 2008; Van Roermund, 2009). Both these rocks have

undergone pressures of 6 to 15GPa. This suggests the possibility of crustal emplacement of the ultramafic rocks into the HP-UHP rocks as well as mafic-ultramafic cumulates inserted in the near-surface crust. These peridotites are therefore exotic (Ernst and Liou, 2008). Peridotite bodies in the form of lenses are found in the fieldwork area. This supports the assumption that these rocks are inserted during subduction. These peridotite bodies play a key factor in understanding or making a (new) conceptional model.

7.3.2 Why are previous geodynamic models incorrect/incomplete

Figure 59 illustrates a cross section A-B in Jämtland (Fig. 9). What can be observed here is the major tectonic contact between the Seve Nappe and the Köli Nappe and between the Eastern Belt of the Seve Nappe with the nappes that belong to the Lower Allochthon. Within this transition zone of the Seve Nappes, an enormous peridotite body in the eastern belt of the Seve Nappe occurs. Between the Eastern Belt and Central Belt, a tectonic contact is present while no tectonic contact has ever been found between the Central and Western Belt. The assumption that the Svartsjöbäcken schist (Western Belt) has approximately the same age as the rocks from the Central Belt, is correct.

A

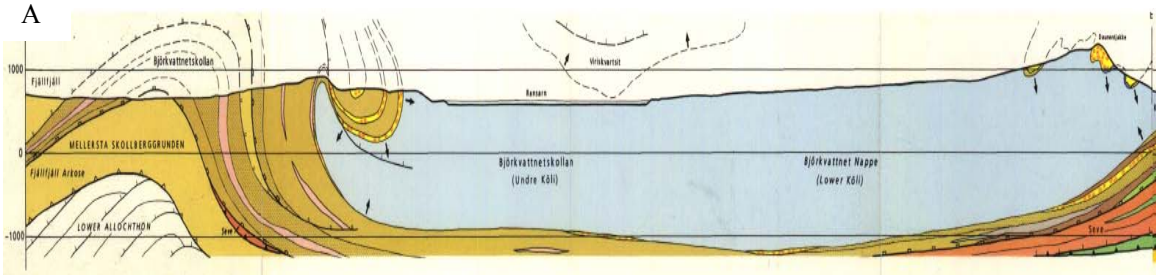

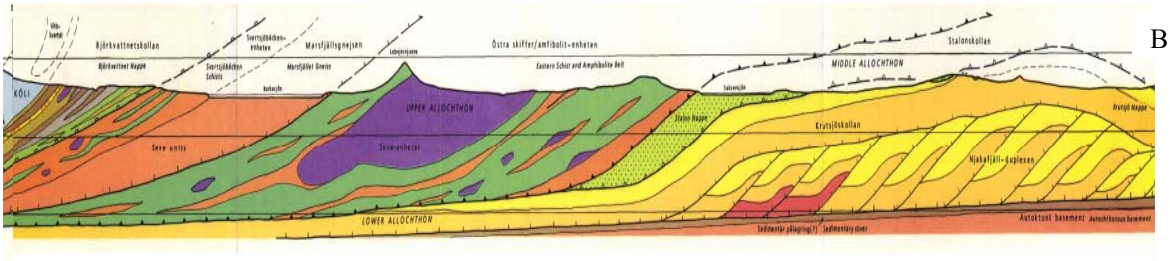

B

Figure 59: Cross section A-B in Jämtland (trace of profile in Appendix 11.2.1) illustrating the different nappes and there main boundaries. Modified after SGU, 1991. Legend can be seen in Appendix 11.2.4.

Another important observation of figure 59 is that the Autochthon can be seen as basement of the Baltic plate that is almost not deformed. The para-Autochthon is the one with the stacking complexes that is responsible for the shortening of approximately 700 km of crust. However, the brittle behaviour of this continental crust is not taken into account here; since this brittle behaviour would have caused many problems, the way it is stacked in this cross section.

The model of Gee (1975) did not involve subduction of plates into the mantle. Gee (1975) only corporate some sort of big décollement on which all the plates are moving (Figs. 7 and 8). In this way the (U)HP metamorphism in the Scandinavian Caledonides cannot be explained. Another big problem is the age that has been found for the rocks (~430 - 410 Ma). This assumed a contemporaneous event, but the 500 Ma found for peak metamorphism in the Central Belt in the SNC in this project is contradicting this assumption. Other outcoming ages of multiple investigators strengthen these age results (Brueckner and Van Roermund, 2004; Roberts, 2003). Hacker and Gans (2005) adapted the ideas of Gee and expanded the model. According to Hacker and Gans (2005; Fig. 13), the peak conditions reached by the Köli Nappes are 9-10 kbar and 550-650 ^{o}C. The peak conditions for the Seve Nappes are higher, with approximately 11-12 kbar and 700-725 ^{o}C. They believe that the (U)HP metamorphism occurred in the latest stages of continental collision. They describe several stages of continental collision. The first one is early arc ophiolite emplacement and continental passive margin contraction. The second stage is emplacement of the oceanic sediments and of the ophiolite assemblages. The third one is emplacement of the upper plate continent and the fourth stage is the plateau formation and intracontinental shortening. They state that the (U)HP rocks where formed as a consequence of the first stage and contact metamorphism is caused by intrusions of 445-432 Ma. This model lacks the incorporation/explanation of multiple subduction stages explained by different ages. Neither can they explain the westwards thinning of the nappes. If the individual thin nappes are assumed to move over each other, how can they manage to do so without breaking them? This is a big mechanical problem in this model.

The model of Terry et al., (2000) describes the exhumation of (U)HP rocks in the WGR. According to them, the upper crustal transtension was enhanced by a reduction of the orogen-normal component of the plate motion vector. Slowing subduction of cold Baltica crust is likely to have caused relaxation of isothermal surfaces and overall weakening in the hinterland. This slowing would have enhanced ongoing upper crustal transtension relative to shortening and would mark the onset of “late orogenic collapse” in other models (Terry et al., 2000). Mechanisms like orogenic collapse and plate divergence (Krabbendam and Dewey, 1998), which involve coaxial thinning of lower crust and extensional faulting of middle and upper crust, may have contributed to the exhumation of (U)HP rocks (Terry et al., 2000).

Brueckner and Van Roermund (2007) suggest that the HP collision recorded in the Jämtland area can be called the Jämtlandian Orogeny with its Early Ordovician age. These ages are evidence for a HP event during Early Ordovician time along the Baltic margin. Andersen et al., (1998) and Corfu et al., (2003) also found metamorphic terranes with Early Ordovician age. The ages found in this research contradict this suggesting. Another interesting connection can be made with the 452 Ma HP terrane in

Trømso Nappe Complex (Corfu et al., 2003). The KNC is composed of ophiolites, volcanic arc terranes, marginal basins, etc and records the closure history of the Iapetus Ocean. The SNC below the KNC records the evolution of the Baltic margin. These HP terranes in the SNC are generally metamorphosed and do not contain fossils. Furthermore, it is cut by numerous low-angle faults with abrupt changes in metamorphic grade across these faults (Brueckner and Van Roermund, 2007). The Finnmarkian Orogeny is interpreted as a collision between the Virisen Arc and a microcontinent or peninsula that had previously rifted away from Baltica instead of with Baltica itself (Brueckner and Van Roermund, 2004). The age found of 458 Ma is most likely representing the peak metamorphic conditions. The amalgamation of the microcontinent and the Virisen Arc occurred during the Finnmarkian Orogeny. Then approximately 42 Myr passed as the ocean between the composite terrane and Baltica narrowed and closed, culminating in the subduction of Baltica. This event has been called the Jämtlandian Orogeny (Brueckner and Van Roermund, 2007; Fig. 11). Nappes became further transported eastwards during final collision when Laurentia collided with Baltica (425-410 Ma). This assumption is fortified with nearly similar ages obtained from the Scandinavian Caledonides. Brueckner and Van Roermund conclude that the 458 Ma HP metamorphism that affected the Jämtland terrane is the first documented tectonic event along the eastern margin of Iapetus. Another conclusion here is that the 458 Ma is almost 50 Myr younger than ages from essentially identical rocks more northwards. Brueckner and Van Roermund (2007) think of 5 to 6 (U)HP collisions that marked the accretionary evolution of the Scandinavian Orogeny: Finnmarkian (500 Ma), Jämtlandian (458 Ma), a separate 450 Ma event on the other side of the Iapetus, another event in the Bergen Arcs (420 Ma; Bingen et al., 2004) and the culminating Scandian Orogeny at 400 Ma (Fig. 12).

Underthrusting of Laurentia by Baltica is generally accepted to account for the different characteristics of the EW-vergent thrust systems (Gee et al., 2008). Ocean derived Allochthons are preserved in the Scandes representing Cambrium-Ordovician Iapetus sea floor, island arcs and back arc basins. Intrusions of dike swarms at c. 600 Ma are probably the cause of the start of the separation of Baltica and Laurentia. Evidence of this separation outside the dike swarms in the Baltoscandian plate is the deposition difference of these plates at that time (Gee et al., 2008). These deposits reflect low latitude location of Laurentia and moderate to high latitude deposits of the Baltoscandian platform. The Baltoscandian platform is dominated by siliciclastics throughout the Cambrium (black shale described by Andersen et al., 1986). Carbonate deposition dominated the Ordovician deposition on both platforms and along the Baltoscandian margin is a change towards the west into turbidites. The Scandinavian Caledoniden show similarities with a classical foreland fold-and-thrust belt, which is developed in the eastern part. To the west, nappes are overridden by long-transported Allochthonous units that are inferred to be the Baltoscandian margin. Precambrian basement becomes more reworked to the west, which goes hand in hand with an increase in PT conditions (Gee et al., 2008). The Upper Allochthon is dominated by sedimentary and igneous rocks derived from the Iapetus Ocean. This

major Allochthon includes metasediments metamorphosed to amphibolite, granulite and locally eclogite facies. The metamorphic grade decreases going to the Middle Allochthon. Just like the inverted metamorphism, these metasedimentary units increased westwards to western Norway, implying that they must have been derived from west of the hinterland (Gee, 1975). The Uppermost Allochthon also has affinities to the Laurentian margin. The oldest dated remnants of arc-related magmatism and ophiolites occur in the upper part of the Upper Allochthon and yield ages around 500 Ma (Dunning and Pedersen, 1988). The present structure of the Scandinavian Caledonides is strongly influenced by extensional shear zones and fabrics indicating W- to NW-directed translations (Gee, 2008). Deposition of coarse siliciclastic sediments occurred during Devonian extension. Tectonic thinning, exhumation of the high pressure rocks and denudation of the Caledonian mountain chain was fast during the Devonian, causing the change from a very deep-rooted crust with high mountains during collisional orogeny to a more normal crustal thickness and a flatter and desert-type landscape towards the end of the Carboniferous (Gee, 2008). In Scandinavia, the E-vergent thrust-sheets were transported from both oceanic and outer continental margin environments and emplaced many hundreds of kilometres onto the Baltoscandian platform. Laurentian margin and proximal island-arc terranes are inferred to comprise the highest Allochthons in this part of the orogen. After the break up of Baltica and Laurentia, about 70 Myr of subduction-related magmatism, sedimentation, deformation and metamorphism are recorded in the fragmented ophiolites, island-arcs and back-arc assemblages of the Scandinavian mountains. Caledonian collisional orogeny in both northeastern Greenland and western Scandinavia culminated in the latest Silurian and early Devonian with rapid exhumation of hinterland high grade complexes, deep erosion, deposition in foreland basins and major extensional faulting

7.3.3 Own adaptation

This new data, combined with the existing data, is used to create a more detailed and quantitative tectonic history of northern Jämtland and southern Västerbotten.

The question ‘when’ did the SNC reached (U)HP conditions can be said to be ~500 Ma (Finnmarkian). The PT conditions reached at that time are approximately 700 ^{o}C with pressures of ~ 16 kbar. This suggests that these rocks were situated on the footwall of a subducting continental slab boundary so that they could endure metamorphism. The HP units are assumed to have endured higher pressures with approximately the same temperatures. This can be accomplished when the Marsfjället gneiss as well as the HP unit is situated at the same continental subducting slab, but only on a different side. It might be possible that the Marsfjället gneiss was situated on the intermediate side, while the HP unit is situated on the bottom side of the continental subducting slab. This way the differences in pressure together with resemblance of temperatures conditions can be explained. The T(0) age of the Marsfjället gneiss is 497 Ma and the HP units is 490 Ma. This might be explained with the assumed

positions in the subducting slab. When the subducting slab is educting again, the HP gneiss is still situated in deeper parts of the earth's mantle and will have more time to realize a possible overprint. This might be enhanced by possible injection of fluids, which have a catalytic property. This is what has been observed in the HP gneiss, were a possible visible second deformation event can be seen. This possible second deformation phase may be due to renewed thrusting (based on Köli ages, 420 Ma) during the Scandian causing second deformation phase.

The shortening of approximately 700 km of crust is achieved by stacking the crust in the para-Autochthon (Fig. 59). Nevertheless the breaking of this crust is inevitable is this model. Maybe part of this shortening can be explained by the slab break-off.

To improve this possible geodynamic model, ages of the Lillfjället gneiss in the southern part of the fieldwork area (Fig. 2), which is assumed to have endured HT and LP conditions, must be included. This way the entire SNC of the n. Jämtland and s. Västerbotten can be incorporated. The ages and PT conditions of these rocks is in progress, done by MSc student M. Gademan.

7.4. Svartsjöbäcken schist

The age of the monazites found within the Svartsjöbäcken schist (488 Ma) is consistent with the geodynamic model. Since no tectonic contact has ever been found or described by someone between the Svartsjöbäcken schist (western belt) and the central belt, the age must be more or less the same. This outcoming age has only been based upon 19 point measurements on eight different monazites from two different rock samples. However, r^2 of these data point in the isochron plot is again perfect with 0,992. Field observations that have been made of the Svartsjöbäcken schist indicate that the temperatures these rocks have endured might be lower than the Central belt. The minerals for instance are much smaller. Therefore, the availability of the mineral monazite at all was doubtful. Nevertheless, monazites have been found but only up to sizes of 20 µm. Monazites found in the Marsfjället gneiss and HP gneiss could reach sizes up to 180 µm. The meaning of this significant smaller size of the monazites is because the rocks are have probably endured lower metamorphic temperatures (schists instead of gneiss).

7.5. Future

7.5.1 Other relevant investigations/projects

BSc M. Gademan is working on his MSc thesis based upon monazite age dating and determination of PT conditions of sillimanite holding gneisses in the area between Saxnäs and Gäddede in Jämtland.

Preliminary ages found in these gneisses are approximately the same as has been found in the Marsfjället gneiss.

Another monazite age dating project in the same area is still in progress by Jarek Majka, supervised by D.Gee. He works in the University of Uppsala on a similar project.

An idea of D.Gee for a drilling project in Jämtland might be approved. Since we do not know exactly what is going on below the surface rocks, the results of this research project might be very interesting to corporate in this geodynamic model.

7.5.2 What needs to be done

The garnet peridotites are playing an important role in the understanding of geodynamic history of the Caledonides. Therefore, it might be interesting to look a bit deeper into these peridotites found in the Central Belt of the SNC. Several peridotite lenses have already been seen and mapped in the area near Marsliden. However, examination and dating of these rocks as well as determination of the PT conditions would in fact give more information about the tectonic history.

Determination of the PT conditions of the HP gneiss would be interesting. This research project did not incorporate these rocks for determination of the PT conditions.

The Svartsjöbäcken schist could also use some more investigation. The data illustrated here is only based on two rock samples. Again, determination of PT conditions would support or contradict the geodynamic models that are discussed.

8. Conclusion

- The standard monazite used as an internal reference during the monazite age dating project, is dated to have a mean age T(0) of 1129.7 Ma (with a known age of 1125 Ma). This age is based on 373 filtered point measurements. The calibration of the EMP based on this monazite standard is accepted because the mean age of the standard is defined as 1125 +/- 10 Myr. R^2 of the isochron plot is 0.9997, which strengthens the correctness of the calibration.

- The metamorphic age (t) of the mineral assemblage in the Marsfjället gneiss is dated to be 502.8 Ma +/- 3, based on 393 filtered point measurements, from 22 different monazites dispersed in 11 different rock samples. This corresponds to an isochron age T(0) of 497.3 Ma, with an R^2 of 0.9756, which strengthens the correctness of the results. A total of 68.2 % of the metamorphic ages fall between 547-459 Ma; a total of 96% would fall between 591-415 Ma. These percentages are indicative for a normal distribution curve.

- The mineral assemblage of the Avardo gneiss has an average metamorphic age (t) of 512.7 Ma +/- 3. This corresponds to an isochron age T(0) of 490.6 Ma. This is slightly younger than the Marsfjället gneiss. This is based on 153 filtered point measurements from 12 different monazites dispersed in 7 different rock samples. R^2 of the isochron plot is 0.9783, which strengthens the correctness of the results.

- The resemblance between T(0) ages, 497,3 Ma for the Marsfjället gneiss and 490,6 Ma for the Avardo HP gneiss is strong. The mineral assemblages in both gneisses are approximately similar and no significant age difference has been found between monazite grains included in different host minerals. This indicates a close relation between monazite growth and growth of the metamorphic mineral parageneses that gave rise to HP conditions. Therefore the monazite ages are interpreted to be coupled to one metamorphic event (deformation phase).

- The PT stability field of the Marsfjället gneiss determined by the computer program Theriak-Domino, lies between pressures of 12.5 – 17 kbar and temperatures of 550 and 850 ^{o}C. Within this field (given the particular sample bulk rock composition), the following minerals are stabile: garnet, 2-feldspars (plagioclase and K-feldspar), biotite, white mica, hematite, rutile, α-quartz and kyanite. This same mineral assemblage has been found with the optical and electron optical microscope.

- EMP mineral compositions do not agree with the endmember chemical compositions obtained by the theoretical program Theriak-Domino.

- The backscatter coefficient (η*) determines whether in a BSE image of a monazite grain the reflectance will be relatively light or dark. The higher η*, the lighter the image. An increase in η* can be explained by a decrease of Th^{4+}, a decrease in Ca^{2+} or alternatively an increase in REE, formed according to the reaction: $2\ REE^{3+} \leftrightarrow Ca^{2+} + Th^{4+}$. Since there is no correlation found between the backscatter coefficient and the corresponding ages, multiple metamorphic recrystallisation stages recorded in the monazites are interpreted not to be present.

- Monazite grains from the Svartsjöbäcken schist have an average crystallisation age of ~488 Ma. This has been based on 19 filtered point measurements of 8 different monazites from 2 rock samples. This strengthens the assumption that there is no tectonic contact between the Western Belt (Svartsjöbäcken schist) and the Central Belt (Marsfjället gneiss). The size of these monazite grains is significant smaller than have been found for the Marsfjallet and HP gneisses, which indicates lower metamorphic temperatures.

- Evaluation of existing geodynamic models has led to a improved geodynamic model which includes a subducting continental slab in Early Caledonian times (Finnmarkian) consisting of Marsfjället and Avardo gneisses that are situated in respectively the intermediate and bottom side of the subducting continental slab. Continental subduction is followed by eduction and compression causing the rocks to migrate and stack upon each other. Finally renewed thrusting (based on Köli ages) during the Scandian causing another deformation phase.

9. Acknowledgements

This project has been build upon the ideas of Dr. H.L.M. v. Roermund. I would like to thank him for introducing me into the geological world of Scandinavia. He coordinated the trip in the summer of 2009 to Lapland, where he was of great assistance in coordinating the fieldwork and helping to do the actual geological fieldwork in a professional way! After the fieldwork part, he guided me with the monazite age dating, the determination of the PT conditions of the rocks, geological thinking and with writing this master thesis. It is nice working with this kind, interesting and intelligent man.

Substantial financial support came from Prof. Dr. M.J.R. Wortel and Dr. H.L.M. v. Roermund. Prof. Dr. M.J.R. Wortel financed the costs of the EMP. Dr. H.L.M. v. Roermund eventually financed the transportation of the fieldtrip in the summer of 2009. Without these financial supports, this project could not have been realised.

I would also like to thank the technical staff of the University of Utrecht. Especially Tilly Bouten, who was of great assistance during working with the EMP.

Finally yet importantly, I would like to thank my student partner BSc Michiel Gademan. Outside the fact that he is a good friend of mine, I thank him for his company and effort during the fieldwork, lab work, writing part and discussing part.

10. References

Andersen, A., Dahlman, B., Gee, D.G. and Snäll, S., (1986), The Scandinavian Alum Shales: Sveriges Geologiska Undersökning, Ser. Ca 56, 50 pp.

Andersen, T.B., (1998). Extensional tectonics in the Caledonides of southern Norway, an overview. Tectonophysics 285, 333–351.

Andréasson, P.G., (1994). The Baltoscandian Margin in Neoproterozoic – Early Palaeozoic time. Some constraints on terrane derivation and accretion in the Arctic Scandinavian Caledonides. Tectonophysics, 231, 1–32.

Andreasson, P. G., Svenningen, O. & Albrecht, L. (1998). Dawn of Phanerozoic Orogeny in the North Atlantic tract: evidence from the Seve---Kalak Superterrane, Scandinavian Caledonides. Geolo- giska Foreningens i Stockholm Forhandlingar 120, 159---172.

Ayers, J.C., Miller, C., Gorisch, B., Milleman, J., (1999) Textural developent of monazite during highgrade metamorphism: Hydrothermal growth kinetics, with implications for U, Th – Pb geochronology, American Mineralogist 84, p. 1766-1780

Bingen, B., Austrheim, H., Whitehouse, M.J. & Davis, W.J. (2004). Trace element signature and U–Pb geochronology of eclogite-facies zircon, Bergen Arcs, Caledonides of W Norway. Contributions to Mineralogy and Petrology, 147, 671–683, doi:10.1007/s00410-004-0585-z.

Brueckner, H. K., (1998). Sinking intrusion model for the emplacement of garnet-bearing peridotites into continent collision orogens, *Geology*, *26/7,* 631-634.

Brueckner, H.K. & Van Roermund, H.L.M. (2004). Dunk tectonics: a multiple subduction/eduction model for the evolution of the Scandinavian Caledonides. Tectonics, 23(TC2004), 1–20, doi:10.1029/2003TC001502.

Brueckner, H.K. & Van Roermund, H.L.M. (2008). Simultaneous HP metamorphism on both margins of Iapetus: Ordovician ages for eclogites and garnet peridotites from the Seve Nappe Complex, Swedish Caledonides. J. Geol. Soc. London. 164, 117-128.

Brueckner, H. K., H. L. M. van Roermund, and N. Pearson. (2003) An Archean to Paleozoic evolution for agarnet peridotite lens with sub-Baltic Shield affinity within the Seve Nappe Complex of Jämtland, Sweden, Central Scandinavian Caledonides, *J. Petrol.*, *in press,*.

Carswell, D.A., Tucker, R.D., O'Brien, P.J., and Krogh, T.E. (2003a) Coesite micro-inclusions and the U-Pb age of zircons from the Hareidland eclogite in the Western Gneiss Region of Norway. Lithos, 67, 181–190.

Carswell, D.A., Brueckner, H.K., Cuthbert, S.J., Mehta, K., and O'Brien, P.J. (2003b) The timing of stabilization and the exhumation rate for ultra-high pressure rocks in the Western Gneiss Region of Norway. Journal of Metamorphic Geology, 21, 601–612.

Chemenda, A. I., M. Mattauer, and A. N. Bokun (1996), Continental subduction and a mechanism for exhumation of high-pressure metamorphic rocks: New modelling and field data from Oman, *Earth Planet. Sci. Lett.*, *143,* 173-182.

Claesson, S. (1987). Isotopic evidence for the Precambrian provenance and Caledonian metamorphism of high grade paragneisses from the Seve Nappes, Scandinavian Caledonides. Contributions to Mineralogy and Petrology 97, 196---204.

Cocks and Torsvik (2002) Cocks, L.R.M., Torsvik, T.H., 2002. Earth history 500– 400 Ma: a faunal and palaeomagnetic review. J. Geol. Soc. Lond. 159,631– 644

Corfu, F., Ravna, E.J.K. & Kullerud, K. (2003). A Late Ordovician U–Pb age for the Tromsø Nappe eclogites, Uppermost Allochthon of the Scandinavian Caledonides. Contributions to Mineralogy and Petrology, 145, 502–513.

Dallmeyer, R.D., (1991). 4oAr/39Ar mineral ages from the western gneiss terrane, Troms, Norway: evidence of a variahle Caledonian record. Terra Abstr., 4: 12.

Dunning, G.R., (1987). U–Pb zircon ages of Caledonian ophiolites and arc sequences: implications for tectonic setting (abstract).Terra Abstr., EUG IV, Strasbourg, 179.

Dunning, G.R., and Pedersen, R.B., (1988), U/Pb dating of ophiolites and arcrelated plutons of the Norwegian Caledonides: implications for the development of the Iapetus Ocean: Contributions to Mineralogy and Petrology, v. 98, pp. 13–23

Eide, E.A., Lardeaux, J.M., (2002). A relict blueschist in meta-ophiolite from the central Norwegian Caledonides—discovery and consequences. Lithos 60, 1 – 19.

Elkins LT, Grove TL (1990) Ternary feldspar experiments and thermodynamic models. Am Mineral 75:544-559

Ernst, W.G. (2001) Subduction, ultrahigh-pressure metamorphism, and regurgitation of buoyant crustal slices—implications for arcs and continental growth. In D. Rubie and R. van der Hilst, Eds., Processes and Consequences of

Deep Subduction. Physics of the Earth and Planetary Interiors, 127, 253–275.

Ernst and Liou (2008): High and Ultrahigh-pressure metamorphism: past and future prospects. American Mineralogist, volume 93, pages 1771-1786.

Ernst, W.G., Maruyama, S., and Wallis, S. (1997) Buoyancy-driven, rapid exhumation of ultrahigh-pressure metamorphosed continental crust. Proceedings of the National Academy of Sciences, 94, 9532–9537.

Ernst, W.G., Mosenfelder, J.L., Leech, M.L., and Liu, J. (1998) H2O recycling during continental collision: Phase-equilibrium and kinetic considerations. In B.R. Hacker and J.G. Liou, Eds., When Continents Collide: Geodynamics and Geochemistry of Ultrahigh-Pressure Rocks, p. 275–295. Kluwer Academic Publishers, Dordrecht.

Fialin, M., Remy, H. Richard, C. and Wagner, C (1999). Trace element analysis with the electron microprobe: new data and perspectives. Am. Mineral**.** 84, pp. 70–77.

Gardes E, Jaoul O, Montel J, Seydoux-Guillaume AM,Wirth R. (2006). Pb diffusion in monazite: an experimental study of Pb2+ + Th4+ ↔ 2Nd3+ interdiffusion. *Geochim. Cosmochim. Acta* 70:2325–36

Gee, D.G., (1975). A tectonic model for the central part of the Scandinavian Caledonides: American Journal of Science, v. 275A, pp. 468–515.

Gee, D.G. (1985). Tectonostratigraphic map. Sveriges Geologiska Undersokning SER. Ba nr 35.

Greiling, R. O., Z. Garfunkel, and E. Zachrisson (1998), The orogenic wedge in the central Scandinavian Caledonides: Scandian structural evolution and possible influence on the foreland basin, in Tectonics and Geological History of some Phanerozoic Orogens, edited by B. Sundquist and M. B. Stephens, Geol. Foeren. Stockholm Foerh., 120, 181 – 190.

Hacker, B.R. (2007) Ascent of the ultrahigh-pressure Western Gneiss Region, Norway. In M. Cloos, W.D. Carlson, M.C. Gilbert, J.G. Liou, and S.S. Sorensen, Eds., Convergent margin terranes and associated regions. Geological Society of America Special Paper 419, 171–184

Hacker and Gans (2005): Continental collisions and the creation of ultrahigh-pressure terranes: Petrology and thermochronology of nappes in the central Scandinavian Caledonides

Kornprobst, J. (2002). Metamorphic rocks and there geodynamic significance, a petrological handbook. Kluwer academin publishers: petrology and structural geology vol.12.

Krabbendam, J.F. and Dewey, M. (1998) Exhumation of UHP rocks by transtension in the Western Gneiss Region, Scandinavian Caledonides. Geological Society of London, Special Publication 135, 159–181.

Krenn, E. and Finger, F. (2007) Formation of monazite and rhabdophane at the expense of allanite during Alpine low temperature retrogression of metapelitic basement rocks from Crete, Greece: Microprobe data and geochronological implications. Lithos, 95, 130-147

Krenn, E., Janak, M., Finger, F., Broska, I., Konecny, P. (2009) Two types of metamorphic monazite with contrasting La/Nd, Th, and Y signatures in an ultrahigh-pressure metapelite from the Pohorje Mountains, Slovenia: Indications for pressure-dependent REE exchange between apatite and monazite? American Mineralogist, volume 94, 2009.

Leake, B.E., Hendry, G.L., Kemp, A., Plant, A.G., Harvey, P.K., Wilson, J.R., Coats, J.S., Aucott, J.W., Lunel, T. and Howarth, R.J., (1969). The chemical analysis of rock powders by automatic X-ray fluorescence. Chem. Geol. 5, pp. 7–86.

Linthout, K. (2007). Tripartite division of the system $2REEPO_4–CaTh(PO_4)_2–2ThSiO_4$, Discreditation of brabantite, and recognition of cheralite as the name for members dominated by $CaTh(PO_4)_2$. *The Canadian Mineralogist*, v.45, pp. 503–508.

Litasov, K.D. and Ohtani, E. (2003) Stability of various hydrous phases in CMAS pyrolite-H2O system up to 25 GPa. Physics and Chemistry of Minerals, 30, 147–156.

Luth, R.W. (1997) Experimental study of the system phlogopite-diopside from 3.5 to 17 GPa. American Mineralogist, 82, 1198–1209.

Matte, P (1998)., Continental subduction and exhumation of HP rocks in Pale9ozoic orogenic belts: Uralides and Variscides, *Geol. Fören. Stockh. Förh, 120,* 209-222.

McFarlane, C.R.M., Connelly, J.N., and Carlson, Q.S. (2006) Contrasting response of monazite and zircon to a high-T thermal overprint. Lithos, 88, 135-149.

Montel J, Foret S, Veschambre M, Nicollet C, Provost A. (1996). Electron microprobe dating of monazite. *Chem. Geol*. 131:37–53

Mørk, M.B.E., Kullerud, K., Stabell, A., (1988). Sm–Nd dating of Seve eclogites, Norbotten, Sweden—evidence for Early Caledonian (505 Ma) subduction. Contrib. Mineral. Petrol. 99, 344–351.

Mørk (1989), Brattvag berggrunnskart 1220 III, 1:50000, voorlopige utgave.

Nelson, S.A. (2000): Triangular Plots in Metamorphic Petrology: Tulane University

Norrish, K. and Chappell, B.W., 1967. X-ray fluorescence spectrography. In: Zussman, J., Editor, , 1967. Physical Methods in

Determinative Mineralogy, Academic Press, London, pp. 161–214.
Poitrasson, F., Chenery, S., Bland, D.J., (1996). Constrasted monazite hydrothermal alteration mechanisms and their geochemical implications, Earth and Planet. Sci. Lett. 145, p. 79-96
Reed, S.J.B. (1983) Electron Microprobe Analysis. Applied Science Publishers Ltd., Analysis of High Temperature Materials pp. 91-127.
Ring, U. and Brandon, M.T. (1994) Kinematic data for the Coast Range fault and implications for the exhumation of the Franciscan subduction complex. Geology, 22, 735–738.
Roberts, D. (2002): the Scandinavian Caledonides: event chronology, palaeogeographic settings and likely modern analogues. Tectonophysics, v. 365, p. 283–299, doi: 10.1016/S0040-1951(03)00026-X
Roberts, D. & Stephens, M. B. (2000). Caledonian orogenic belt. In: Lundqvist, Th. & Autio, S. (eds) Description to the Bedrock Map of Central Fennoscandia (Mid-Norden). Geological Survey of Finland, Special Paper 28, 79---108.
Sveriges Geologiska Undersokning Berggrundskartan (1991). C 689, 1-155.
SGU, Uppsala (1998). Beskrivning till bergrundskartan over Jamtlands lan. By: Karis, L and Stromberg, A.G.B. SGU series Ca 53:2.
Stöckhert, B. and Renner, J. (1998) Rheology of crustal rocks at ultrahigh pressure. In B.R. Hacker and J.G. Liou, Eds., When Continents Collide: Geodynamics and Geochemistry of Ultrahigh-Pressure Rocks, p. 57–95. Kluwer Academic Publishers, Dordrecht.
Sturt, B.A., Pringle, I., Ramsay, D.M., (1978). The Finnmarkian phase of the Caledonian orogeny. J. Geol. Soc. Lond. 135, 597– 610.
Suzuki K. & Adachi M. (1991). The chemical Th-U-total Pb Isochron Ages of zircon and monazite from the Gray Granite of the Hida Terrane, Japan. J.Earth Sci. Nagoya Univ., 38; 11-38.
Terry, M.P., Robinson, P., Hamilton, M.A., Jercinovic, M.J., (2000). Monazite geochronology of UHP and HP metamorphism, deformation and exhumation, Nordøyane, Western Gneiss Region, Norway. Am. Mineral. 85, 1651– 1664
THERIAK-DOMINO Vers. 20.03.07 User's Guide *Christian de Capitani Konstantin Petrakakis*
Torsvik, T.H., (1998). Palaeozoic palaeogeography: a North Atlantic viewpoint. Geol. Fo¨ren. Stockh. Fo¨rh. 120, 109–118.
Torsvik, T. H. & Cocks, L. R. M. 2005. Norway in space and time: a centennial cavalcade. Norwegian Journal of Geology, 85, 73–86.
Torsvik, T. H., Smethurst, M. A., Van der Voo, R., Trench, A., Abrahamsen, N. & Halvorsen, E. (1992). Baltica. A synopsis of Vendian---Permian paleomagnetic data and their paleotectonic implications. Earth-Science Reviews 33, 133---152.
Trouw, R.A.E. (1973): structural geology of the Marsfjallen area, Caledoniden of Vasterbotten, Sweden. Sveriges Geologiska Undersokning C 689, 1-155.
Van der Stijl 1976
Van Roermund, HLM., (1985). Eclogites of the Seve Nappe, central Scandinavian Caledonides. In: Gee D.G. & Sturt, B.A. (eds) The Caledonide Orogen – Scandinavia and Related Areas. Wiley, Chichester, 873-886.
van Roermund, H. L. M. (1989), High-pressure ultramafic rocks from the allochthonous nappes of the Swedish Caledonides, in The Caledonide Geology of Scandinavia, edited by R. A. Grayer, pp. 205 – 219, Graham and Trotman, Norwell, Mass.
Van Roermund, H.L.M. (2009). Mantle garnet peridotites from the northermost ultra-high pressure domain of the Western Gneiss Region, SW Norway
Van Roermund, H. L .M. and E. Bakker (1983), Structure and metamorphism of the Tången-Inviken area, Seve Nappe, Central Scandinavian Caledonides, *Geol. Fören. Stockh. Förh., 105,* 301-319.
Vannay, J. C. and B. Grasemann (2001), Himalayan inverted metamorphism and syn-convergence extension as a consequence of a general shear extrusion, *Geol. Mag., 138,* 253-276.
Von Blanckenburg, F. and Davies, J.H. (1995) Slab breakoff: A model for syncollision magmatism and tectonics in the Alps. Tectonics, 14, 120–131.
Williams ML, Jercinovic MJ, Goncalves P, Mahan KH. (2006). Format and philosophy for collecting, compiling, and reporting microprobe monazite ages. *Chem. Geol*. 225:1–15
Williams, M.L., Jercinovic, M.J., Hetherington, C.J. (2007). Microprobe monazite geochronology: Understanding geologic processes by integrating composition and chronology. Annual review of Earth planet. Science, 35:137-75
Wortel, M. J. R. and W. Spakman (2000), Subduction and slab detachment in the Mediterranean-Carpathian Region, *Science, 290*, 1910-1917.
Zeitler, P.K., Koons, P.O., Bishop, M.P., Chamberlain, C.P., Craw, D., Edwards, M.A., Hamidullah, S., Jan, M.Q., Khan, M.A., Khattak, U.K., Kidd, W.S.F., Mackie, R.L., Meltzer, A.S., Park, S.K., Pecher, A., Poage, M.A., Sarker, G., Schneider, D.A., Seeber, L., and Shroder, J.F. (2001) Crustal reworking at

Nanga Parbat, Pakistan: Metamorphic consequences of thermal-mechanical coupling facilitated by erosion. Tectonics, 20, 712–728.

Zhang, R.Y., Liou, J.G., Yang, J.S., and Yui, T.F. (2000) Petrochemical constraints for dual origin of garnet peridotites from the Dabie-Sulu UHP terrane, eastern-central China. Journal of Metamorphic Geology, 18, 149–166.

Zhu, X.K., O'nions, R.K., (1999) Zonation of monazite in metamorphic rocks and its implications for high temperature thermochronology: a case study from the Lewisian terrain, Earth Planet. Sci. Lett. 171, p. 209-220

Zwart, H.J. (1974). Structure and metamorphism in the Seve–Ko¨li Nappe Complex (Scandinavian Caledonides) and its implications concerning the formation of metamorphic nappes. In: Bellie`re, J. & Duchesne, J.C. (eds) Ge´ologie des Domains Cristallins. Centenaire de la Socie´te´ Ge´ologique de Belgique, Lie`ge, 129–144.

Websites:
http://www.earth.ox.ac.uk/~davewa/pt/index.html

http://gcmd.nasa.gov/records/StereoNet.html

www.webmineral.com